# SYNCHROPHASOR MEASUREMENT BASED MODE DETECTION AND DAMPING ESTIMATION IN POWER SYSTEM USING FFT - CONTINUOUS WAVELET TRANSFORM APPROACH

**FFTと連続ウェーブレット変換法を用いた同期位相計測に基づく電力システムのモード検出とダンピング推定**

KHAIRUDIN

DEPARTMENT OF ELECTRICAL AND ELECTRONIC ENGINEERING

GRADUATE SCHOOL OF ENGINEERING

KYUSHU INSTITUTE OF TECHNOLOGY

**March 2016**

# SYNCHROPHASOR MEASUREMENT BASED MODE DETECTION AND DAMPING ESTIMATION IN POWER SYSTEM USING FFT - CONTINUOUS WAVELET TRANSFORM APPROACH

FFTと連続ウェーブレット変換法を用いた同期位相計測に基づく電力システムのモード検出とダンピング推定

by

**KHAIRUDIN**

(Student ID: 12589505)

**Supervisor: Prof Yasunori MITANI**

**Thesis**

Submitted to the Graduate School of Engineering

Kyushu Institute of Technology

in Fulfillment of the Requirements for the Degree of

**Philosophy Doctoral Degree (Ph.D.) in Electrical Engineering**

In the

DEPARTMENT OF ELECTRICAL AND ELECTRONIC ENGINEERING

GRADUATE SCHOOL OF ENGINEERING

**KYUSHU INSTITUTE OF TECHNOLOGY**

**March 2016**

# Dedication

I dedicate this thesis to my late father Hasan Basri and late mother Aisyah, whom always accompanied me with their prayer while they were alive. May Allah enlarges their graves, forgives their entire mistakes, bestows on them His Mercy and grants them to the paradise. I also dedicate this thesis to my beloved family; my wife Mardiana, my daughter Rahma, my sons Naufal, Iqbal, Hamzah, Al-Faruq and Luthfi for all their sacrifices and understanding for this "old man goes to school".

# Acknowledgements

doing a great effort for my sons Naufal's and Iqbal's during their preparation and admittance process to their Senior High School.

Last but not the least, I would like to express my appreciation to the Directorate General of Higher Education, Research and Higher Education Ministry of republic of Indonesia that allowed me to undertake the Ph.D. program in Kyushu Institute of Technology.

# Abstract

## SYNCHROPHASOR MEASUREMENT BASED MODE DETECTION AND DAMPING ESTIMATION IN POWER SYSTEM USING FFT - CONTINUOUS WAVELET TRANSFORM APPROACH

KHAIRUDIN

Kyushu Institute of Technology, 2016


Supervisor: Prof. Yasunori Mitani

The thesis carries out the estimation of damping as well as the frequency mode of inter area oscillations in the range of 0.1 to 1.0 Hz. This belongs under the topic of angle stability management of power systems. Previously some other studies had been conducted in this area at which most of them employed the methods such as the least squares, Yule-Walker, autoregressive (AR), autoregressive moving average (ARMA), the Kalman filter and the subspace method. Another research also had been conducted which based on Fast Fourier Transform (FFT) analysis individually, the damping ratio and frequency oscillation were estimated from eigenvalue of the matrix associated to a Single Machine Infinite Bus (SMIB) model. An output-only-based simplified oscillation model was developed to estimate the characteristic of inter-area power oscillation based on extracted oscillation data. However, this previous method did not explain how to calculate damping ratio without considering any simplified model.

Furthermore, the behavior of the signal during certain time of analysis could not be described.

This thesis promotes a novel approach in analyzing PMU data based on Fast Fourier Transform (FFT) and Continuous Wavelet Transform (CWT) algorithm. Then proceed by demodulating the slicing signal at a particular peak and ridge of the signal using a decrement technique. The approach applied in this thesis can be classified into the non-parametric approach, where it works directly on the data. The damping calculation method in this thesis emphasized on the accurate and robust damping estimations which was proved by attempting the simulation towards various level of signal to noise ratio (SNR).

To verify the outcome of this method a synthesized signal contains of three ringdown modes representing a real signal from PMU was analyzed. The results were compared to the given parameters and it was clearly shown that this method gave the result within an acceptable range of error. Additionally, the acceptability of this method was also verified by comparing to the result of eigenvalue-based calculation on a standard power system model. The simulation indicated the results of the two approaches fitted each other means this FFT-CWT is workable to assess the damping ratio of a small signal oscillation in power system. The advantage of this method is no prior data of the system required; hence this approach is very applicable in the power system where gathering data from the network is not attainable.

This thesis also elaborated the application of wide area signal recorded by PMU, refined by the FFT-CWT method, for controlling the oscillation damping of power system. The simulation showed the application of wide area signal as an input to the damping controller has a great prospective to countermeasure the inter area oscillation in the system.

# Table of Contents

# List of Tables

# List of Figures

# Chapter 1.

# INTRODUCTION

## 1.1.    MOTIVATION

The important issue in modern power system operation is the system stability. It has been acknowledged as a main problem for secure system operation since the1920s. Many blackouts ever happened in history is the proof of this phenomenon [1], [2].

The unceasing growth in demand, generations and interconnections and the using of new technologies and controls has lead to a high stress in power system operation. This situation forces the power systems to evolve time by time and precede to the emergence of new instability such as voltage stability, frequency stability and inter-area oscillations which becoming greater concerns than in the past.

Conventionally, the stability of a power system is elaborated based on some extensive simulations studies, which might be able to be done for a limited set of operating conditions only. These kinds of studies require a comprehensive simulation model that could reflect the behavior of the real power system in a precise way. Yet, in practice, there are many factors may initiate differences between the dynamic behavior of the simulated model and the real power system.

Moreover, in such circumstance, it is not easy to obtain the system parameters due to missing or improper data, which may cause discrepancies between the simulated and the real dynamic behavior of the power system. In the real operation, components are added and reordered but in the simulation model it might remain un-updated. This situation challenges to the author to elaborate an approach to dealing with power system stability especially the dynamic stability of power system without involving the real data of the system.

Taking advantage of some digital signal processing technology and the uses of synchrophasor measurement system, the power system – small signal – stability is dealt with. Damping ratio and frequency mode are the main keyword in assessing the power system small signal stability. This thesis promotes an easy and direct way of analyzing and monitoring the power system dynamic stability based on the Phasor Measurement Unit (PMU) data using the combination of the well-known Fast Fourier Transform (FFT) and the Continuous Wavelet Transform (CWT).

In addition, the information of frequency mode and the phase angle differences from the PMUs can be exploited as a global signal input to increase the system stability through a wide area damping controller strategy.

## 1.2. BACKGROUND

In last two decades, the interconnection of power systems grows wider and more complex due to increase in power demands and supplies, deregulation of electricity markets, growth in distributed generations and in some countries, the ageing of substations apparatus such as Transformer, Breaker, etc. which were built more than 40 years ago, could lead the system to critical condition.

Under this circumstance, any failure in the planning, operation, protection and control of any part of the entire power system could evolve into the cause of cascading events that may eventually lead to a large area power blackout. Several recently happened major widespread blackouts as follows:

- Java and Bali, Indonesia on August 18th 2005, recovered after 11 hrs. Affected 100 million people.

- Germany, France, Italy, And Spain on November 4th 2006, affected 10-15 million people.

- Changzhou, China on January 24th - February 2008 for 2 weeks. Affected 4.6 million people.

- Brazil and Paraguay on November 10th -11th, 2009 for 2 days.

- India on July 30th-31st, 2012 for several hrs. Affected 670 mill people.

This situation needs a big concern from the stakeholders including researchers in universities in the development of power system stability monitoring and controls. Although some studies have been conducted in this area, still some problem remains unsolved; such as the need of clear depiction of the system behavior under certain condition, a free modeling based stability analysis and a direct and simple assessment tool for the damping calculation and mode identification.

## 1.3. PREVIOUS WORK

Damping estimation of a power system has been a topic of great interest recently. Many publications have been attempted to deal with this issue such as in [3], [4], [5], [6], [7], [8], [9], [10], [11], [12], [13], [14], [15] and many more. In these works, various unique procedures for damping estimation of the power system have been presented. Yet, the approaches presented in all of those papers

are diverse from the method in this thesis. None of the methods was based on the combination of fast Fourier Transform and Continuous Wavelet Transform (FFT-CWT) approach. Most of them employed the methods such as the least squares, regularized robust recursive least squares, Yule-Walker with autoregressive (AR) and autoregressive moving average (ARMA) model, the Kalman filter model and the subspace method. Those approaches belong to parametric class, which assume a certain model and fit the parameters of the model to minimize the difference between the model output and the system output. The main disadvantage of the parametric approaches is that the requirement of the assumption of the model structure [16]. Incorrect assumption of the model structure and/or order might lead to incorrect damping estimates.

The approach applied in this thesis can be classified to the non-parametric approach, where it works directly on the data. Emphasize of the approach in this thesis is on the accuracy and robustness of the calculation. The only disadvantage of this method is the difficulty of parameters tuning, nevertheless compared to the parametric methods, the tuning process of the nonparametric methods as elaborated in this thesis is less intricate.

Traditionally, power system small signal stability is done based on model analysis. Here, "model" actually means a set of mathematic equations which are derived to describe the dynamic of generators and their associated control devices like exciter and automation voltage regulator (AVR), the dynamic of other control devices like power system stabilizer (PSS), as well as the interaction between generators and power network and loads. In order to construct such a mathematic model for either a simple system or a large interconnected system, all information about the studied system (i.e. grid topology, component parameters, loads profile and control settings, etc.) must be collected prior to starting any analysis.

4

Obviously, it is a tedious process, especially for a relatively large system to be analyzed. This is first disadvantage of traditional model-based small-signal stability analysis.

Generally, part of these model equations is a group of nonlinear differential equations and the remaining part is a group of nonlinear algebraic equations, since the physical nature of these dynamics is nonlinear. Therefore, the entire system model is finally constructed in the following form:

$$\dot{x} = f(x, u, t)$$
$$y = g(x, u, t) \tag{1}$$

where *x, y, u* and *t* are the state vector, output vector, input vector and time vector respectively. *f(..)* and *g(..)* represent the differential functions and algebraic functions respectively. If the system is autonomous, time *t* can be eliminated from above equations.

With all necessary information known, the next step is to specify multiple normal operating conditions and linearize the system model for each normal operating condition to obtain a linearized system small-signal model. Hence, each small-signal model just corresponds to a specific normal operating condition. Because of each normal operating condition differs in the generation and load setting, the final analysis result of every small-signal model is also just applicable to the corresponding operating condition. One has to repeat the same analysis process when the operating condition changes. This is second disadvantage of model-based traditional small-signal stability analysis.

The linearized system small-signal model is usually in the state-space form as follows:

$$\Delta\dot{x} = A\Delta x + B\Delta u$$
$$\Delta y = C\Delta x + D\Delta u \tag{2}$$

where **A, B, C** and **D** are the state matrix, input matrix, output matrix and feed-forward matrix respectively.

Then all subsequent analysis focuses on the state matrix of the linearized model. From the stability analysis principle of a dynamic system, it is known that the eigenvalues of the state matrix **A** have close relation with the characteristic of the small-signal stability under the considered operating condition. In particular, a real eigenvalue corresponds to a non-oscillatory mode while a negative real eigenvalue represents a decaying mode [17]. The larger its magnitude means the faster the decay. A positive real eigenvalue represents non-periodic instability.

Complex eigenvalues occur in conjugate pairs, and each pair corresponds to an oscillatory mode. The real part of the eigenvalues gives the damping, and the imaginary part gives the frequency of oscillation. A negative real part represents a damped oscillation whereas a positive real part represents oscillation of increasing amplitude [18]. That is to say, for a given pair of complex eigenvalues:

$$\lambda = \sigma \pm j\omega \tag{3}$$

The frequency of oscillation in Hz, i.e. the actual or damped frequency, is:

$$f = \frac{\omega}{2\pi} \tag{4}$$

The damping ratio, which determines the rate of decay of the amplitude of the oscillation, is given by:

$$\xi = \frac{\sigma}{\sqrt{\sigma^2 + \omega^2}} \tag{5}$$

For a large power system, the dimension of state matrix of its linearized small-signal model is usually very high, for example, up to several hundred, which is a very serious problem when the eigenvalues are computed. This can be said as third inconvenience of model-based traditional small-signal stability

6

analysis. On the other hand, however, by observing the eigenvalues, it is easy to identify all modes in the system simultaneously: stable and unstable, non-oscillatory or oscillatory, as well as the associated mode parameters. This is the merit of model-based traditional small-signal stability analysis.

Further analysis can be performed based on the computed eigenvalues to get more insight into each identified mode, especially for those oscillatory modes, such as mode shape and mode participation.

Surely, all model-based analysis is generally performed by utilizing a set of computer programs, which can easily memory system parameters, carry on repetitive computation for different operating conditions, save computation time and improve computation accuracy. However, the inconveniences of using these programs still exist. Moreover, one of the most obvious problems is that the operator found it is very difficult to match a model-based analysis result to a scenario of real power system because the real power system is always in the changing operating conditions. In one word, the model-based analysis method cannot reflect the real dynamic and its characteristic of a practical power system.

Several analysis techniques for digital signal processing and system identification can be applied to realize measurement-based approach to estimate the low-frequency oscillation. Among these techniques, Prony method and a family of autoregressive (AR) methods have been most often used in many previous publications.

Prony method is a signal processing technique for extracting the sinusoid or exponential signals from a uniformly sampled signal by solving a set of linear equations for the coefficients of the recurrence equation that the signals satisfy. It extends Fourier analysis by directly estimating the frequency, damping, strength, and relative phase of modal components presenting in a given signal. Therefore,

Prony method belongs to the type of parametric analysis, which is defined as any tool that estimates the modal (Eigen) properties of oscillation modes based upon finite measurements of output signals.

The Prony analysis directly estimates the parameters of the Eigen-properties by fitting a sum of complex damped sinusoids to evenly spaced sample (in time) values of the output as [19]:

$$\hat{y}(t) = \sum_{i=1}^{L} A_i e^{(\sigma_i t)} \cos(2\pi f_i t + \phi_i)$$

(6)

where $A_i$, $\sigma_i$, $\phi_i$ , and $f_i$ are the amplitude, damping coefficient, phase and frequency of component respectively; $L$ is the total number of damped exponential components; $\hat{y}(t)$ is the estimate of the perceived data for $y(t)$ consisting of $N$ samples $y(t) = y[k],k=0,1,2,3,…,N-1$ that are evenly spaced.

The family of Auto Regressive (AR) methods is also a type of parametric mode-estimation approach, though it differs from Prony method. It is more applicable to the estimation of modal properties using measurements under normal operating conditions with constant small load changes. The key point of Prony method is that it assumes the analyzed signal is the sum of multiple complex-exponential. From this point, this is actually a priori determination of signal model, which can simplify the estimation. However, on the other hand, this point also limits the applicability of Prony method only to specific such as ringdown signals. In other words, applying Prony method to the signal with small signal-to-noise ratio would fail to produce satisfactory estimation results due to no obvious sign of complex exponential components. In this situation, a general linear model of signal without any component assumption has to be considered [20].

For the family of AR methods, as illustrated in Figure-1, the power system response output can be regarded as the result of an approximately stationary white noise input, i.e. constantly varying loads, in the frequency band of interest over an analysis window. From this angle, the characteristic of the studied power system can be represented by a discrete transfer function as in Figure-1:

Input Noise $\longrightarrow$ $\boxed{G(z) = \dfrac{B(z)}{A(z)}}$ $\longrightarrow$ Output
$u(t)$ $y(t)$
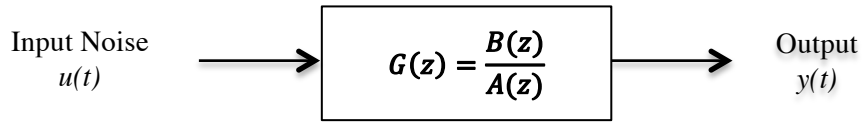
Figure-1. The linier model of power system

The denominator polynomial in model (7) is the characteristic polynomial of transfer function $G(z)$ in Figure-1. The roots of characteristic polynomial are the system poles that describe the system Eigen-properties of oscillation modes. Hence, as long as the coefficients $a_1$, $a_2$,..., $a_p$ of the characteristic polynomial $A(z)$ can be estimated, then the polynomial is rooted and the system poles can be found as the dominant roots in the frequency band of interest. This is the fundamental theory of AR-family models can be used for power system small-signal analysis. Various algorithms have been proposed to calculate the coefficients $a_1$, $a_2$,..., $a_p$ of the characteristic polynomial $A(z)$ from either time-domain or frequency-domain.

$$y(t) = \frac{1}{\left(1 + a_1 z^{-1} + a_2 z^{-2} + \cdots + a_p z^{-p}\right)} u(t) \qquad (7)$$

Another way of estimating the damping apart from Prony and AR method as describe above is using the subspace method combining with the Fast Fourier Transform (FFT). The power system model in Figure-1 can be represented using a state space model as follows:

9

$$\begin{bmatrix} x(k+1) \\ y(k) \end{bmatrix} = \begin{bmatrix} A & K \\ C & 0 \end{bmatrix} \begin{bmatrix} x(k) \\ u(k) \end{bmatrix} \qquad (8)$$

where $A$ is the state matrix whose eigenvalues describe the characteristic of the small signal stability. Similarly, the eigenvalues can be readily calculated from the state matrix $A$ that can be obtained from the measured data of system responses.
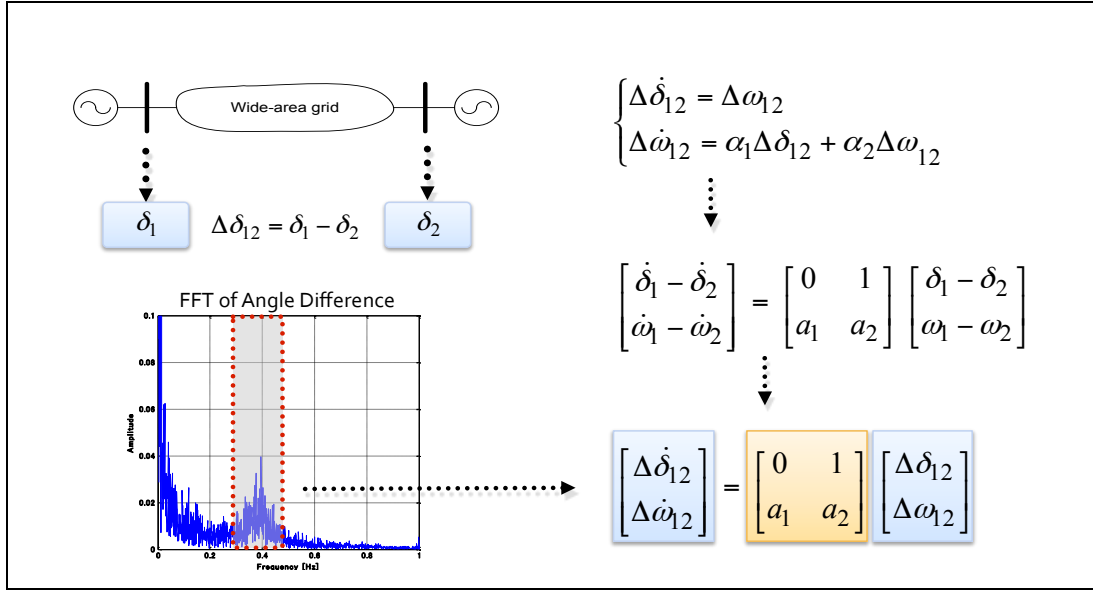


Figure-2. Subspace method using FFT and SMIB model [20]

The later scheme, which recently done in the same laboratory of the author of this thesis, only focuses on the estimation of single dominant inter-area oscillation mode through the following steps: estimating the center frequency of single mode of interest, extracting the oscillation data from original phasor measurements, analyzing the oscillation shape, identifying the oscillation model, and estimating the oscillation parameters. However, this kind of approach still needs to associate to the state space model, which is derived from Single Machine Infinite Bus (SMIB) model, and treated them as if they represent the real system under analysis. The following Figure-2 illustrates the procedure of calculation of this method.

Hilbert Huang Transform analysis also has been attempted to deal with PMU data. However, the ability of this approach to estimate damping ratio and modal parameters cannot satisfactorily distinguish two separate modes unless there is a large difference in either frequency or damping ratio [9], [21].

The Hilbert transform is a linear operator which takes a function, *u(t)*, and produces a function, H(u)*(t)*, with the same domain. The Hilbert Huang Transform (HHT) is the transform advancement of Hilbert transforms which is initiated by prof. Huang et al. on 1996 using the Intrinsic Mode Functions (IMF) and Hilbert Space Analysis (HSA). Recently, this method is very famous especially for analyzing the non-stationary and non-linier data.

One of the differences from the proposed approach in this thesis is that in this thesis no model or parameters are required in its calculation process. All the calculation is based on the signal input from the synchrophasor measurement system.

## 1.4. OBJECTIVES

The objective of this research is to develop a new synchrophasor measurement based method for identifying low frequency inter-area oscillation mode and damping estimation in power system. The damping information will be useful to admit the power system operators driving their system to the maximum capability while keep preserving its security level.

In addition, applying wide area signal for power system control to enable the maximum power transfer and to keep the system remains stable when an inter-area oscillation occurred is included.

## 1.5. SCOPE OF THE RESEARCH

The thesis carries out the estimation of damping as well as the frequency mode of inter area oscillations in the range of 0.1 to 1.0 Hz. This belongs under the topic of angle stability management of power systems and the study case is the Japan Campus Wide Area Monitoring System (Campus-WAMS). The assessment of damping and frequency are computed based on synchrophasor measurement signals come from PMU measurements, simulated signals and power system model.
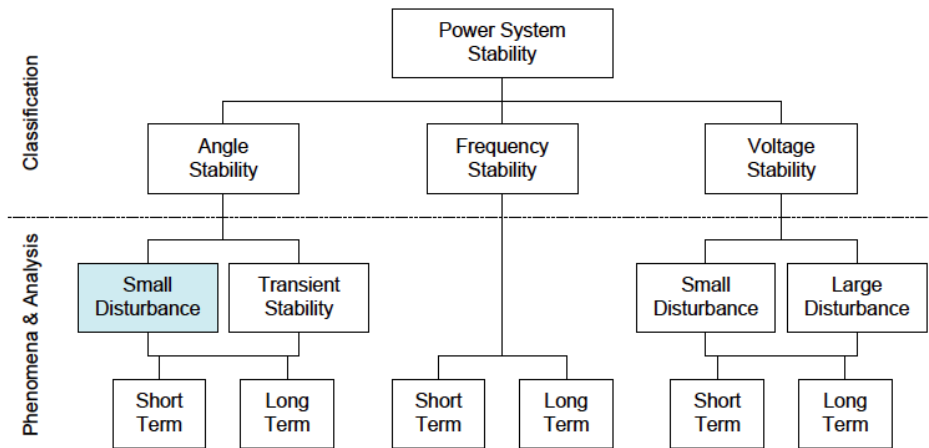


Figure-3. Power system stability classification [2]

The small-signal (also referred to small-disturbance or oscillatory) rotor angle stability is associated with the ability of generators to maintain synchronism after small disturbances, with "small" meaning that the perturbations should be of a magnitude such that the phenomenon can be studied through a linearization of system model equations. This problem is usually associated with the appearance of low-damped or un-damped oscillations in the system due to lack of sufficient damping torque [1], [17], [22], [23], [24]. Figure-3 describes the classification of power system stability problem.

In detail the scope of this research are processing the signal from PMU for the need of power system stability monitoring and applying the wide area signal for power system stability control. Figure-4 illustrates this research scope in the form of block diagram.
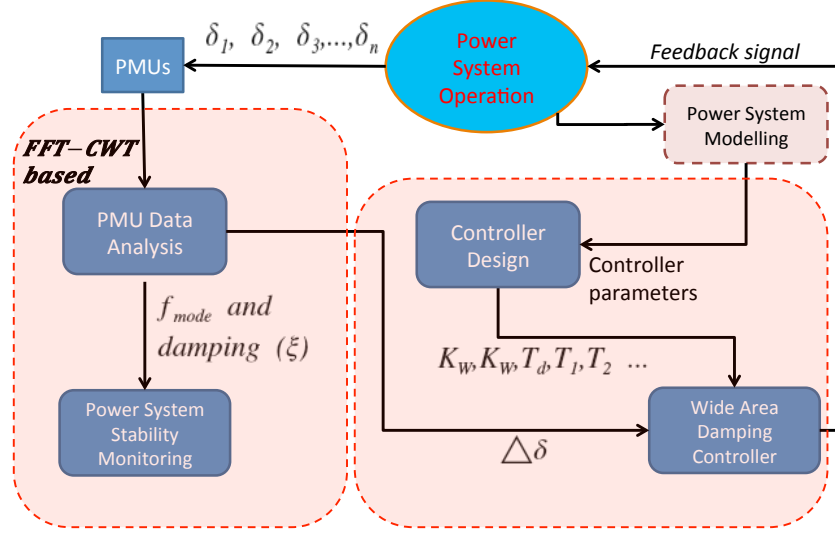


Figure-4. Research scope

## 1.6. THESIS CONTRIBUTION

The main scientific contribution of this thesis is a novel approach in estimating the damping and identifying the frequency mode of the power system inter area oscillation. The process is based on applying the Fast Fourier Transform and The Continuous Wavelet Transform. The mode identification is based on the Fast Fourier Transform only and the damping estimation is based on the hybrid combination of the Fast Fourier Transform and the Continuous Wavelet Transform. A logarithmic decrement technique is also utilized for the de-modulation of wavelet modulus envelop in final step of damping calculation.

In summary, this thesis contributes in the forms of:

- Promoting a novel approach in power system stability analysis, with no parameters and no modeling of power system are required in its calculation process.

- Presenting the time and frequency localization simultaneously and identifying multi-modes of frequency oscillation in the system.

- The combination of the Fast Fourier Transform and Continuous Wavelet Transform produces an easy and simple technique of identification of modes in power system and calculation of its damping ratio.

- Propose a combination of conventional damping controller and a wide area signal based damping controller in power system.

## 1.7. OUTLINE OF THE THESIS

This thesis is managed in 6 chapters resumed as follows;

**Chapter 1**. The research background, previous approach and literature research concerning the inter area oscillation and damping estimation are reviewed. On the previous researches, which were only based on FFT analysis, the damping ratio and frequency oscillation were estimated from eigenvalue of the matrix associated to a Single Machine Infinite Bus (SMIB) model. However, this previous method was unsuccessful to explain how to calculate damping ratio without considering any simplified model, especially when the system under studied cannot be modeled as a SMIB. HHT analysis also has been attempted to deal with PMU data. However, the ability of this approach to estimate damping ratio and modal parameters cannot satisfactorily distinguish two separate modes unless there is a large difference in either frequency or damping ratio.

**Chapter 2**. The concept of synchrophasor measurement system and the Phasor Measurement Unit (PMU) are explored in this chapter. The application of

FFT and Continuous Wavelet Transform in PMU signal analysis as well as the reason why the CWT is used as the tools is discussed in detail. Mode detection and Damping Estimation procedure using Complex Morlet as a mother function of wavelet and the background of the selection this function among others such as Gabor, Symlet or Mexican Hat is discussed here. Finally, the review of other method in dealing with PMU signal, i.e. Prony Analysis and eigenvalue Based are described. The tuning of wavelet parameters, i.e. Center of Frequency and Bandwidth parameters is very important to the performance of calculation. The application of Genetic Algorithm to optimize the parameters selection is explored in this chapter.

**Chapter 3**. Chapter 3 promotes a new approach in analyzing PMU data to identify Low Frequency Inter-area Oscillation (LFIO) mode and to calculate damping ratio based on the CWT. The capability of CWT to construct the 3D representation simultaneously, i.e. time, frequency and modulus of a signal offering time and frequency localization becomes the main reason of applying this method for the PMU Signal analysis. In this chapter, the PMU signal is transformed to time-frequency-modulus and plotted in three-dimension sketch so that it is easy to investigate any oscillation mode in the system. Complex Morlet is selected as a mother wavelet function considering its performance in dealing with ringdown type signal compared to the other wavelet function.

**Chapter 4**. By combining the advantageous of the Fast Fourier Transform (FFT) and the Complex Morlet Function of the Continuous Wavelet Transform (CWT), some simulated signals representing PMU data and a Two Area Four Machine System model are examined. The calculation results of FFT-CWT approach are compared to the eigenvalue based method result for convincing the acceptability of the proposed method. Some sets of PMU data from Japan Campus

WAMS at some disturbances are also evaluated using this method as a practical attempt.

**Chapter 5** is the application to the control system. This chapter depicts the application of wide area signal recorded by PMU, which is refined using the proposed method, for controlling the oscillation damping of power system. The gains of the wide area controller are determined by solving Linear Matrix Inequalities (LMI). Kundur's two-area four-machine system is used to investigate the performance of the wide area damping control. In this chapter the small signal stability analysis, modal analysis, and phase plane analysis have been studied to analyze the damping ratio enhancement using direct load control. The simulation shows direct load control with PMU measurement as an input has a great prospective to countermeasure the oscillation in the system.

The thesis is concluded in **Chapter 6**. The FFT-CWT approach is very promising for the identifying inter area oscillation mode in the system as well as estimating the damping ratio based on the information extracted from the PMU data without knowing the parameters of the system. The validity of this method was verified by comparing the result to the eigenvalue-based calculation. It was demonstrated that the results of the two approaches confirmed each other, means that this FFT-CWT is feasible enough to estimate the damping ratio of a small signal oscillation in a power system.

The advantageous of this study are: it requires no system parameters in the calculation process, the ability of time-frequency localization simultaneously and the ability of identifying multi-modes oscillation in power system. In addition, FFT has been efficiently utilized to determine the center of the oscillation as one of the wavelet parameters.

# Chapter 2.

# SYNCHROPHASOR MEASUREMENT AND THE METHOD OF ANALYSIS

## 2.1. POWER SYSTEM OSCILLATION

Power system electromechanical oscillation is an inherent property of an AC transmission system. The oscillations cannot be eliminated altogether, however, in some particular power systems (e.g. with short lines) they do not cause any problems due to a high damping system. Under certain operating conditions, the oscillations set the limits for power transfer capacity and may pose a serious threat to system stability [25].

There are different types of electromechanical oscillations and they can be classified by their interaction characteristics: inter-area mode oscillations, local plant mode oscillations, intra-plant mode oscillations, torsional (sub synchronous) mode oscillations, and control mode oscillations. In this thesis, only the inter-area mode oscillations are considered.

Inter-area oscillation is a complex and non-linear phenomenon and its damping characteristic is dictated by the strength of the transmission path, the nature of the loads, the power flow through the interconnection, and the interaction of loads with the dynamics of generators and their associated controls

[26]. Typically the oscillations in power system are stable however when the system experiences too much stress, the Hopf bifurcation may occur then the real parts of a complex conjugate eigenvalue pair cross the imaginary axis and the system becomes unstable.

A weak transmission path means high effective impedance between the oscillating generator groups. The high impedance causes the amortisseur windings of the generators to lose their effect on the inter-area oscillation damping. In addition, the adverse interactions among the automatic controls, especially the automatic voltage regulators (AVRs), decrease inter-area oscillation damping. Even without the adverse effects among the automatic controls, the uncontrolled system's damping for inter-area oscillations is commonly poor when the transmission path is weak. Additionally, when the loading of the interconnecting lines grow, the damping decreases, mainly because the angle difference between the oscillating generator groups grow and thus the voltage oscillations at the generator terminals grow, causing the AVRs to act and produce negative damping [26].

The analysis and monitoring of power system oscillations can be accomplished by means of several methodological approaches. Each approach has its own advantages and feasible applications, providing a different view of the system dynamic behavior. Eigenvalue analysis technique is based on the linearization of the nonlinear equations that represent the power system around an operating point that is the result of electromechanical modal characteristics: frequency, damping and shape. Direct spectral analysis of power response signals use the Fourier Transforms or Short Time Fourier Transform (STFT), Prony or Wavelet analysis technique or any combination among those method [27].

## 2.2. SMALL SIGNAL STABILITY AND DAMPING ESTIMATION METHOD

### 2.2.1. MODAL ANALYSIS

Small signal stability analysis of practical power systems involves the simultaneous solution of equations representing the following [28]:

- Synchronous machines, excitation systems and prime movers.

- Interconnecting transmission network.

- Static and dynamic (motor) loads, and

- Other additional devices such, as HVDC converters, static VAR compensators, etc.

Low frequency electromechanical oscillations range from less than 1 Hz to 3 Hz in it is different from those with sub-synchronous resonance. Multi-machine power system dynamic behavior in this frequency range is usually expressed as a set of non-linear differential and algebraic equations. The algebraic equations result from the network power balance and generator stator current equations. The high frequency network and stator transients are usually ignored when the analysis is focused on low frequency electromechanical oscillations [2].

The initial operating state of the algebraic variables such as bus voltages and angles are obtained through a standard power flow solution. The initial values of the dynamic variables are obtained by solving the differential equations through simple substitution of algebraic variables into the set of differential equations. The set of differential and algebraic equations is then linearized around the equilibrium point and a set of linear differential and algebraic equations is obtained [23].

### 2.2.2. FAST FOURIER TRANSFORM

The Fourier Transform decomposes a signal function in time domain into the frequency domain. The Fourier transform as a function of time itself is a complex-valued function of frequency, whose absolute value represents the amount of that frequency present in the original function, and whose complex argument is the phase offset of the basic sinusoid in that frequency. The Fourier transform is called the frequency domain representation of the original signal. The term Fourier Transform refers to both the frequency domain representation and the mathematical operation that associates the frequency domain representation to a function of time [29].

Fourier Transforms are widely used for many applications in engineering, science, and mathematics. The basic ideas were popularized in 1965, but some algorithms had been derived as early as 1805 [30]. Fourier Transform converts a signal from its original domain (often time or space) to a representation in the frequency domain and vice versa.

Discrete Fourier Transform (DFT) is obtained by decomposing a sequence of values into components of different frequencies and a Fast Fourier Transform (FFT) is a way to compute the same result more quickly.

Suppose that $T$ is large enough so that the interval $[-T/2, T/2]$ contains the interval on which f is not identically zero. Then the $n^{\text{th}}$ series coefficient $c_n$ is given by:

$$c_n = \frac{1}{T} \int_{-T/2}^{T/2} f(x)e^{-j2\pi\left(\frac{n}{T}\right)x}dx \tag{9}$$

Under appropriate conditions, the Fourier series of $f$ can be written:

$$f(x) = \sum_{-\infty}^{\infty} c_n \, e^{-j2\pi\left(\frac{n}{T}\right)x} = \sum_{-\infty}^{\infty} \hat{f}(\zeta_n) \, e^{-j2\pi\zeta_n x} \, \Delta\zeta \tag{10}$$

This second sum is a *Riemann sum*, and so by letting $T \to \infty$ it will converge to the integral for the inverse Fourier Transform. Figure-5 and Figure-6 provide a visual illustration of how the Fourier Transform measures whether a frequency is present in a particular function.
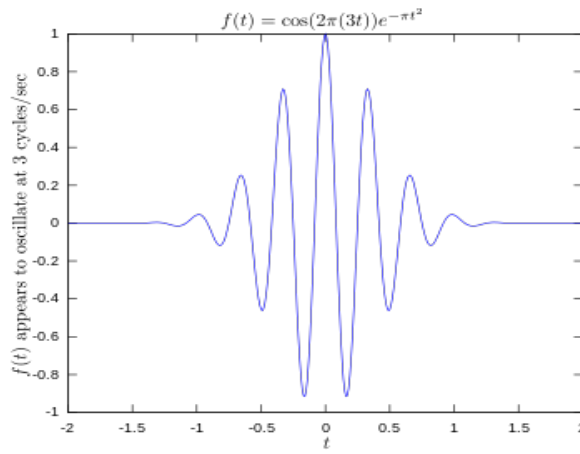


Figure-5. Signal in cosine function
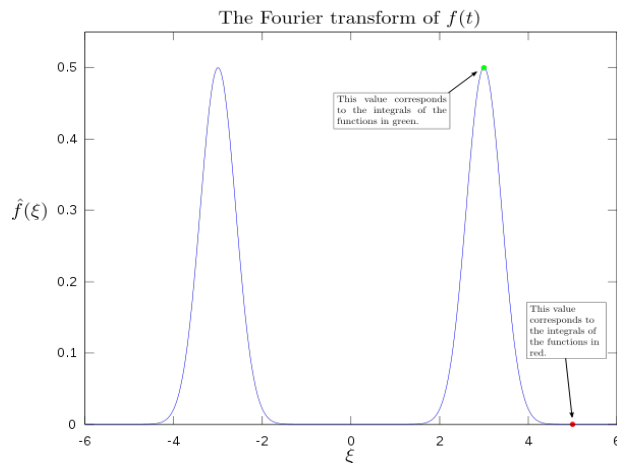


Figure-6. Fourier transform of *f(t)*

### 2.2.3. CONTINUOUS WAVELET TRANSFORM

Wavelet analysis is a relatively new signal-processing tool and is applied recently by many researchers in power systems due to its strong capability of time and frequency domain analysis [31], [10], [9], [11], [12]. The Wavelet transform is a mathematical tool, like the Fourier transform for signal analysis.

In mathematics, a continuous wavelet transform (CWT) is used to divide a continuous-time function into wavelets. The CWT possesses the ability to construct a time-frequency representation of a signal simultaneously that offers very good time and frequency localization.

In definition, the continuous wavelet transform is a convolution of the input data sequence with a set of functions generated by the mother wavelet. The convolution can be computed by using the FFT. Normally, the output $X_w(a,b)$ is a real valued function except when the mother wavelet is complex. A complex mother wavelet will convert the continuous wavelet transform to a complex valued function. The power spectrum of the continuous wavelet transform can be represented by $|X_w(a,b)|^2$.

Wavelet Transform can be applied to the following scientific research areas: edge and corner detection, partial differential equation solving, transient detection, filter design, electrocardiogram (ECG) analysis, texture analysis, business information analysis and gait analysis. Continuous Wavelet Transform (CWT) is very efficient in determining the damping ratio of oscillating signals (e.g. identification of damping in dynamical systems). CWT is also very resistant to the noise in the signal [31].

There are some wavelet families typically used in signal analysis. They are Gabor, Symlet-wavelet, Mexican hat and the Complex Morlet wavelet that is used

in this study. The choice of wavelet is dictated by the signal or image characteristics and the nature of the application.

Gabor wavelets are wavelets invented by Dennis Gabor using complex functions constructed to serve as a basis for Fourier transforms in information theory applications. The important property of the wavelet is that it minimizes the product of its standard deviations in the time and frequency domain. Put another way, the uncertainty in information carried by this wavelet is minimized. However, they have the downside of being non-orthogonal, so efficient decomposition into the basis is difficult. Since their inception, various applications have appeared, from image processing to analyzing neurons in the human visual system.

In applied mathematics, Symlets-wavelets are a family of wavelets. They are a modified version of Daubechies wavelets that increased the symmetrical function of wavelet. Symlets is short of symmetrical wavelet. The Symlets are more symmetric than the external phase wavelets. This kind of wavelet family is suitable for the image reconstruction and filter.

Mexican hat is usually only referred to as the Mexican hat wavelet in the Americas due to taking the shape of a *sombrero* when used as a 2D image processing kernel. The multidimensional generalization of this wavelet is called the Laplacian of Gaussian function. In practice, this wavelet is sometimes approximated by the difference of Gaussians function, because it is separable and can therefore save considerable computation time in two or more dimensions. It is frequently used as a blob detector and for automatic scale selection in computer vision applications.

The complex Morlet wavelet is a wavelet composed of a complex exponential multiplied by a Gaussian window (envelope). This is the complex

version of Gabor wavelet as mentioned above. The Morlet wavelet transform method presented offers an intuitive bridge between frequency and time information and suitable for the decay analysis. This reason makes the author take this kind of wavelet function for the ringdown type signal analysis.

### 2.2.4. PRONY ANALYSIS

Prony analysis is a signal processing method that extends Fourier analysis. It is a technique of analyzing signals to determine model, damping, phase, frequency and magnitude information contain within the signal. Prony method is a technique for sample data modeling as a linear combination of exponentials. It has a close relationship to the least squares linear prediction algorithm used for AR (Autoregressive) and ARMA (Autoregressive moving average) parameter estimation. Prony analysis is a method of fitting a linear combination of exponential terms to a signal. Each term in (13) has four elements: the magnitude $A_n$, the damping factor $\sigma_n$, the frequency $f_n$, and the phase angle $\theta_n$. Each exponential component with a different frequency is viewed as a unique mode of the original signal $y(t)$. The four elements of each mode can be identified from the state space representation of an equally sampled data record. The time interval between each sample is $T$ [28]:

$$y(t) = \sum_{n=1}^{N} A_n \ e^{\sigma_n t} cos \ (2\pi f_n t + \theta_n) \tag{11}$$

Using Euler's theorem and letting $t = MT$, the samples of $y(t)$ are:

$$y_M = \sum_{n=1}^{N} B_n \lambda_n^M \tag{12}$$

$$B_n = \frac{A_n}{2} e^{j\theta_n} \tag{13}$$

24

$$\lambda_n = e^{(\sigma_n + j2\pi f_n)T} \tag{14}$$

Prony analysis consists of three steps. In the first step, the coefficients of a linear predication model are calculated. The linear prediction model (LPM) of order *N*, shown in (15), is built to fit the equally sampled data record *y(t)* with length *M*. Normally, the length M should be at least three times larger than the order *N*.

$$y_M = a_1 y_{M-1} + a_2 y_{M-2} + \cdots + a_N y_{M-N} \tag{15}$$

Estimation of the LPM coefficients $a_n$ is crucial for the derivation of the frequency, damping, magnitude, and phase angle of a signal. To estimate these coefficients accurately, many algorithms can be used. A matrix representation of the signal at various sample times can be formed by sequentially writing the linear prediction of $y_M$ repetitively.

In the second step, the roots $\lambda_n$ of the characteristic polynomial shown as (16) associated with the LPM from the first step are derived. The damping factor $\sigma_n$ and frequency $f_n$ are calculated from the root $\lambda_n$ according to (14).

$$\begin{aligned} \lambda^N - a_1 \lambda^{N-1} &- \cdots - a_{N-1} \lambda^{-a_N} \\ &= (\lambda - \lambda_1)(\lambda - \lambda_2) \dots (\lambda - \lambda_n) \dots (\lambda - \lambda_N) \end{aligned} \tag{16}$$

In the last step, the magnitudes and the phase angles of the signal are solved in the least square sense. Based on (12), equation (17) is built using the solved roots $\lambda_n$.

$$Y = \begin{bmatrix} 1 & 1 & \dots & 1 \\ \lambda_1 & \lambda_2 & \dots & \lambda_N \\ \vdots & \vdots & \vdots & \vdots \\ \lambda_1^{M-1} & \lambda_2^{M-1} & \dots & \lambda_N^{M-1} \end{bmatrix} [B_1 \quad B_2 \quad \dots \quad B_N]^T \tag{17}$$

Where the magnitude $A_n$ and phase angle $\theta_n$ are thus calculated from the variables $B_n$ as in equation (13).

### 2.2.5. HILBERT HUANG TRANSFORM

The Hilbert Huang Transform (HHT) was proposed by Huang et al. in period of 1996 - 2012. It is the result of the empirical mode decomposition (EMD) and the Hilbert Spectral Analysis (HSA). The HHT uses the EMD method to decompose a signal into so-called intrinsic mode functions (IMF) with a trend, and applies the HSA method to the IMFs to obtain instantaneous frequency data. Since the signal is decomposed in time domain and the length of the IMFs is the same as the original signal, HHT preserves the characteristics of the varying frequency. This is an important advantage of HHT since real-world signal usually has multiple causes happening in different time intervals. The HHT provides a new method of analyzing non-stationary and non-linier time series data.

The limitation oh this method as mentioned by Chen and Feng is that the EMD is limited in distinguishing different components in narrow-band signals. The narrow band may contain either (a) components that have adjacent frequencies or (b) components that are not adjacent in frequency but for which one of the components has much higher energy intensity than the other components [32].

### 2.3. THE GLOBAL POSITIONING SYSTEM

The Global Positioning System (GPS) was introduced in 1960 under the auspices of the U.S. Air Force. The first satellites were launched into space in 1978. The System was declared operational in April 1995. The Global Positioning System consists of 24 satellites, that circle the globe once every 12 hours, to provide worldwide position, time and velocity information. GPS makes it possible to precisely identify locations on the earth by measuring distance from the satellites. GPS allows you to record or create locations from places on the earth and help you navigate to and from those places. Originally, the system was

designed only for military purposes until the 1980's that it was made available non-military use [33].

The GPS synchronization concept is based on *time*. The satellites carry very stable atomic clocks that are synchronized to each other and to ground clocks. Any drift from true time maintained on the ground is corrected daily. Likewise, the satellite locations are monitored precisely. GPS receivers have clocks as well—however, they are not synchronized with true time, and are less stable. GPS satellites continuously transmit their current time and position. A GPS receiver monitors multiple satellites and solves equations to determine the exact position of the receiver and its deviation from true time. At a minimum, four satellites must be in view of the receiver for it to compute four unknown quantities (three position coordinates and clock deviation from satellite time).

There are many non-military applications use of the GPS in daily application such as in the field below:

- *Navigation*: for digitally precise velocity and orientation measurements.

- *Surveying*: surveyors use absolute locations to make maps and determine property boundaries.

- *Tectonics*: GPS enables direct fault motion measurement of earthquakes. Between earthquakes, GPS can be used to measure crustal motion and deformation to estimate seismic strain buildup for creating seismic hazard maps.

- *Robotics*: self-navigating and autonomous system. Autonomous Robots uses GPS sensors to calculate latitude, longitude, time, speed, and heading.

- *Phasor measurements*: GPS enables highly accurate time stamping of power system measurements, making it possible to compute phasor.

27

## 2.4.  INTRODUCTION TO SYNCHROPHASOR MEASUREMENT

Phasor are basic tools of ac circuit analysis, usually introduced as a means of representing steady state sinusoidal waveforms of fundamental power frequency. Even when a power system is not quite in a steady state, phasor are often useful in describing the behavior of the power system [2].

A phasor measurement unit (PMU) is a device that measures the electrical waves on an electricity grid using a common time stamp for the synchronization. Time synchronization allows synchronized real-time measurements of multiple remote measurement points on the grid. The resulting measurement is known as a synchrophasor. PMUs are considered as one of the most important measuring devices in the future of power systems [34], [35]. A PMU can be a dedicated device, or the PMU function can be incorporated into a protective relay or other device.

Synchronized Phasor Measurement Unit (PMU) was invented in 1988 by Dr. Arun G. Phadke and Dr. James S. Thorp at Virginia Tech. Since then, the subject of wide-area measurements in power systems using PMUs and other measuring instruments has been receiving considerable attention from researchers in the field Phasor measuring units (PMUs) using synchronization signals from the Global Positioning System (GPS) satellite system have evolved into mature tools and are now being manufactured commercially [34], [36].

Synchronized phasor (synchrophasor) provide a real-time measurement of electrical quantities from across the power system. Applications include wide-area control, system model validation, determining stability margins, maximizing stable system loading, islanding detection, system-wide disturbance recording, and visualization of dynamic system response. The basic system building blocks are GPS satellite-synchronized clocks, phasor measurement units (PMUs), a

phasor data concentrator (PDC), communication equipment, and visualization software. Figure-7 shows hardware block of the PMU.
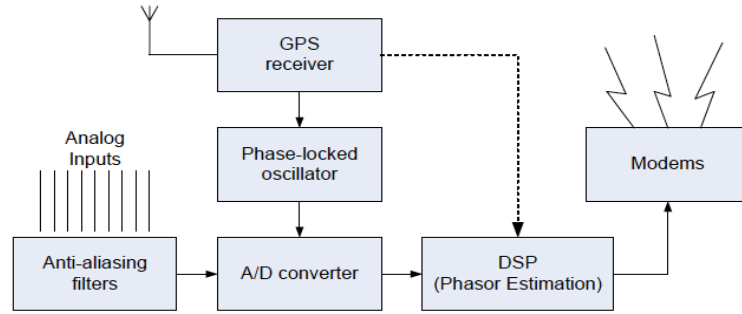


Figure-7. Hardware block of a PMU

Motivation for Synchronized Measurements: Need for High Resolution Synchronized Data [37]:

- The data from different locations are not captured at precisely the same time.

- However, V, P, and Q normally do not change abruptly, unless there is a large disturbance nearby.

- System monitoring is more critical during disturbance and transients Faster synchronized data is needed to capture the dynamics

- Fast real time control is possible only with real time situational awareness

## 2.5. PHASOR MEASUREMENT CONCEPTS

A phasor is a complex number representing the magnitude and phase angle of the sine waves found in an alternating current (AC) type of electrical system. Mathematically, it can be represented as a unique complex number known as a phasor equation.

Lets consider the sinusoidal equation below:

$$x(t) = X_m cos\left(\omega t + \phi\right) \tag{18}$$

29

where $X_m$ is magnitude of the sinusoidal waveform, $\omega$ is the instantaneous frequency $(2.\pi.f)$ and $\phi$ is an angular starting point of the waveform.

The phasor representation of this sinusoidal is given by:

$$x(t) = \frac{X_m}{\sqrt{2}} e^{j\phi} = \frac{X_m}{\sqrt{2}} (cos\,\phi + jsin\,\phi) = \frac{X_m}{\sqrt{2}} \angle\,\phi \qquad (19)$$

The sinusoidal signal and its phasor representation given by (18) and (19) are illustrated in Figure-8.

Phasor measurements that occur at the same time are named synchrophasors. Sometimes the terms of *PMU* and synchrophasor are used interchangeably whereas they actually represent two independent technical meanings. A synchrophasor is the metered value while the Phasor Measurement Unit (PMU) is the metering device to measure the phasor itself.



(a) Sinusoidal signal.                    (b) Phasor representation
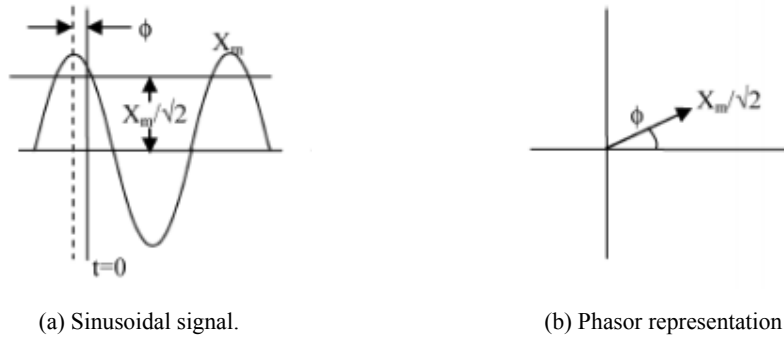
Figure-8. Phasor representation of a sinusoidal block of a PMU

In practical applications, PMUs are sampled from widely distributed locations in the power system network and synchronized from the common time source of a GPS time stamp.

To standardize the data format and measurement concept, The IEEE Standard 1344-1995 was introduced. In 2005 that standard was updated with the new standard IEEE C37.118, it was around 10 years of WAMS experience and

research. The latest IEEE C37.118 improves PMU interoperability with the following three major contributions [38]:

- Refined definition of a "Absolute Phasor" referred to GPS-based and nominal frequency phasor, as well as time-stamping rule;

- Introduction of the TVE (Total Vector Error) to quantify the phasor measurement error; and

- Introduction of the PMU compliance test procedure.

Synchronized phasor technology is the preferred basis of a wide area measurement system (WAMS). Phasor quantities are logged from digital samples of the AC waveforms. To ensure that all phasor are synchronized using the same time reference, the standard defines a synchronized phasor angle as an instantaneous phase angle relative to a cosine function at nominal system frequency synchronized to UTC. This angle is defined to be 0 degrees when the maximum of the measured sinusoidal waveform occurs at the UTC second rollover (1 pulse per second time signal), and -90 degrees when the positive zero crossing occurs at the UTC second rollover. Figure-9 illustrates the concept showing the nominal 'reference' waveform (dotted line) synchronized with UTC (peaks at 0, $T_0$, $2T_0$, etc.) and the actual waveform (solid line) with growing phase angle ($\phi$i) relative to the reference [39].
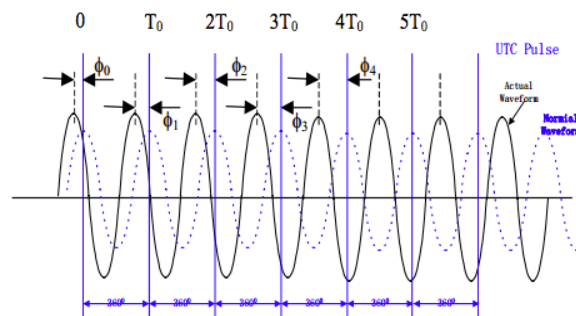


Figure-9. Absolut phasor

## 2.6.  APPLICATIONS OF PMU IN POWER SYSTEMS

The synchronized phasor measurement technology is relatively new, and consequently several research groups around the world are actively developing applications of this technology. The following are some of current development of PMU application in power system [40], [41]:

- Power system automation, as in smart grids

- Load shedding and other load control techniques such as demand response mechanisms to manage a power system. (i.e. Directing power where it is needed in real-time)

- Increase the reliability of the power grid by detecting faults early, allowing for isolation of operative system, and the prevention of power outages.

- Increase power quality by precise analysis and automated correction of sources of system degradation.

- Wide area measurement and control through state estimation, in transmission networks or distribution grids.

- Phasor measurement technology and synchronized time stamping can be used for Security improvement through synchronized encryptions like trusted sensing base.

Dealing with the WAMS, currently there are two kinds of WAMS strategy approach in the power system. First is the application of WAMS in transmission level, where the PMUs are installed in the substation as it is shown in Figure-10. The other is deploying PMUs in the wall laboratory outlet such as in Japan Campus WAMS, Malaysia-Singapore WAMS and Thailand WAMS. Figure-11 illustrates the typical installation of PMU in 220V domestic outlet.
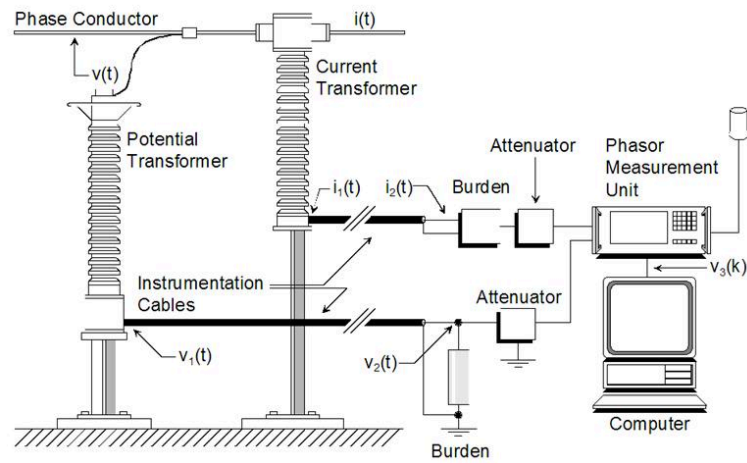
Figure-10. PMU installed in substation [42]
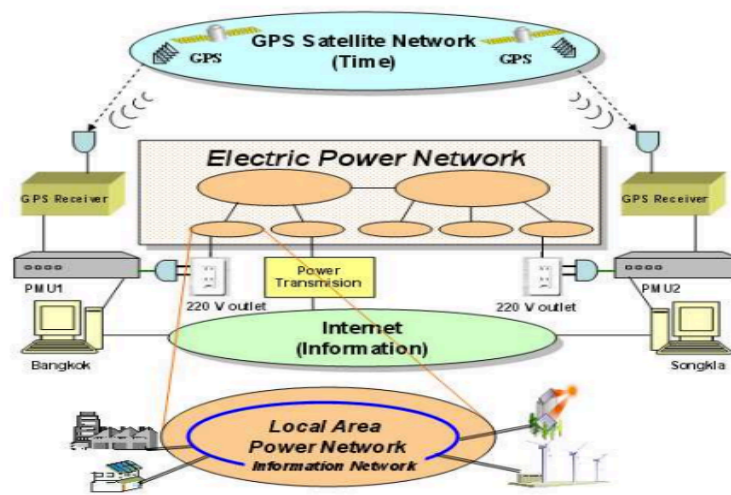


Figure-11. Typical PMU deployment in domestic wall outlet on WAMS system [43]

## 2.6.1. EXAMPLE OF PMU FOR WAMS IN THE WORLD

The application of PMU technology for power system wide area monitoring started in the 1980s and continuously gains the worldwide acceptance. Many projects are going on in Europe, America and Asia to deploy PMUs in large scale.

33

In the US through the Smart Grid Investment Grant (SGIG) program sponsored by the US government, there are a total of at least 921-networked PMUs installed and operational across the country until 2014 [44]. Figure-12 pictures the PMU Network in the US.

China has already started their application of WAMS since 1995. Around 2000 PMUs have been already installed in Chinese power grids. The installed PMUs cover all the 500 kV substations, important 220 kV substations and generating stations above 100 MW [45].

Other countries also follow to apply the PMU such as in India, Russian, Scandinavia, Croatia, Japan and Indonesia, which is just starting their PMU installation in the National Grid Company.
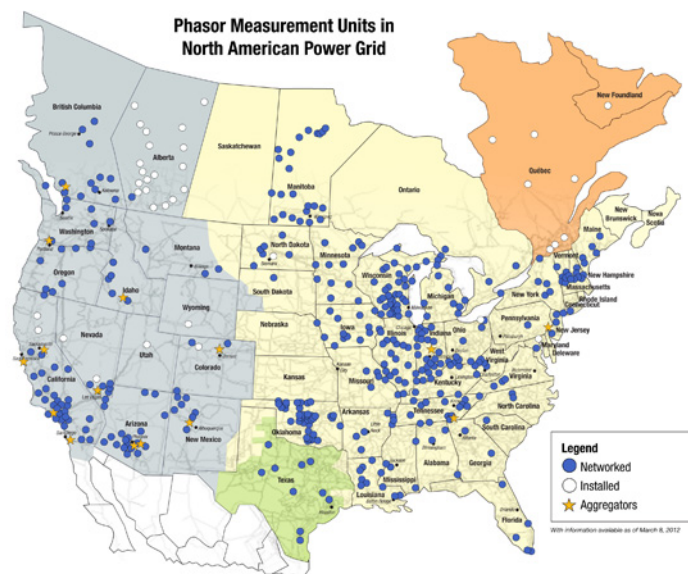


Figure-12. PMU deployment in US

## 2.6.2. THE CAMPUS WAMS

Another implementation for wide area measurement system is trough the Campus Wide Area Measurement System (Campus WAMS) initiated by several

universities in Japan. This project started on 2002 and continuously develops for the better result of power system monitoring through the low voltage network. Figure-13 shows PMU locations in Western Japan 60-Hz power system.

This Campus WAMS, consisting of eight commercial PMUs, which are installed at eight universities, covers typical power supply area of all six electric power companies of Western Japan 60-Hz power system. Because of each power company is independent operating entity; there is no way to collect synchronized phasor measurements of transmission high voltage level from all power companies at present. However, with the availability of Campus WAMS it becomes possible to observe and analysis system wide dynamics for overall Western Japan 60-Hz power system [46].
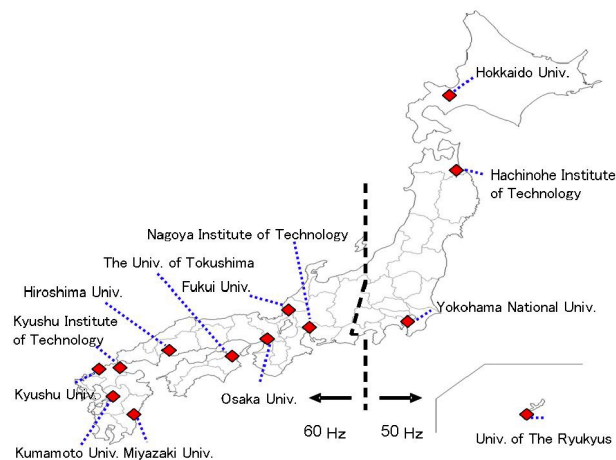


Figure-13. Japan Campus WAMS

All PMUs measure the single-phase voltage phasor of 100V outlet on the wall of laboratory with GPS-synchronized time tag. The voltage phasor is calculated by using 96 sample data per voltage sine-wave cycle. The calculated voltage phasor data are saved in PMU at interval of 1/30s from H:50 min to H:10 min, H:10 min to H:30 and from H:30 min to H:50 min, in every hour. All phasor

measurements of all locations are automatically collected into a data server through Internet. The background application program running in other computers reads data from server and performs analysis [47].

For the Campus WAMS, two following points need to be addressed. First point is that the single-phase voltage of end user voltage level is recorded by PMUs. Due to the constant sampling interval at off-nominal frequencies, the single-phase phasor measurement will produce some slight errors. Second point is that low voltage switching events are also measured and may interfuses with oscillation mode. Based on these two points, the previous work results have verified the validity of phasor data of the Campus WAMS.

Dealing with the two conditions above, some previous work in [43] and [48] had verified the validity of this measurement type. In [43] the single voltage phase difference from PMUs measurement in low voltage level were compared to the actual power flow of a 230kV tie line between center area and south area of Thailand power system. In [48] the phasor measurements from PMUs installed in 100 V power outlets at the central supply area of Kyushu, Kansai, and Chubu electric power company were compared to the measurement of PMU in 500 kV power station at west end of Chubu, PMU located in 500 kV power stations at east end, and PMUs which are installed in 275 kV generating stations. From those two investigations, it showed a strong correlation between two sets of data confirming the validity of the phase difference data of PMUs measured from low voltage level. Those results indicated 100V power outlet phasor properly reflects the oscillatory characteristics of upper power system including the power outlet. Additionally, as for second issue, the influence caused by relative high frequency low voltage switching events could be eliminated by applying signal filtering method [49], [50].

Like in Japan, Thailand 50-Hz interconnection power system that is linking central and southern areas developed in a longitudinal structure. Therefore, various system oscillations such as long-term oscillations, local generator oscillations etc., especially, an inter-area oscillation in interconnected tie lines 230 and 115 kV could raise between two areas. As stated in [51], the effects of system structure, load characteristic, excitation type of generating unit much influence the system stability of inter-area oscillation performance.

As an overview, the architecture of the PMU based monitoring system in Thailand WAMS is shown in Figure-14. PMUs are located at Thammasat University (TU), Bangkok and Prince of Songkla University (PSU), Songkla. The purpose of the monitoring system is to detect the inter-area oscillation between central and southern areas by assuming that group of generators in each area oscillate in the same rhythm. Both coherent groups are connected by a 230 kV tie-line so that the phase angles at PSU and TU are used as the representative phase angles of the southern area and the remaining areas of EGAT system, respectively.



Figure-14. Thailand WAMS

37

The PMU measure a single-phase instantaneous voltage at 220 V outlets. The phase angle of the measured voltage is accumulated in the PMU as the time sequential data. The PMU records the calculated phasor voltages every 40ms (2 cycles) and measures at the domestic outlets for 20 minutes twice an hour and transmitting it through Internet to the server at TU [52].

The map of Campus WAMS installation in Malay is shown in Figure-15. The tie line between Malaysia and Singapore is linked by AC and the tie-line between Malaysia and Thailand is by DC, so the power system in Malay Peninsula is one large AC interconnected system with a longitudinal structure which is similar to the West Japan power system. In this longitudinal power system a low-frequency power oscillation mode around 0.3 - 0.5 Hz is observed, which is the dominant mode among some electro-mechanical oscillations.



Figure-15. Singapore-Malaysia WAMS

## 2.7. APPLICATION OF GENETIC ALGORITHM IN WAVELET PARAMETERS OPTIMIZATION

The performance of the Wavelet calculation is much determined by the tuning of parameters; center of frequency $f_c$ and the bandwidth $f_b$. An optimum tuning of parameters will result smooth envelope with a less edge effect. The following figures describe how the edge effects influence the process of obtaining the gradient of logarithmic decrement function. Applying such an optimization tools helps to manage this edge effect. Genetic Algorithm is one of the prospective tools to dealing with this problem [21], [53]. The edge effect existence in wavelet envelope signal is shown in Figure-16.

The wavelet transform is calculated as shifting the wavelet function in time along the input signal and calculating the convolution of them. In most practical applications, the signals of interest have finite support. As the wavelet gets closer to the edge of the signal, computing the convolution requires the non-existent values beyond the boundary. This creates boundary effects caused by incomplete information in the boundary regions. Thus, the results of wavelet transform in these boundary effects regions have questionable accuracy [54].

Actually, the particular impacts of boundary effects become increasingly significant for some systems that may possess longer period sequence and thus require higher frequency resolutions [54].

Genetic algorithm simulates the genetic and evolutionary process of organisms in the natural environment, and form a kind of adaptive global optimization probability search algorithm, which is a kind of mathematical simulation of biological evolution process, is also one of the most important form of evolutionary computation.
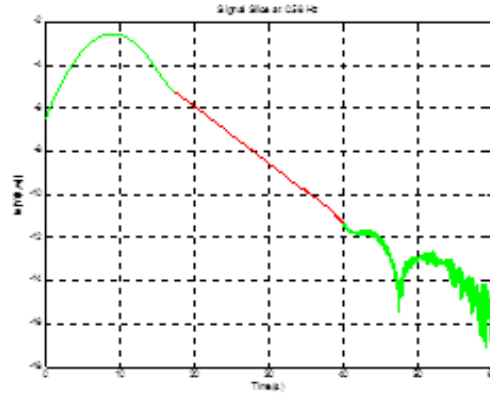
Figure-16. Edge effect in wavelet envelop

According to the genetic theory, two genes are excellent individuals; the possibility of their offspring is excellent than general of the offspring of two individuals to produce, so in theory, this algorithm is feasible, and more conducive to search to the global optimal solution [55].

Considering a three-layered network (*1xNx1*) as shown in Figure-17, the input and output are linear elements and the output function of the hidden units that satisfies both admissibility and stability conditions. It is assumed that the network sufficiently approximates the target. The estimate of the network $\hat{f}$ can be represented as:

$$\hat{f}(x) = \sum_{n,m} c_{n,m} \psi_{n,m}(x)$$

$$= \sum_{n,m} c_{n,m} 2^{\frac{n}{2}} \psi(2^n x - mb_0) \tag{20}$$

where $c_{n,m}$ is a weight parameter between the hidden layer and the output unit.

$x$

1

$2^n$  $i$  $c_{n,m}$  $\hat{f}(x)$

input unit  $2^n mb_0$  output unit

N

hidden layer
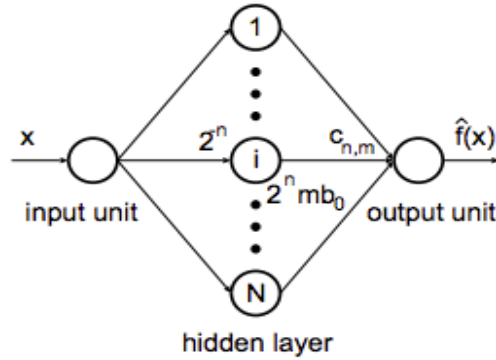
Figure-17. Wavelet network for GA

## 2.8. SUMMARY

With the invention of PMU in 1988 by DR. Arun G. Phadke and DR. James S. Thorp, the research in the field of wide area measurement system has evolved significantly.

The analysis and monitoring of power system oscillations can be accomplished by means of several methodological approaches. Each approach has its own advantages and feasible applications, providing a different view of the system dynamic behavior. Eigenvalue analysis technique is based on the linearization of the nonlinear equations that represent the power system around an operating point that is the result of electromechanical modal characteristics: frequency, damping and shape. Direct spectral analysis of power response signals use the Fourier Transforms or Short Time Fourier Transform (STFT), Prony or Wavelet analysis technique or any combination among those method.

The application of genetic algorithm is possible to make a better tuning in wavelet parameters to minimize the edge effect that might be exist.

# Chapter 3.

# FAST FOURIER TRANSFORM AND CONTINUOUS WAVELET TRANSFORM APPROACH

## 3.1.   INTRODUCTION

On the previous researches [20] and [46], which were based on Fast Fourier Transform (FFT) analysis, the damping ratio and frequency oscillation were estimated from eigenvalue of the matrix associated to a Single Machine Infinite Bus (SMIB) model. An output-only-based simplified oscillation model is developed to estimate the characteristic of inter-area power oscillation based on extracted oscillation data. However, this previous method did not explain how to calculate the damping ratio without considering any simplified model, especially when the system considered cannot be modeled as a SMIB.

In fact, there are some other techniques to recognize the mode of set of signals, from the classical Prony Analysis to the relatively new method Hilbert Huang Transform (HHT) as it has been compared in [56]. Prony analysis is more suitable for stationary signal, therefore a window signal where the system does not change so much should be selected to get an accurate result as discussed in [56]. HHT analysis also has been attempted to deal with PMU data. However, the

ability of this approach to estimate damping ratio and modal parameters cannot satisfactorily distinguish two separate modes unless there is a large difference in either frequency or damping ratio [10], [56], [32], [57].

In this thesis, PMU data used in the calculations come from the Japan Campus WAMS where the PMUs are deployed in laboratory wall outlet. Working with PMU data acquired from a domestic outlet is a fascinating challenge since all system data i.e. generators, transformers, tie lines and load parameters are all unknown. The analysis must be carried out merely rely on to the phasor signals. Therefore, a robust method is unavoidably needed. This research elaborates a novel approach in dealing with PMU data to estimate system's damping ratio based on the combination of FFT and Continuous Wavelet Transform (CWT) algorithm and demodulating the slicing signal at a ridge of 3D waveform.

The modulation signal is the signals envelop which measures the dissipation of oscillation energy caused by damping hence calculation of damping can be done by extracting the signal envelop using logarithmic decrement technique. The logarithmic modulus and phase decrement of the CM-CWT are calculated using one order polynomial regression routine to extract the damping ratio and frequency mode from the signal envelope. The main contribution of this work is the calculations are purely based on information from the signal regardless to any network model assumption.

## 3.2. THE APPLICATION OF FFT AND CWT APPROACH

### 3.2.1. MODE IDENTIFICATION USING FFT

In general, the Fourier Transform (FT) is a mathematical function that transforms a signal from the time domain to the frequency domain. This transformation makes it possible to identify the frequencies concealed in a signal.

The Discrete Fourier Transform (DFT) is a discrete version of FT, which transforms a signal (discrete sequence) from Time Domain representation to Frequency Domain representation. The Fast Fourier Transform (FFT) is a numerical algorithm that is commonly used to computes the Discrete Fourier Transform (DFT) of an *n*-dimensional signal in a very efficient time compared to other method such as solving simultaneous linear equation or the correlation method [58].

Taking an advantage of FFT to separate each frequency contain in a composite signal, in this work the oscillation mode is detected using FFT algorithm in Matlab. The DFT is a very important discrete transform to carry out Fourier analysis in many practical applications. A DFT with an *n*-length can be defined as:

$$X(k) = r(t) + \sum_{n=0}^{N-1} x(n) \, e^{\frac{-2\pi}{N}jkn}$$

(21)

where *X(k)* and *x(n)* are in general complex value. $k \geq 0$ and $n \leq N - 1$ [14].

The Oscillation mode of a set of signal can be easily revealed using spectral analysis. Taking advantage of the well-known mathematical function FFT that can transform a signal from the time domain to the frequency domain, it is possible to identify the frequencies concealed in a signal. The FFT is a numerical algorithm that is commonly used to compute the Discrete Fourier Transform (DFT) of an n-dimensional signal in a very efficient time compared to other methods such as solving simultaneous linear equation or the correlation method [58], [59]. In this work, the oscillation modes are discovered using FFT by separating each dominant frequency contained in a composite signal.

To demonstrate the ability of the FFT method in recognizing modes from a set of signals, a synthesized signal in time domain in (22) is converted to

frequency domain using FFT algorithm to identify the centre of oscillation. The parameter values of individual mode are given in Table-1. A random noise signal *r(t)* represents local switching and other noises in the real PMU signal. The amplitude of the noise is selected so that not bigger than the amplitude of the ringdown signal in order not burying off the actual signal we need to analyse.

$$f(t) = r(t) + \sum_{i=1}^{3} A_i e^{-2\pi\zeta t} \cos(2\pi f_i t + \theta_i) \tag{22}$$

Table-1. Signal parameters

| Mode (i) | Amplitude (A) | Frequency (f) | Damping (ξ) | Shift angle (θ) |
|----------|---------------|---------------|-------------|------------------|
| 1 | 1.0 | 0.35 | 0.26 | $0^o$ |
| 2 | 0.5 | 0.50 | 0.50 | $30^o$ |
| 3 | 0.9 | 0.9 | 0.11 | $60^o$ |

The comparison between expected value and the result of estimation using FFT-CWT approach are given in Table-2.

Table-2. Expected and estimated value of each signal mode

| Mode (i) | Center of oscillation frequency | |
|----------|----------|-----------|
| | Expected | Estimation |
| 1 | 0.35 | 0.35 |
| 2 | 0.5 | 0.50 |
| 3 | 0.9 | 0.90 |

The experimental signal in time domain is shown in Figure-18 and the result of estimation using this FFT Algorithm is depicted in Figure-19. It confirms that this FFT method is appropriate to identify the mode contained in a set of synthesized signal.
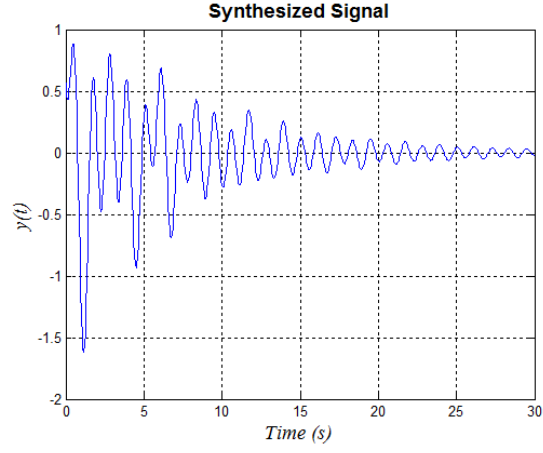
Figure-18. The synthesized signal of three modes
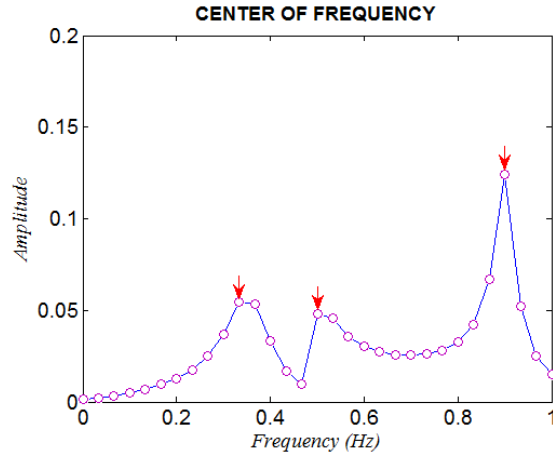


Figure-19. FFT estimation of frequency mode

### 3.2.2. DAMPING CALCULATION USING CONTINUOUS WAVELET TRANSFORM

The wavelet transform decomposes signals over dilated and translated wavelets. A wavelet is a function of $f(t) \in L2(R)$ with a zero average. It has been proved that the CWT is very indisputable to identify the damping ratio and shown to be highly resistant to noise, i.e. of up to 0 dB signal-to-noise ratio [60], [9].

46

Suppose that all function *f(t)* satisfy the condition:

$$\int_{-\infty}^{+\infty} |f(t)|^2 dt \leq 0 \tag{23}$$

Then, the continuous wavelet transform of the signal can be defined as:

$$Wf(u,s) = \int_{-\infty}^{+\infty} f(t)\,\psi_{u,s}^*(t)dt \tag{24}$$

where *u* and *s* are the translation and the scale parameters respectively. $\psi^*_{u,s}(t)$ is the translated and scaled complex conjugate of the mother wavelet function *f(t)* ∈ $L^2(R)$. The wavelet function is a normalized function i.e. the norm is equal to one with an average of zero [31].

The scaled-and-translated wavelet function is expressed as:

$$W_{(u,s)}(t) = \frac{1}{\sqrt{s}}\psi\left(t - u/s\right) \tag{25}$$

It can be noted that the CWT is the sum over all time of the signal *f(t)* multiplied by scaled, shifted versions of the mother wavelet (which are also called son wavelets). Thus, the CWT possesses localization properties in both time and frequency domains and consequently provides valuable information about *f(t)* at different levels of resolution and measures the similarity between and each son wavelet [10].

### 3.2.3. SELECTING MOTHER WAVELET FUNCTION

The wavelet transform is more alike to the well-known Windowed Fourier Transform (WFT). However, they are in a completely different advantage and purpose. The disparity is that Fourier transform decomposes the signal into *sines* and *cosines*, which means that the function is localized in a Fourier Space. On the

other hand, the wavelet transform uses functions that are localized in both the real and Fourier Space [31].

The wavelet transform decomposes signals over dilated and translated wavelets. A wavelet is a function of $f(t) \in L^2 R$ with a zero average. It has been proved that the CWT is very dexterous to identify the damping ratio and shown to be highly resistant to noise, i.e. of up to 0 dB signal-to-noise ratio [12].

Suppose that all function *x(t)* satisfy the condition:

$$\int_{-\infty}^{+\infty} |x(t)|^2 dt < \infty, \tag{26}$$

Then, the CWT of a signal can be defined as:

$$Wf(u,s) = \int_{-\infty}^{+\infty} f(t)\psi_{u,s}^*(t)dt, \tag{27}$$

Here, *u* and *s* are the translation and scale parameters respectively while $\psi_{u,s}{}^*(t)$ is the translated and scaled complex conjugate of the mother wavelet function $\psi^*(t) \in L2(R)$ . The wavelet function is a normalized function i.e. the norm is equal to 1 with an average of zero [31].

The scaled-and-translated wavelet function is expressed as:

$$\psi_{(u,s)}(t) = \frac{1}{\sqrt{s}} \psi\left(\frac{t-u}{s}\right) \tag{28}$$

It can be noted that the CWT is the sum over all time of the signal *f(t)* multiplied by scaled, shifted versions of the mother wavelet (which are also called son wavelets). Thus, the CWT possesses localization properties in both time and frequency domains and consequently provides valuable information about *f(t)* at different levels of resolution and measures the similarity between and each son wavelet [10].

The admissibility condition implies $\psi(0) = 0$, which means that a wavelet must integrate to zero. In some literatures, it was stated that there are several different types of mother wavelet functions satisfying the admissibility condition such as the Mexican hat, Gabor and Morlet, which can be selected according to the nature of the signal to be analysed. According to those literatures the complex Morlet Wavelet Function (CMWF) would be appropriate for the analysis of ring down signals due to its capabilities in time-frequency localization for analytical signals [9], [10], [12], [61]. According to [31], the CMWF is capable of analysing data in a multi-resolution domain which means it can automatically filter out the noise from *f(t)* and thus no additional filters are needed.

### 3.2.4. DETERMINING CWT PARAMETERS

The performance of FFT-CWT method is based on the selection of parameters. The center of frequency $f_c$ can be approximated near the typical modal frequency in the case of small signal stability analysis. Typically, these oscillatory modes have frequencies in the range of 0.1 to 1.0 Hz; that is lower compared to the local modes with frequencies ranging from 1 to 2 Hz. The center of frequency also can be calculated using Auto spectrum method, contour plot of CWT, Wavelet Scalograms or Wavelet Coefficients Charts [9], [62].

When selecting the range of scales, these two issues have to be taken into consideration. First, the lower scales correspond to the most compressed wavelets, which allow detecting rapidly changing signal features related to high-frequency components. Second, the higher scales correspond to the most stretched wavelets, which allow detecting slowly changing signal features related to low-frequency components. In fact, selecting an appropriate range of scales will determined the accuracy of the calculation as practiced in this research. In addition, a suitable

selection of scales range is very important since in practice the CWT is computed within a predefined range of scale and it must be able to identify the individual oscillatory modes. When the complex Morlet mother-wavelet function is dilated by a scaling factor s, then the center frequency becomes $f_c = f_b.\Delta t.s$.

To dealing with PMU Data, first the PMU signals are read from MPU database center in *.csv format. Auto-spectrum method is then employed to this data to determine the center of low frequency oscillation. The next is using CW-CWT method to transform the data to three-dimensional form; i.e. Time-Frequency-Modulus.

Using a special function written in Matlab the ridge and peak of the 3D wave is decided. The damping ratio begin to be calculated starting from the peak of the wave using demodulation method and finally linear regression is applied to estimate decay constant and angular velocity of the signals.

### 3.2.5. COMPLEX MORLET FUNCTION

Following the work on [9], [10], [31], the CWT of a continuous time signal can be expressed by the inner product of the Hilbert Space as follows:

$$W_h f(a,b) = \frac{1}{\sqrt{a}} \int_{-\infty}^{+\infty} f(t) h^*_{(t-a/b)} \, dt \tag{29}$$

where **a** is a dilation or scaling factor, **b** is a translation or time shift factor, and $h^*(t)$ is complex conjugate of a mother wavelet function h(t).

Again, taking advantage of the work on [9], [10], The Complex Morlet Wavelet Function is selected and formulated as:

$$h(t) = e^{j2\pi f_c t} e^{\frac{-t^2}{f_b}} \tag{30}$$

$f_c$ is the center of oscillation and $f_b$ is bandwidth frequency parameters.

Let's have a look at a function of a ringdown type signal in (31:

$$x(t) = ae^{-\alpha t}\cos(\omega t + \theta) \tag{31}$$

This can be re-written as:

$$x(t) = A(t)\left|\frac{e^{j(\omega t+\theta)} + e^{-j(\omega t+\theta)}}{2}\right| \tag{32}$$

where $A(t) = e^{-\alpha t}$, $a$ is the relative amplitude and $\theta$ is the mode phase shift. $t$ is lying in a certain interval of time.

The logarithmic decrement constant $\alpha$ and the angular frequency $\omega$ correspond to the real and the imaginary components, respectively. The eigenvalues of the $i_{th}$ mode expressed as $\lambda_i = \alpha_i + j\omega_i$. $f_c$ is the wavelet central frequency parameter and $f_b$ is a bandwidth parameter that controls the shape of the wavelet [10].

Representing $A(t)$ with its Taylor Series around the reference point $t = b$ returns:

$$A(t) = A(b) + \sum_{n=1}^{\infty}(t - b)^n \frac{A^{(n)}(b)}{n!} \tag{33}$$

By substituting (32) into (31) the CWT of $f(t)$ can be expressed as:

$$W_h x(a,b) = \frac{1}{\sqrt{a}}\int_{-\infty}^{+\infty} A(t)\left(\frac{e^{j(\omega t+\theta)} + e^{-j(\omega t+\theta)}}{2}\right)h^*_{(t-b/a)}dt \tag{34}$$

Jumping to the result as derived in [9], in the form of time varying amplitude and phase angle the equation can be defined as:

$$W_h x(a_k, t) = \frac{\sqrt{\pi a_k f_b}\,Ae^{-\alpha t}}{2}\,e^{j(\omega t+\theta)} \tag{35}$$

where $a_k = (2\pi/\omega)f_c$ and $k$ is the corresponding mode to be analyzed. For the detail please refer to [9], [10].

The logarithmic and argument of the modulus $W_h x(a_k,t)$ can be written as (36) and (37) respectively.

$$ln|W_h x(a_k,t)| = -\alpha t + ln\left(\frac{\sqrt{\pi a_k f_b}\, A e^{-\alpha t}}{2}\right) e^{j(\omega t + \theta)} \tag{36}$$

$$arg|W_h x(a_k,t)| = -\omega t + \theta \tag{37}$$

The logarithmic decrement constant $\alpha$ and the phase decrement constant $\omega$ are extracted from (36) and (37) correspondingly.

The damping ratio is then calculated using:

$$\xi = \frac{-\alpha}{\sqrt{\alpha^2 + \omega^2}} \tag{38}$$

For the multi-mode signal with $m$ sets of data, the value of $\alpha$ and $\omega$ can be determined as in (39) and (40).

$$\alpha = \frac{-m\sum_{i=1}^{m} b_i \ln|W_h x(a_k,b_i)| - \sum_{i=1}^{m} b_i \sum_{i=1}^{m} \ln|W_h(a_k,b_i)|}{m\sum_{i=1}^{m} b_i^2 - \left(\sum_{i=1}^{m} b_i\right)^2} \tag{39}$$

$$\omega = \frac{-m\sum_{i=1}^{m} b_i \arg|W_h x(a_k,b_i)| - \sum_{i=1}^{m} b_i \sum_{i=1}^{m} \arg|W_h(a_k,b_i)|}{m\sum_{i=1}^{m} b_i^2 - \left(\sum_{i=1}^{m} b_i\right)^2} \tag{40}$$

Therefore, to dealing with the multimode signal, the Complex Morlet CWT is expressed as in (42) [9]:

$$W_h\left(x\sum_{i=1}^{N} x_i\right)(a,b) = \sum_{i=1}^{N} W_h x_i(a,b) \tag{41}$$

where $N$ is the maximum number of modes in the signal.

Figure-20 summarizes the process of identification of oscillation mode and calculation of damping ratio in this study. PMU Signal or simulated signal is

transformed the Time-Frequency-Modulus representation using CWT where the center of oscillation taken from FFT calculation is employed as one of the wavelet parameters. On the other works [9], [10], [12], [11] and [60] the center of oscillation is predicted using CWT itself. The advantage of using FFT to estimate the center of oscillation is its simplicity and clarity to break away each mode contained in the signal. This is one of the contributions of this work.
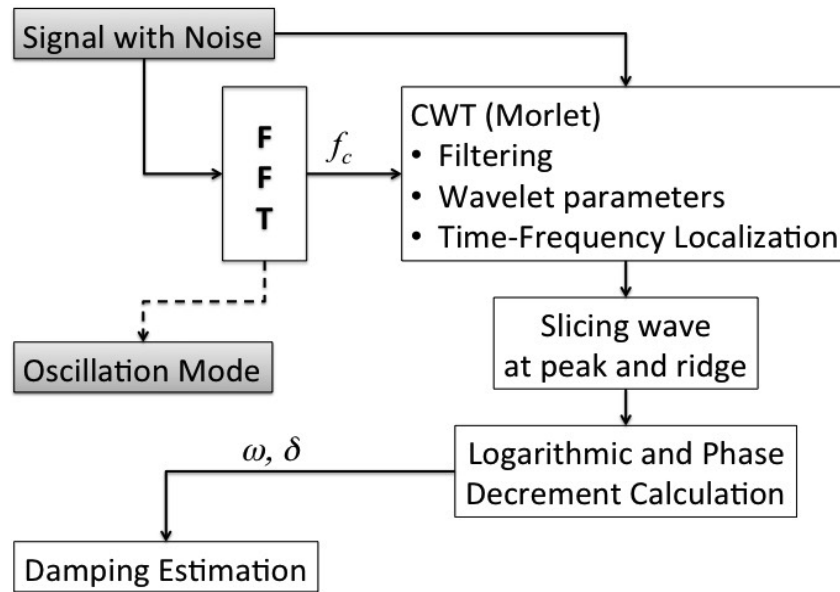


Figure-20. Calculation process

## 3.3. PERFORMANCE OF THE FFT-CWT COMPARED TO PRONY UNDER NOISY RINGDOWN SIGNAL

Signal-to-noise ratio (SNR) is an essential quantity used in signal processing that associates the level of a desired signal to the level of background noise. It is defined as the ratio of signal power to the noise power that usually expressed in *decibels*. A ratio higher than 1:1 (greater than 0 dB) indicates more signal than noise.

53

Signal-to-noise ratio is defined as the ratio of the power of a signal (meaningful information) and the power of background noise (unwanted signal):

$$SNR = \frac{P_{signal}}{P_{noise}} \qquad (42)$$

where $P$ is average power. Both signal and noise power must be measured at the same and equivalent points in a system, and within the same system bandwidth.

In this section various level of SNR are applied to the signal in order to inspect the performance between Prony and FFT-CWT approach in dealing with the corresponding signal. To generate the signal and manipulating the noise, a Simulink block is employed as shown in Figure-21.



Figure-21. Simulink block to generate signal and noise

Table-3 shows the performance of FFT-CWT towards the various level of noise contains in the main signal. The simulation begins with signal and noise power at the same level that means signal and noise are mixed together or the SNR approach zero. The higher SNR denotes the better quality of signal.

54

Table-3. Performance of FFT-CWT under various noise level
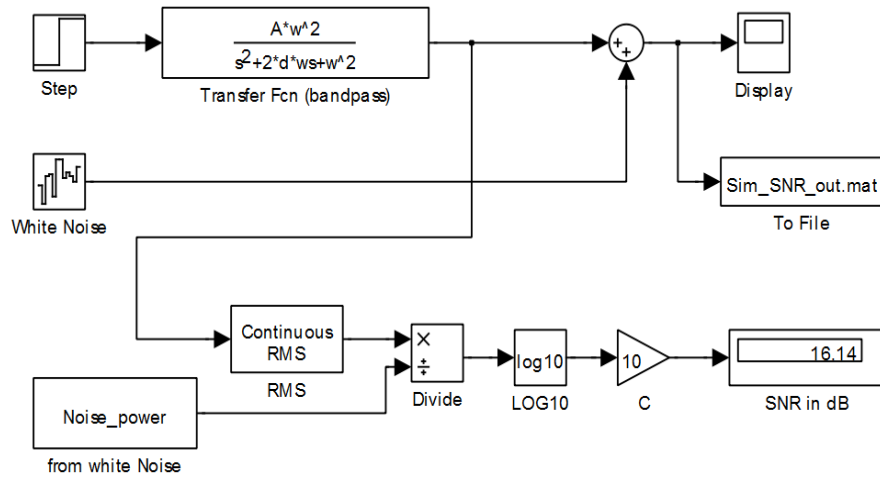
| No. | Signal Power (RMS) | Noise Power (RMS) | SNR (dB) | Expected value | | Calculated value | | Error margin | |
|---|---|---|---|---|---|---|---|---|---|
| | | | | Freq. (Hz) | Damping (%) | Freq. (Hz) | Damping (%) | Frequency | Damping |
| 1. | 4 | 4 | 0.04 | 0.35 | 2 | 0.54 | NA | 54 % | NA |
| 2. | 4 | 3 | 1.29 | 0.35 | 2 | 0.54 | NA | 54 % | NA |
| 3. | 4 | 2 | 3.051 | 0.35 | 2 | 0.54 | NA | 54 % | NA |
| 4. | 4 | 1 | 6.061 | 0.35 | 2 | 0.35 | 1.50 | 1 % | 25 % |
| 5. | 4 | 0.1 | 16.061 | 0.35 | 2 | 0.35 | 1.95 | 0 | 1 % |
| 6. | 4 | 0.01 | 26.061 | 0.35 | 2 | 0.35 | 1.98 | 0 | 0 |
| 7. | 4 | 0.001 | 36.061 | 0.35 | 2 | 0.35 | 1.99 | 0 | 0 |
| 8. | 4 | 0.0001 | 46.061 | 0.35 | 2 | 0.35 | 2.00 | 0 | 0 |
| 9. | 4 | 0.00001 | 56.061 | 0.35 | 2 | 0.35 | 2.00 | 0 | 0 |
| 10. | 4 | 0.000001 | 66.061 | 0.35 | 2 | 0.35 | 2.00 | 0 | 0 |

The Rose criterion (named after Albert Rose) states that an SNR of at least 5 is needed to be able to distinguish image features at 100% certainty. An SNR less than 5 means less than 100% certainty in identifying image detail [63]. It is clearly demonstrates by this FFT-CWT method as shown in Table-3 where the calculation revealed the correct result after SNR 6.061 *dB*.

Table-4 shows the performance of Prony analysis towards the various level of noise contains in the main signal. Similar to the prior, the simulation begins with signal and noise power at the same level that means signal and noise are mixed together or the SNR approach zero where logically it will be impossible to separate between noise and real signal.

From the result illustrated in Table-4, it can be seen the Prony approach start to reveal the correct estimation after SNR 16.0 *dB* for mode frequency and SNR 36.061 dB for the damping estimation.

Table-4. Performance of PRONY under various noise level

| No. | Signal Power (RMS) | Noise Power (RMS) | SNR (dB) | Expected value | | Calculated value | | Error margin | |
|---|---|---|---|---|---|---|---|---|---|
| | | | | Freq. (Hz) | Damping (%) | Freq. (Hz) | Damping (%) | Frequency | Damping |
| 1. | 4 | 4 | 0.04 | 0.35 | 2 | 5.00 | 95 | 1329 % | 4650 % |
| 2. | 4 | 3 | 1.29 | 0.35 | 2 | 1.20 | 90 | 243 % | 4445 % |
| 3. | 4 | 2 | 3.051 | 0.35 | 2 | 1.10 | 72.70 | 63 % | 3535 % |
| 4. | 4 | 1 | 6.061 | 0.35 | 2 | 0.57 | 68.18 | 11 % | 764 % |
| 5. | 4 | 0.1 | 16.061 | 0.35 | 2 | 0.39 | 7.27 | 0 | 61 % |
| 6. | 4 | 0.01 | 26.061 | 0.35 | 2 | 0.35 | 3.23 | 0 | 11 % |
| 7. | 4 | 0.001 | 36.061 | 0.35 | 2 | 0.35 | 2.05 | 0 | 2 % |
| 8. | 4 | 0.0001 | 46.061 | 0.35 | 2 | 0.35 | 2.00 | 0 | 0 |
| 9. | 4 | 0.00001 | 56.061 | 0.35 | 2 | 0.35 | 2.00 | 0 | 0 |
| 10. | 4 | 0.000001 | 66.061 | 0.35 | 2 | 0.35 | 2.00 | 0 | 0 |

From Table-3 and Table-4, it can be concluded that the FFT-CWT approach is much better than the Prony method in dealing with signal with noise.

## 3.4. THE INFLUENCE OF THRESHOLD LEVEL ADJUSTMENT

As it has been discussed in the previous section, the level of threshold will influence the number of impulse can be analyzed. Higher threshold level will collect samples with higher magnitude but less in number. Lower threshold gather more samples but prone to noise interference or coinciding samples. To obtain the relationship of this phenomenon, a Simulink model was built to generate several

kinds of signal with noise and various damping ratio as presented in the Figure-22.



$$\frac{A.\omega^2}{s^2+2.\xi.\omega.s+\omega^2}$$

Band-Limited White Noise

Step

FFT-CWT

Best Damping Estimation
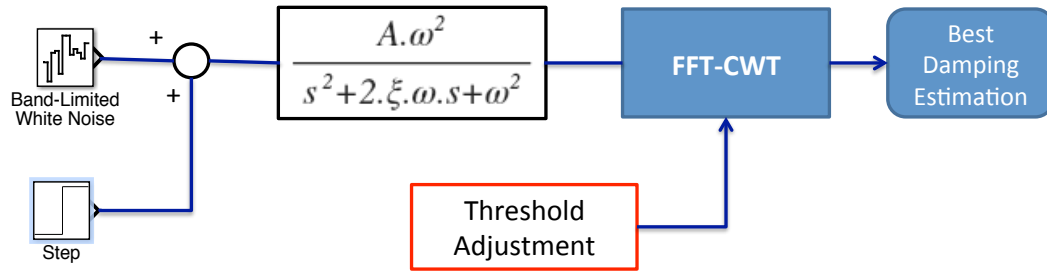
Threshold Adjustment

Figure-22. Simulink model to generate signal with various damping and noise value

Simulation using three ringdown signals with similar damping ratio and triggered at 50s, 700s and 720s respectively yields the result presented in Figure-23 and Table-5.
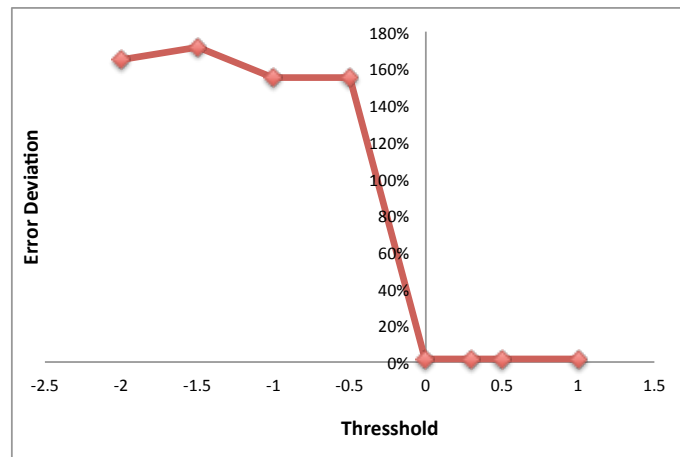


Figure-23. Simulation of threshold level adjustment

Table-5. Simulation of threshold level adjustment

SNR = 43.79 dB
Damping Ratio = 3 %
Oscillation frequency = 0.3 Hz., Standard deviation of signal = 0.3

| No. | Threshold | Damping (Calculated) | N (Number of impulse) | Error deviation (%) |
|------|-----------|----------------------|------------------------|----------------------|
| 1. | -2.0 | -1.95 | 22 | 165 |
| 2. | -1.5 | -2.14 | 15 | 171 |
| 3. | -1.0 | -1.65 | 4 | 155 |
| 4. | -0.5 | -1.65 | 4 | 155 |
| 5. | 0 | 3.05 | 3 | 2 |
| 6. | 0.3 | 3.05 | 2 | 2 |
| 7. | 0.5 | 3.05 | 2 | 2 |
| 8. | 1.0 | 3.05 | 1 | 2 |

From Figure-23 and Table-5 above, it can be seen that the adjustment of threshold level is very crucial to obtain the precise result of estimation. From a bounce of simulation already conducted, the minimum threshold level is equal to its standard deviation of the corresponding signal. In this simulation the standard deviation is 0.3 as shown in the table.

## 3.5.  VALIDATION PROCESS

To validate the method some known parameters signals are employed. Cases 1 to 3, individual signal with a random noise are used for representing the signal from PMU. Case 4 is a synthesized of three ringdown signal to verify the ability of the method to separate the modes which are hidden in a set of signal input. The synthesized signals are contains of 3 modes signals below:

$$f(x) = r(t) + e^{-0.2639t} \cos{(2\pi(0.35)t + 0^0)} \qquad \text{CASE 1}$$

The contour plot is given in Figure-24. This figure shows the center of frequency as well as the ridge of the signal in the frequency axis.
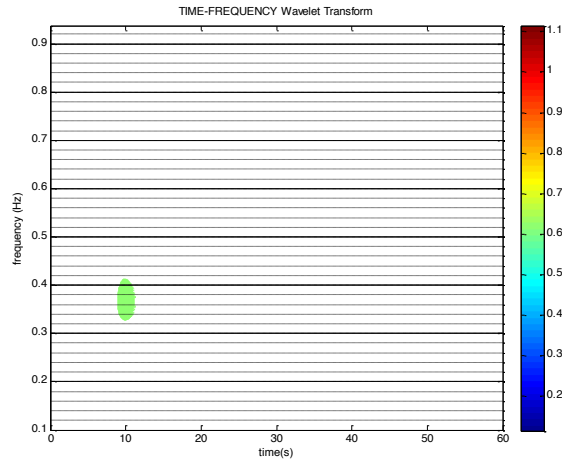


Figure-24. Contour Plot of function *f(t)*

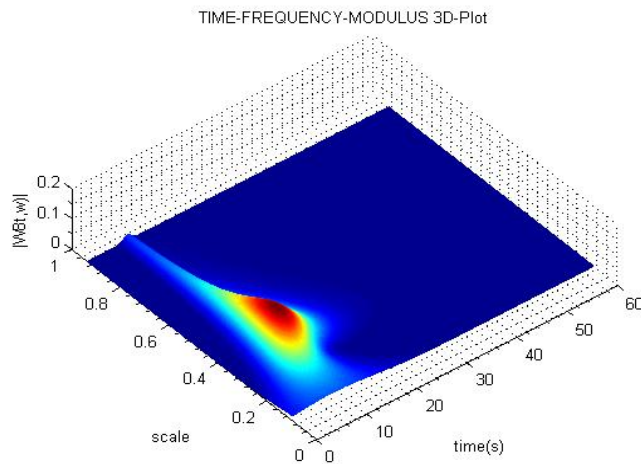In Figure-25, it is clearly shown the ridge of the signal as well as how it decays along the time.



Figure-25. A 3D plot of the *f(t)* signal showing the peak of Wavelet

Figure-26 and Figure-27 demonstrate the logarithmic decrement of the wave and phase decrement of the corresponding signal at the center of frequency

oscillation respectively. This calculation results damping ratio estimation $(\xi_{calc})$ = *0.1191*.

Comparing to the real parameter value of damping $(\zeta_{real})$ is 0.12, which means the error margin of calculation is about 0.7%.
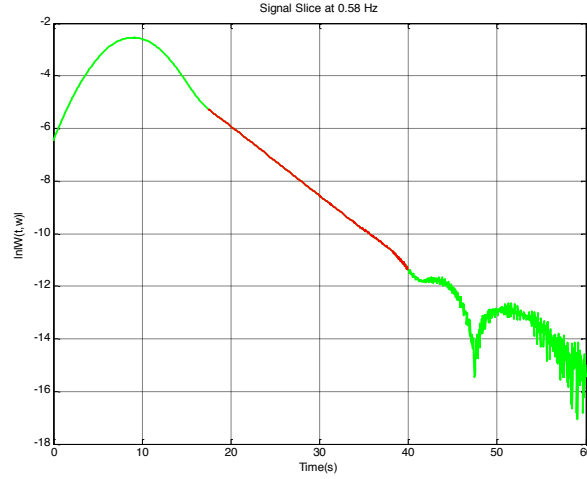


Figure-26. Logarithmic decrement of wavelet envelop of signal in case 1
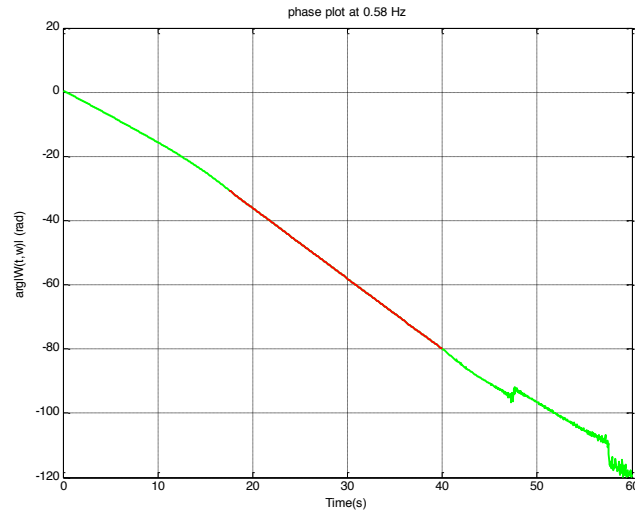


Figure-27. Phase decrement of wavelet envelop of signal in case 1

Similar to the above case, the proses is employed to the others following signals of case-2 and case-3. The summary of given parameters of the all three

cases are listed in Table-6 and the comparing of estimation result to the given value are presented in Table-7.

$$f(x) = r(t) + e^{-0.1571t} \cos\left(2\pi(0.5)t + 30^0\right) \qquad \text{CASE 2}$$

and,

$$f(x) = r(t) + e^{-0.1131t} \cos\left(2\pi(0.9)t + 165\right) \qquad \text{CASE 3}$$

Table-6. List of parameters of signal in case1, case 2 and case 3

| Case ($N$) | $f_N$ | $a_N$ | $\xi_N$ | $\theta_N$ |
|---|---|---|---|---|
| 1 | 0.35 | 1.0 | 0.12 | $0^o$ |
| 2 | 0.5 | 0.5 | 0.05 | $30^o$ |
| 3 | 0.9 | 0.9 | 0.02 | $165^o$ |

Table-7. Expected value and result of estimation

| $f_N$ (Hz) | $\xi_{expected}$ | $\xi_{estimated}$ | Error (%) |
|---|---|---|---|
| 0.35 | 0.12 | 0.1191 | 0.7 |
| 0.50 | 0.05 | 0.05 | 0 |
| 0.90 | 0.02 | 0.02 | 0 |

A 3-D visualization in Figure-25 and Figure-30 demonstrate a ringdown signal behavior simultaneously in the time domain as well as in frequency domain. This is actually the advantage of this method i.e. Wavelet analysis is able to reveal signal aspects that other analysis techniques miss them, such as trends, breakdown points, and discontinuities. As it has been mentioned in 3.3.1, using wavelet analysis makes it possible to perform a multi-resolution analysis.

In case-4, a synthesized signal contains three modes that develop from signals in case-1, case-2 and case-3 all together.

$$f(x) = r(t) + \sum_{i=1}^{3} M_i e^{-\alpha_i t} \cos(2\pi(f_i)t + \theta_i)$$  CASE 4

In this case all the signals are merged and a random noise is added to represent a real condition of PMU signal. The synthesized signal of these three modes is shown in Figure-28.

Figure-29 clearly shows the modes contained in the signals and depicts the center of frequency of each mode.
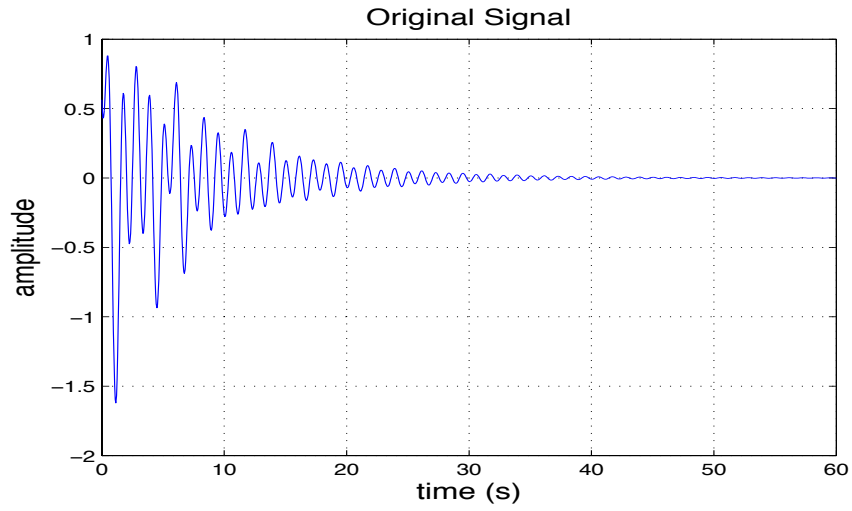


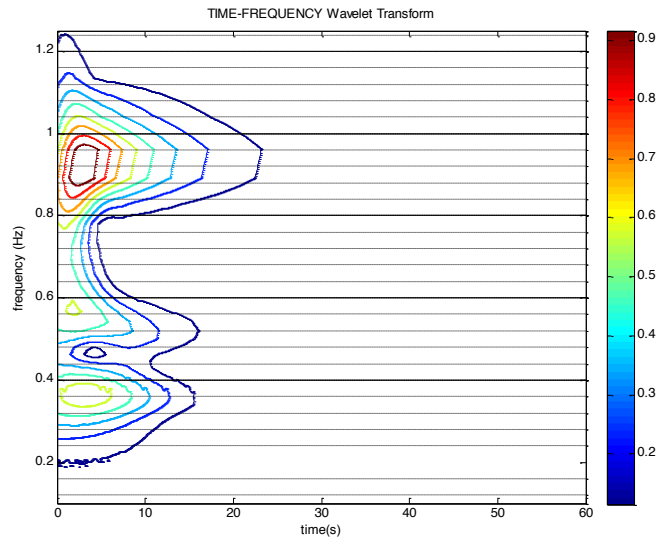Figure-28. Signal in case 4 in time domain

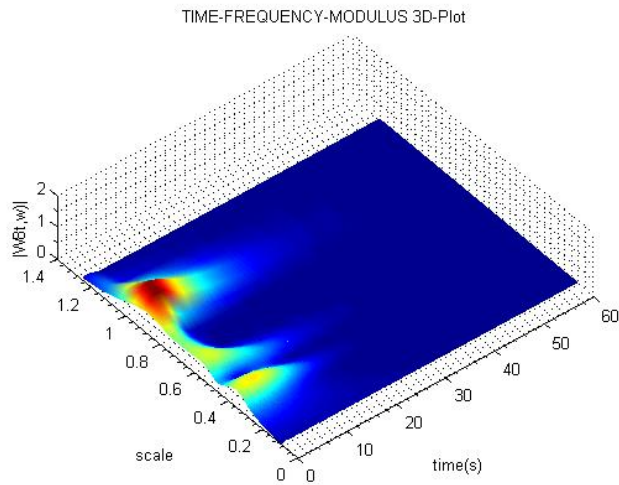Figure-29. Center of frequency of all mode in case 4



Figure-30. The 3-D wavelet representation of signal in case 4

The comparison between real value and calculated value in Table-8 are convincing the worth of this method. The accuracy of this method exceeds 99% according to this simulation.

Table-8. Expected value and result of estimation in case-4

| Mode | $f_{exp}$ (Hz) | $f_{est}$ (Hz) | $\xi_{exp}$ | $\xi_{est}$ | Damping Error (%) |
|---|---|---|---|---|---|
| 1 | 0.35 | 0.347 | 0.12 | 0.119 | 0.67 |
| 2 | 0.50 | 0.500 | 0.05 | 0.050 | 0 |
| 3 | 0.90 | 0.901 | 0.02 | 0.020 | 0 |

## 3.6.    SUMMARY

In this chapter the performance of FFT-CWT approach has been compared to the Prony analysis towards various level of signal to noise ratio (SNR). The simulation convinced that the proposed approach is much better than the Prony method in dealing with signal with noise.

It also presented the FFT-CWT approach is capable to detect modal frequency oscillation as well as calculating the damping ratio based on the information extracted from the PMU data without associating the parameters to a power system model.

# Chapter 4.

# APPLICATION OF THE APPROACH FOR MODE AND DAMPING CALCULATION

## 4.1. INTRODUCTION

The application of Phasor Measurement Unit (PMU) in power system has been widely used in the last decades. Since then many research works have been conducted and research topic in the field of security assessment, fault location detection, wide area protection, instability prediction and power system state estimation are widely opened [13], [14], [34], [64], [65].

Generally, a PMU is installed in substation or generation station. It measures the magnitude and angle of current and voltage of the corresponding bus. The capability of this device to measures the phasor of voltage and current in a very high accuracy and synchronizing it using Global Positioning System (GPS) clock makes it possible to assess the system state or to locate a disturbance in the transmission line. Recently, the deployment of PMU in a domestic network is beginning popular constituted by a variety of reasons. One of them is in Japan, where many different companies operate the power system; sharing data is an uneasy thing to do. Hence, the application of PMU in a campus scale where some

universities working in collaboration in a Japan Campus WAMS is a reasonable choice.

Indeed, there is no way to check the accuracy of the estimation without involving the system modeling. Since it is not possible to have a complete modeling from a real power system, in this thesis a well-known test bed system is used. The validity of this method is verified by comparing the result of damping ratio of Kundur Two Area Four Machine System (TAFM) by using eigenvalue-based analysis using Power System Analysis Toolbox (PSAT) to the result from this proposed method.

## 4.2. SIMULATION USING TWO AREA FOUR MACHINE SYSTEM MODEL

Figure-31 shows a system consists of two identical areas interconnected by a weak tie line. The model used is as same as the system in example-12.6 page-813 in [2]. The small signal stability analysis is carried out by applying a three-phase fault in bus 8 that is cleared out after 0.05 second. The one line diagram of the system is presented in the following figure.
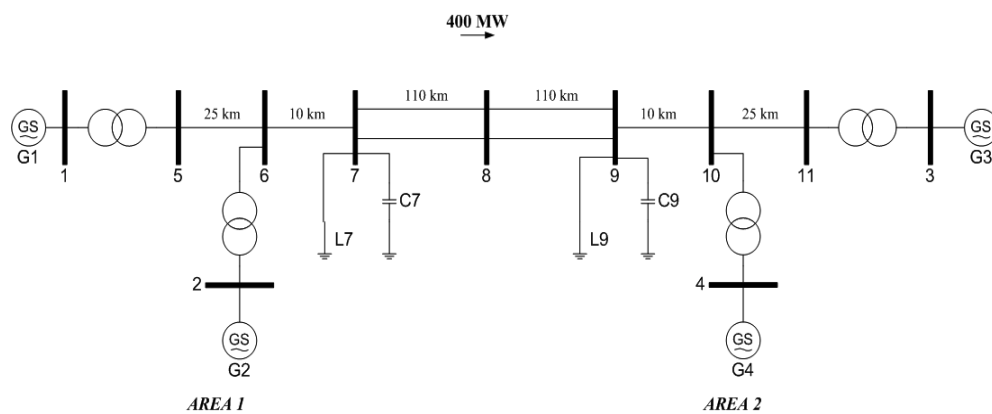


Figure-31. Two Area Four Machine System model

Scenarios are managed by simulating load in L7 (area 1) and L9 (area 2). First attempt analyzes the system using eigenvalue-based method using PSAT toolbox and the Second evaluates the system applying FFT-CWT approach.

## 4.2.1. SIMULATION USING EIGENVALUE BASED METHOD

There are two groups of assessment are applied. First keeps load in area 2 constant and step-by-step increases the load in area 1 as presented in Table-9. The second simulation keeps the load in area 1 constant and increases the load in area 2 from 98MVA to 120MVA as illustrated in Table-10. The calculation is attempted at every load scenario using eigenvalue based PSAT toolbox developed by Prof F. Milano [66], which based on eigenvalue approach. The example of calculation result from PSAT toolbox is given in the Appendix C.

Table-9. Simulation result for L9 keeps constant at 100 MVA – using PSAT toolbox

| No. | L7 (MVA) | Estimated damping (%) | | | Mode freq. (Hz) |
|-----|----------|-----------|------------|---------|-----------------|
|     |          | Real part | Imag. part | Damping |                 |
| 1.  | 98       | -0.14624  | 3.3501     | 4.361   | 0.534           |
| 2.  | 100      | -0.14092  | 3.3925     | 4.150   | 0.540           |
| 3.  | 102      | -0.14367  | 3.3613     | 4.270   | 0.535           |
| 4.  | 104      | -0.13581  | 3.4297     | 3.957   | 0.546           |
| 5.  | 106      | -0.13016  | 3.4805     | 3.737   | 0.554           |
| 6.  | 108      | -0.12582  | 3.5217     | 3.570   | 0.561           |
| 7.  | 110      | -0.1224   | 3.5574     | 3.439   | 0.567           |
| 8.  | 112      | -0.11985  | 3.59       | 3.337   | 0.572           |
| 9.  | 114      | -0.11876  | 3.6191     | 3.280   | 0.576           |
| 10. | 116      | -0.12317  | 3.6297     | 3.391   | 0.578           |

Table-10. Simulation result for L7 keeps constant at 100 MVA – using PSAT
toolbox

| No. | L9 (MVA) | Estimated damping (%) | | | Mode freq. (Hz) |
|-----|----------|-----------|-----------|---------|-----------------|
|     |          | Real part | Imag. part | Damping |                 |
| 1.  | 98       | -0.14903  | 3.3548    | 4.438   | 0.534           |
| 2.  | 100      | -0.14031  | 3.0741    | 4.560   | 0.490           |
| 3.  | 102      | -0.13621  | 3.0819    | 4.415   | 0.491           |
| 4.  | 104      | -0.13244  | 3.0901    | 4.282   | 0.492           |
| 5.  | 106      | -0.12903  | 3.0985    | 4.161   | 0.494           |
| 6.  | 108      | -0.12591  | 3.1087    | 4.047   | 0.495           |
| 7.  | 110      | -0.12306  | 3.1235    | 3.937   | 0.498           |
| 8.  | 112      | -0.12099  | 3.1468    | 3.842   | 0.501           |
| 9.  | 114      | -0.12471  | 3.1751    | 3.925   | 0.506           |

## 4.2.2. SIMULATION USING FFT-CWT APPROACH

Using the loading scheme as the previous section, there are two groups of calculation are applied. First keeps load in area 2 constant and step-by-step increase the load in area 1. First assessment keeps L9 constant and varies load in L7 as given in Table-11. The next keeps L7 to remain at 100MVA and varies the load in L9 from 98MVA to 116MVA as presented in Table-12. The details of calculation are presented from Figure-32 until Figure-50.

Table-11. Simulation result for L9 keeps constant at 100 MVA –
using FFT-CWT

| No. | L7 (MVA) | Estimated damping (%) | Mode freq. (Hz) |
|---|---|---|---|
| 1. | 98 | 4.4921 | 0.5143 |
| 2. | 100 | 4.0400 | 0.5306 |
| 3. | 102 | 3.9055 | 0.5306 |
| 4. | 104 | 3.6412 | 0.5388 |
| 5. | 106 | 3.5163 | 0.5469 |
| 6. | 108 | 3.4193 | 0.5469 |
| 7. | 110 | 3.3364 | 0.5551 |
| 8. | 112 | 3.2788 | 0.5551 |
| 9. | 114 | 3.2770 | 0.5551 |
| 10. | 116 | 3.1596 | 0.5633 |

Table-12. Simulation result for L7 keeps constant at 100 MVA – using
FFT-CWT

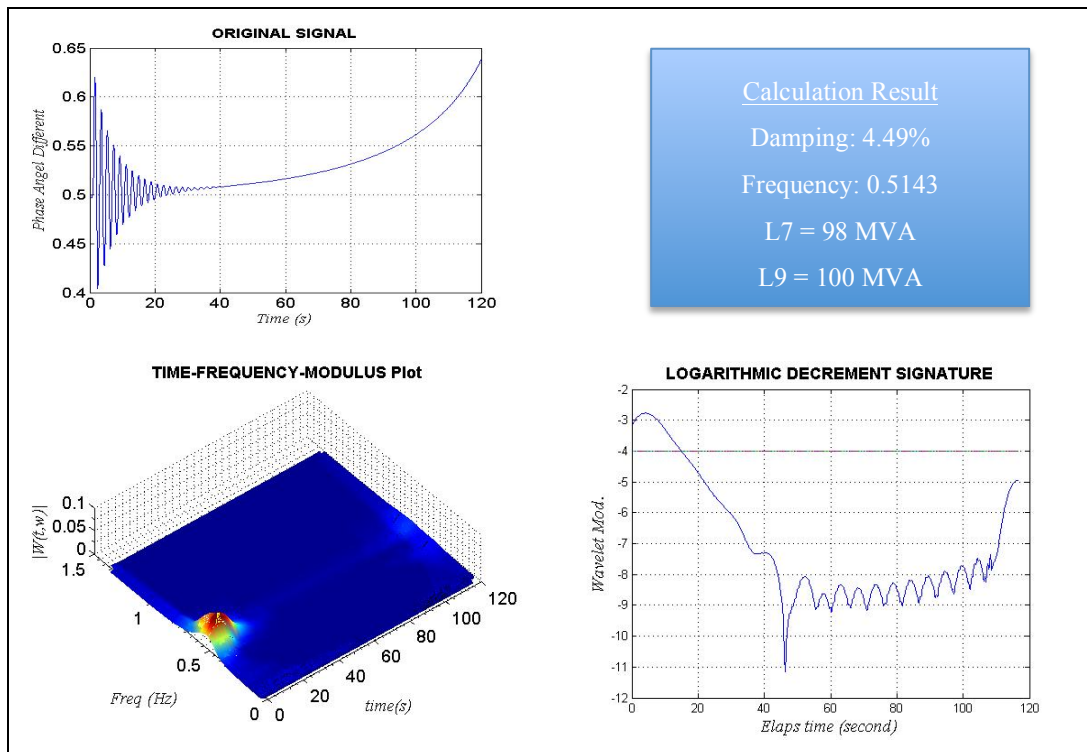| No. | L9 (MVA) | Estimated damping (%) | Mode freq. (Hz) |
|---|---|---|---|
| 1. | 98 | 4.6039 | 0.5280 |
| 2. | 100 | 4.4532 | 0.4800 |
| 3. | 102 | 4.4261 | 0.4800 |
| 4. | 104 | 4.3481 | 0.4800 |
| 5. | 106 | 4.2376 | 0.4800 |
| 6. | 108 | 4.1110 | 0.4800 |
| 7. | 110 | 3.9722 | 0.4800 |
| 8. | 112 | 3.8362 | 0.4800 |
| 9. | 114 | 3.2223 | 0.4960 |

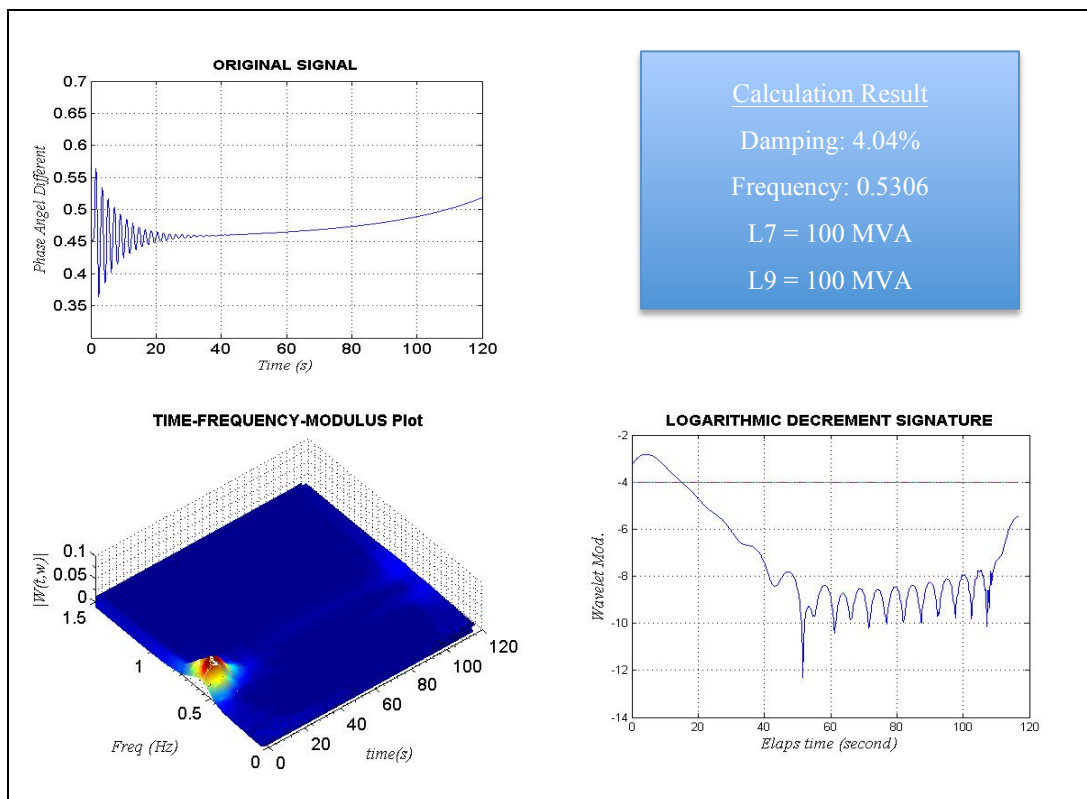Figure-32. Load in area 1: 98MVA and area 2: 100MVA



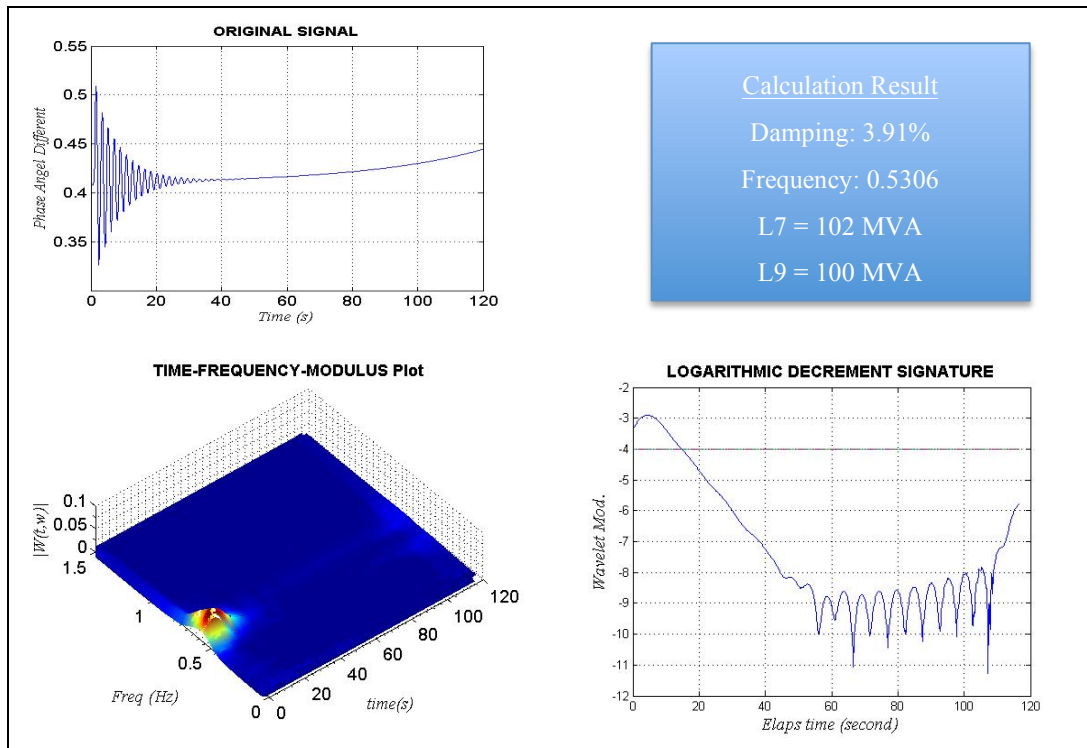Figure-33. Load in area 1: 100MVA and area 2: 100MVA

70

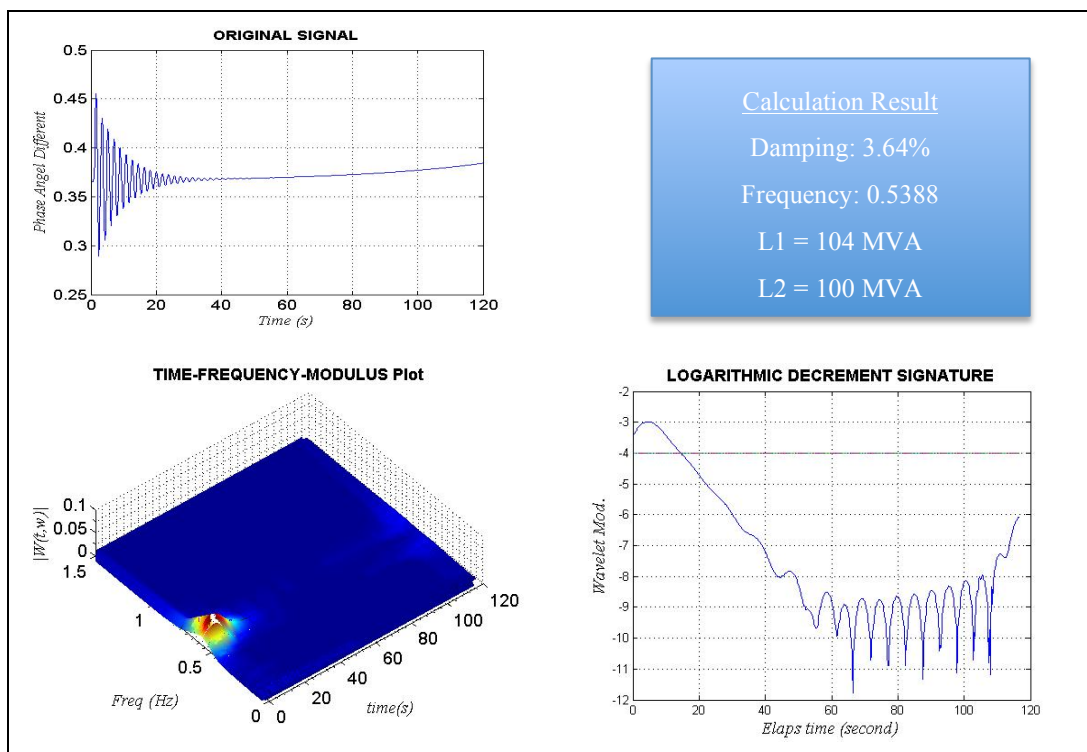Figure-34. Load in area 1: 102MVA and area 2: 100MVA



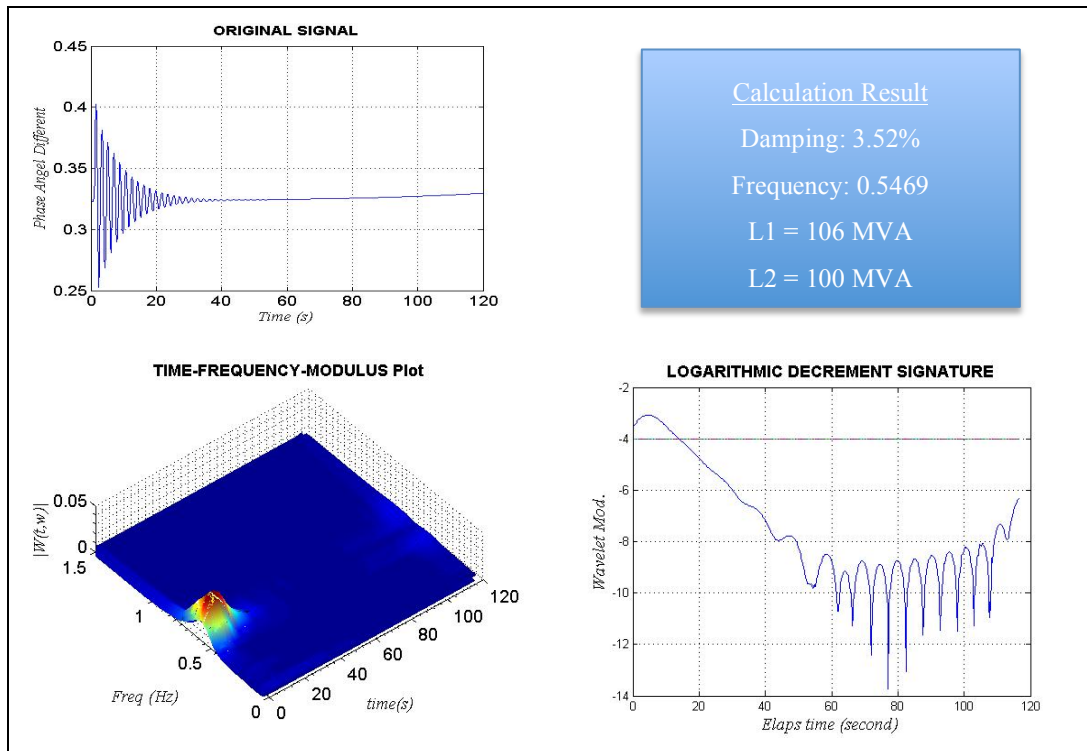Figure-35. Load in area 1: 104MVA and area 2: 100MVA

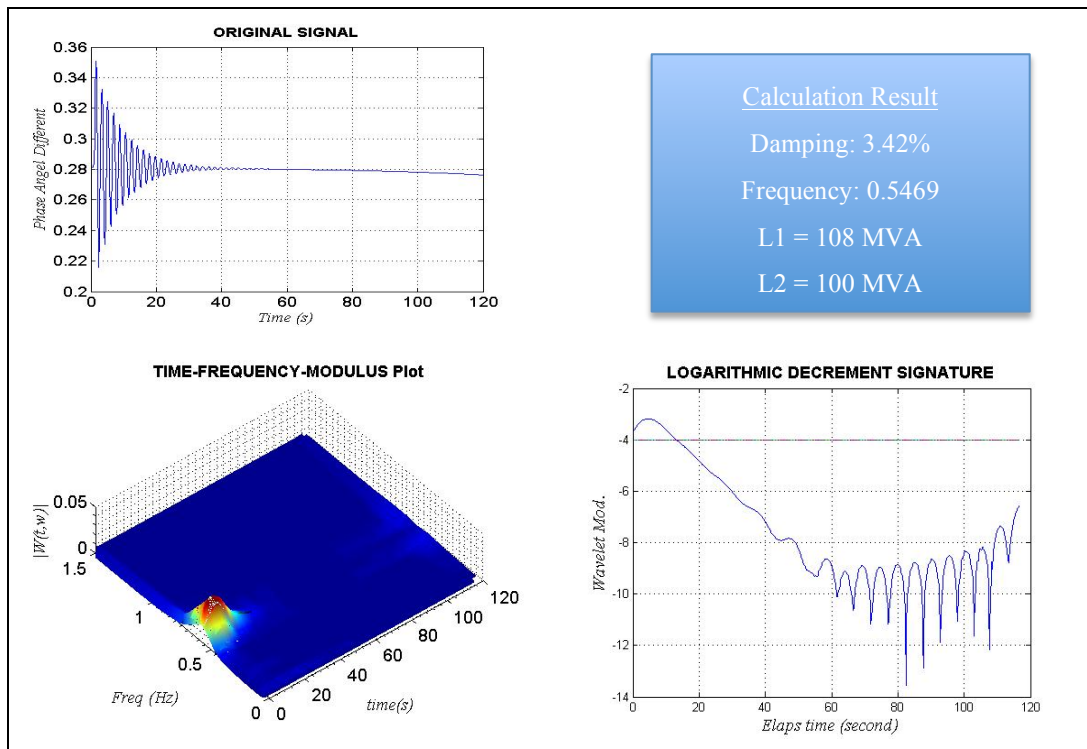Figure-36. Load in area 1: 106MVA and area 2: 100MVA



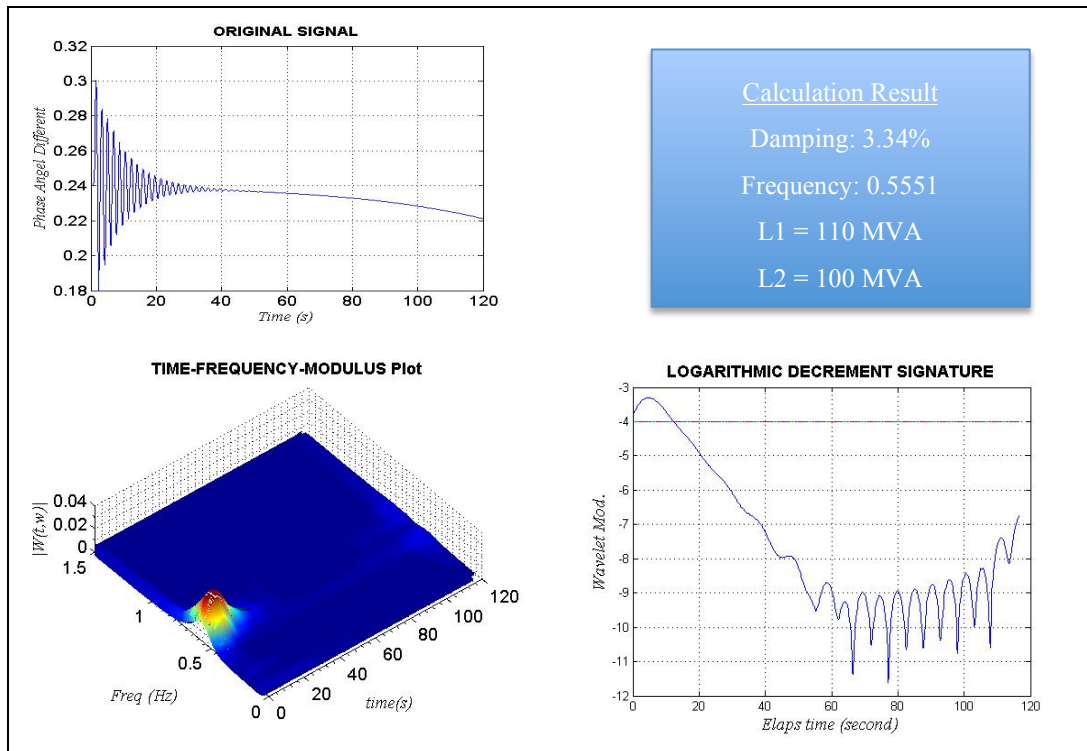Figure-37. Load in area 1: 108MVA and area 2: 100MVA

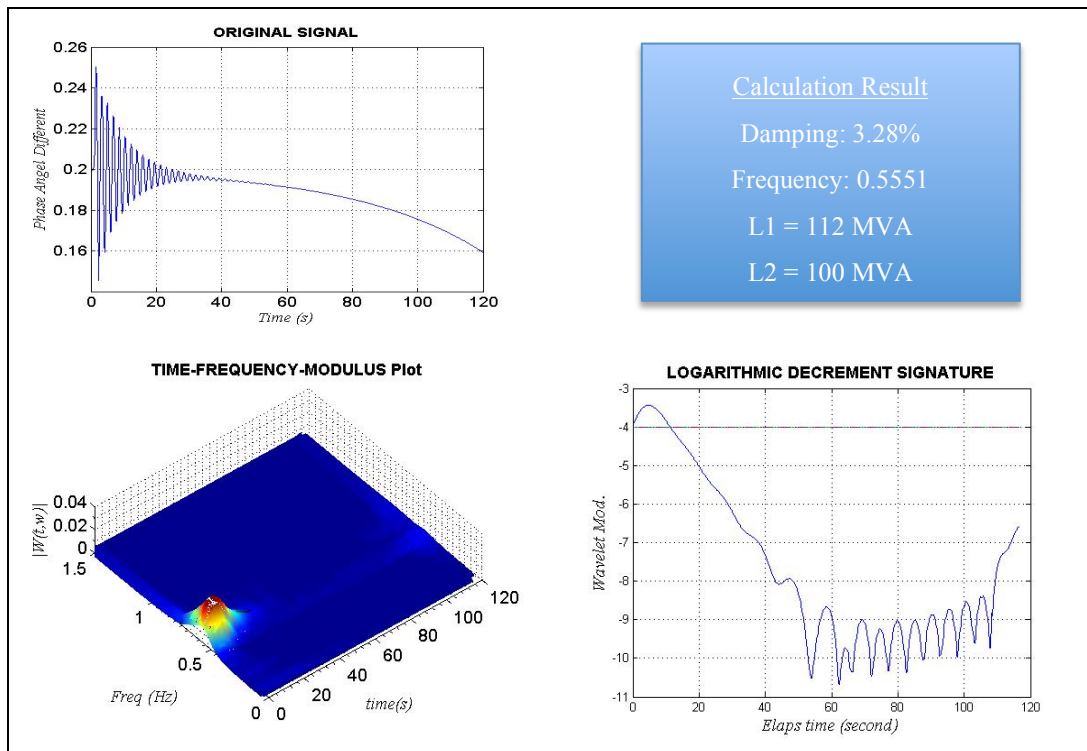Figure-38. Load in area 1: 110MVA and area 2: 100MVA



Figure-39. Load in area 1: 112MVA and area 2: 100MVA

Figure-40. Load in area 1: 114MVA and area 2: 100MVA



Figure-41. Load in area 1: 116MVA and area 2: 100MVA

Figure-42. Load in area 1: 100MVA and area 2: 98MVA



Figure-43. Load in area 1: 100MVA and area 2: 100MVA
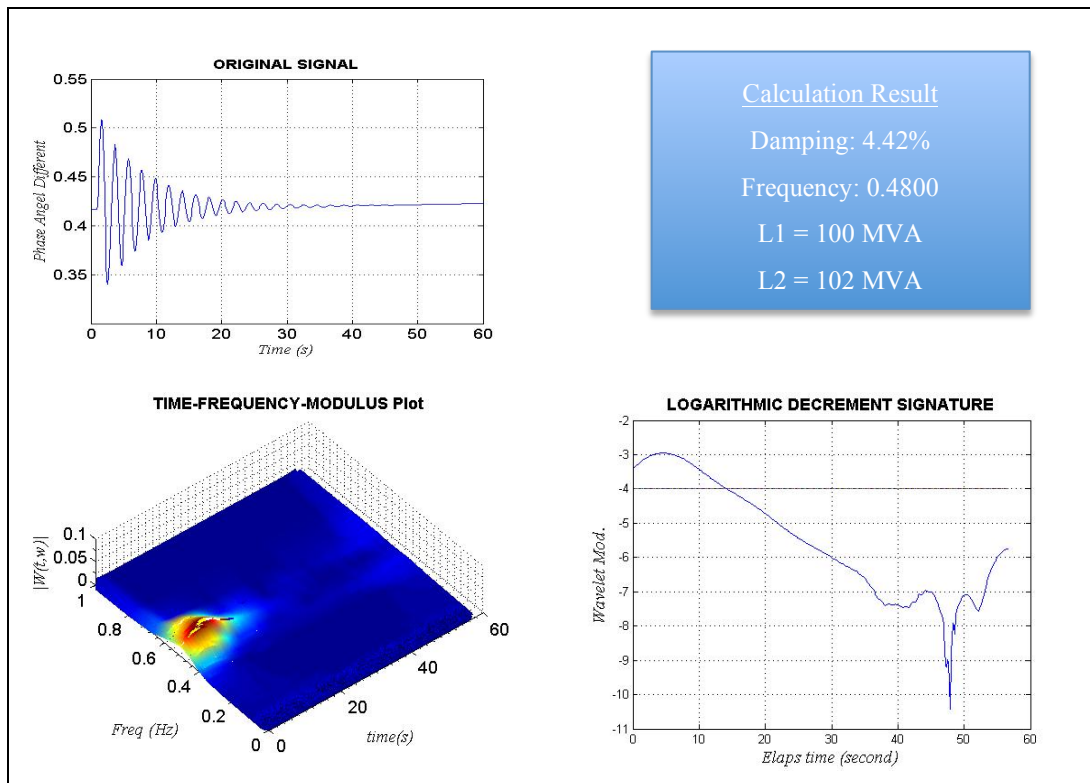
Figure-44. Load in area 1: 100MVA and area 2: 102MVA
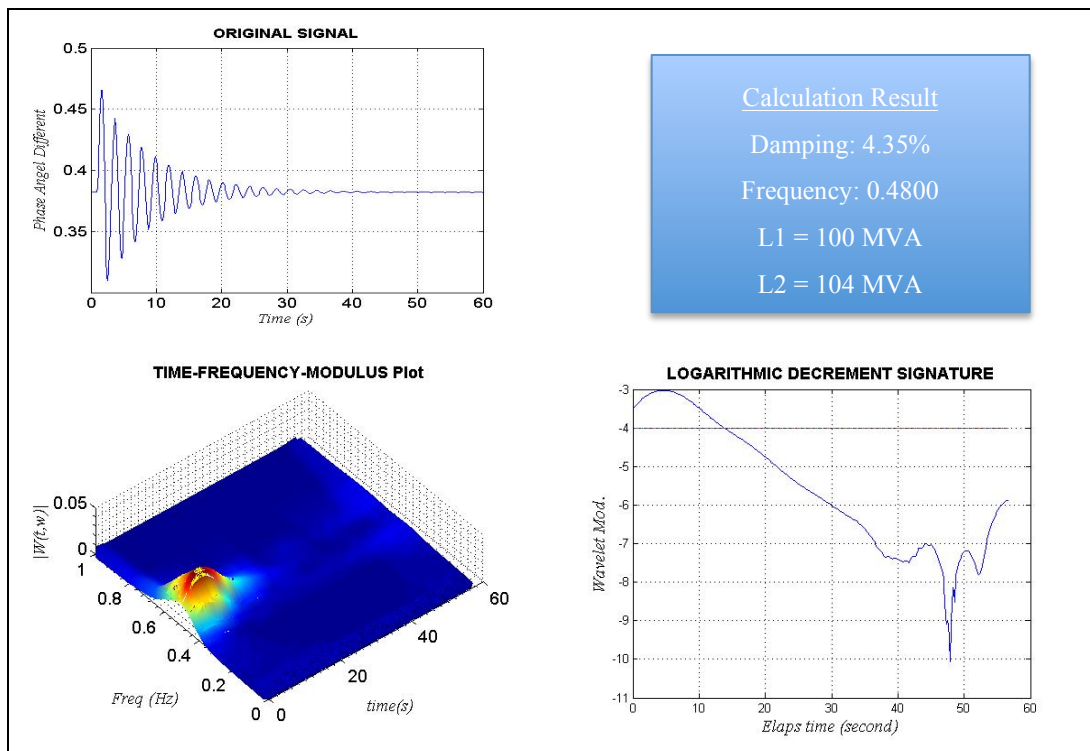


Figure-45. Load in area 1: 100MVA and area 2: 104MVA
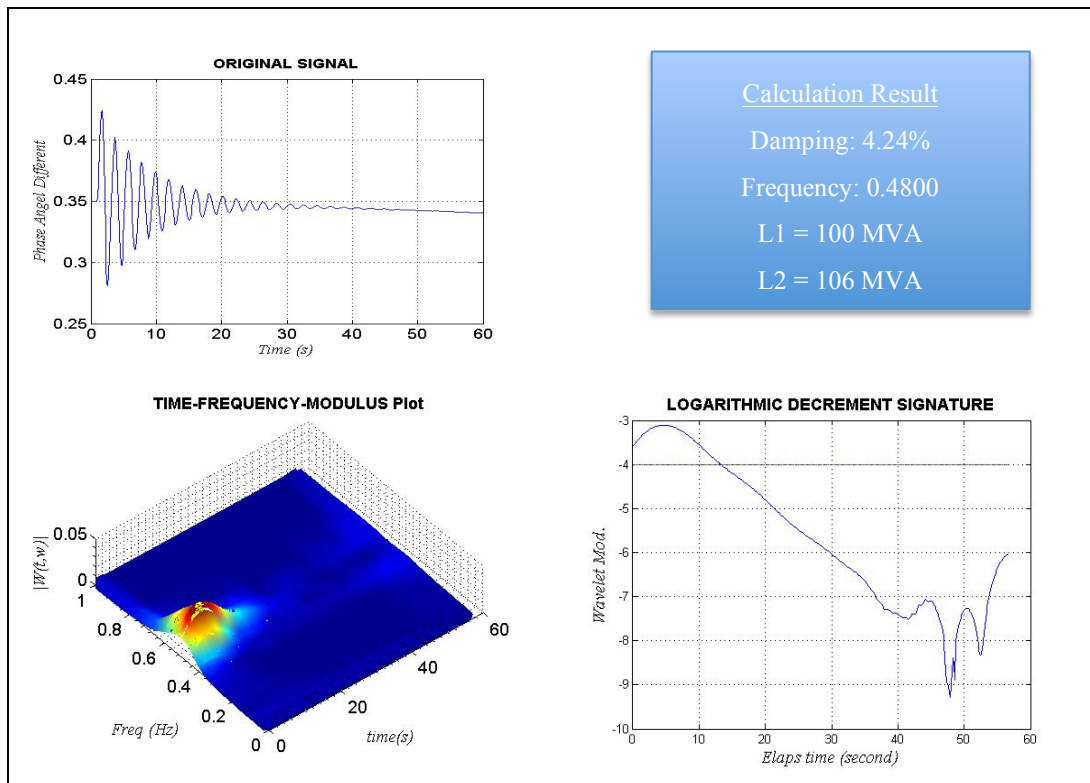
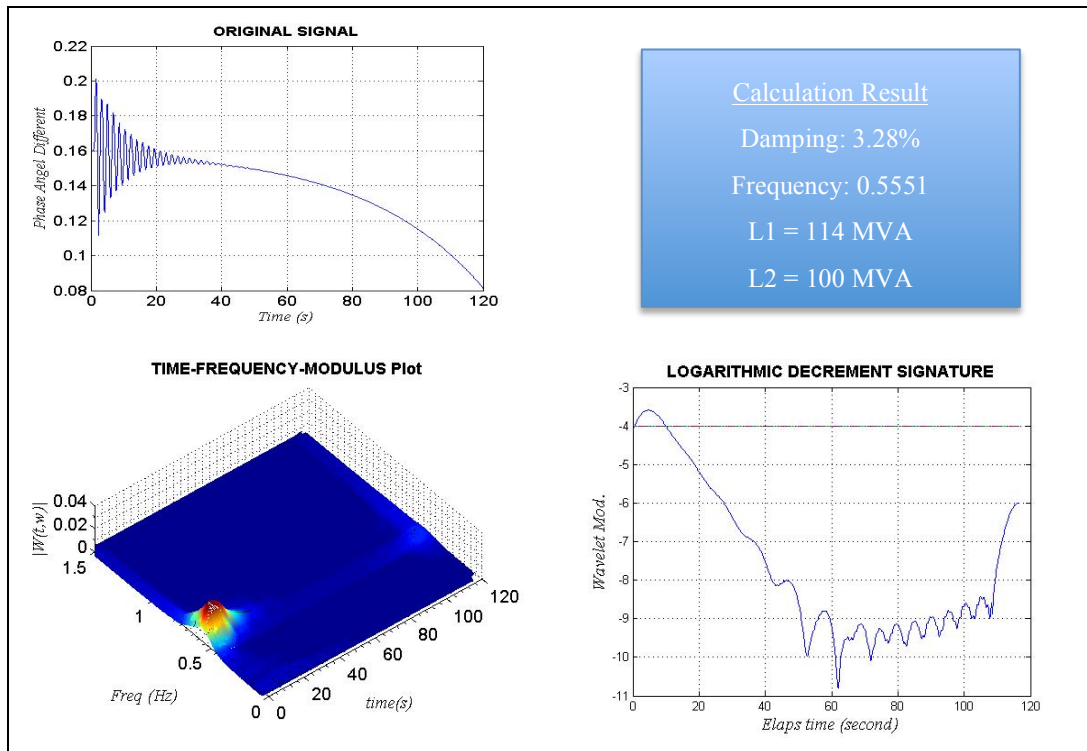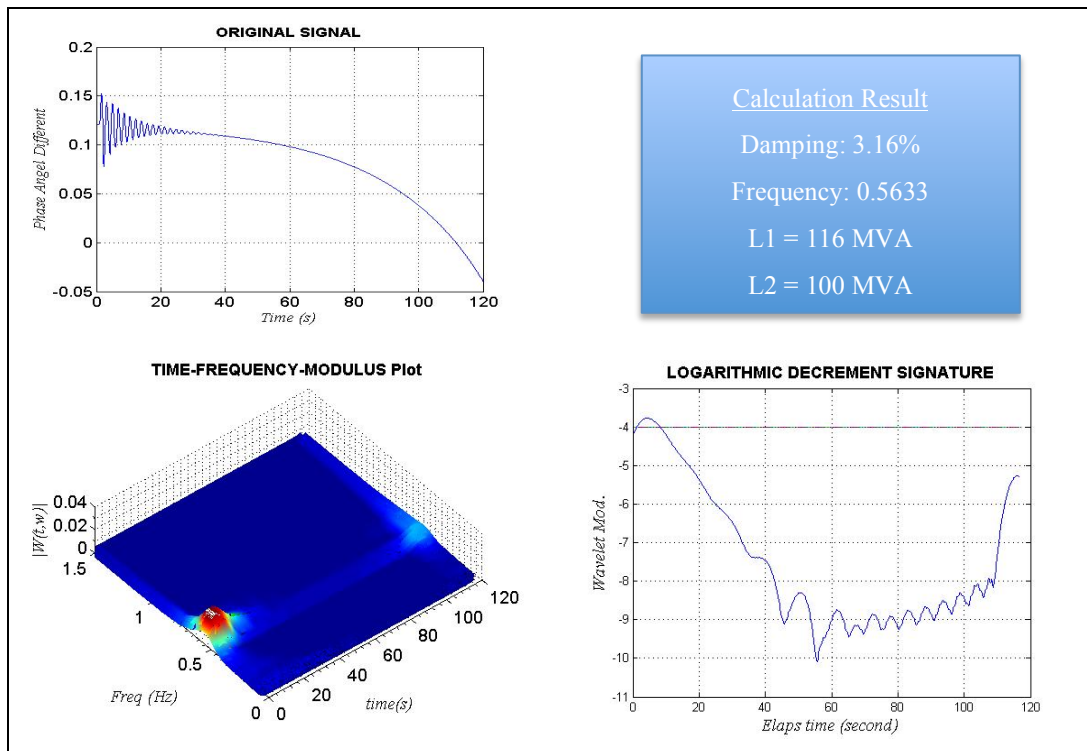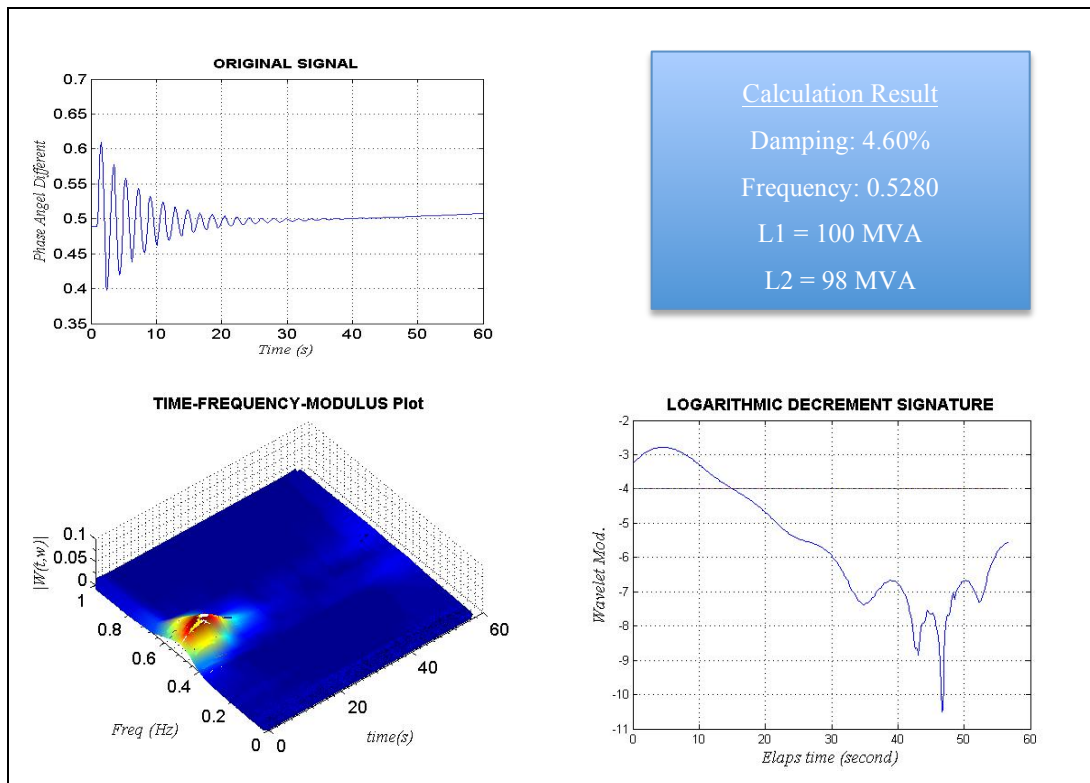Figure-46. Load in area 1: 100MVA and area 2: 106MVA
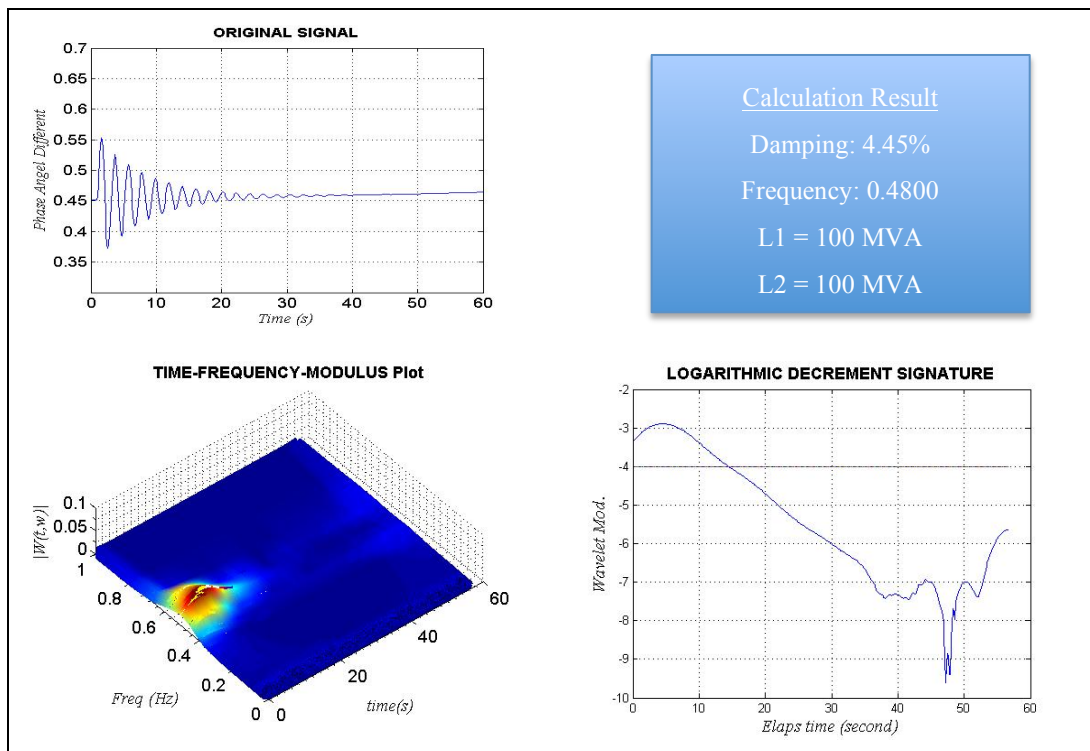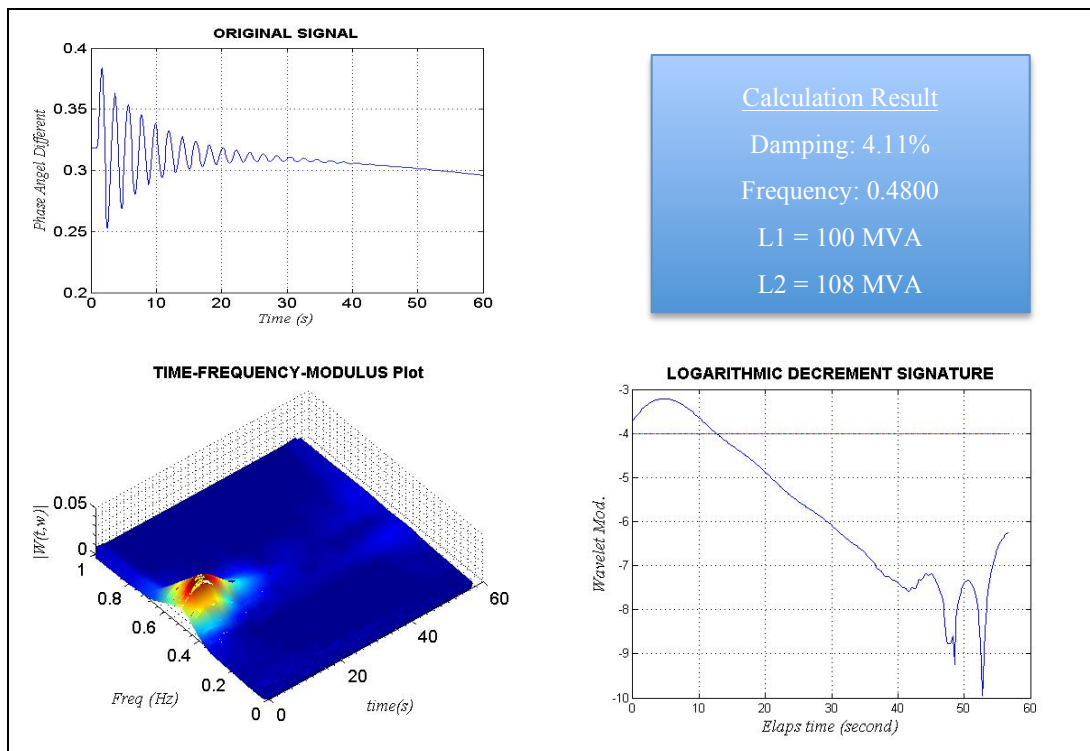


Figure-47. Load in area 1: 100MVA and area 2: 108MVA
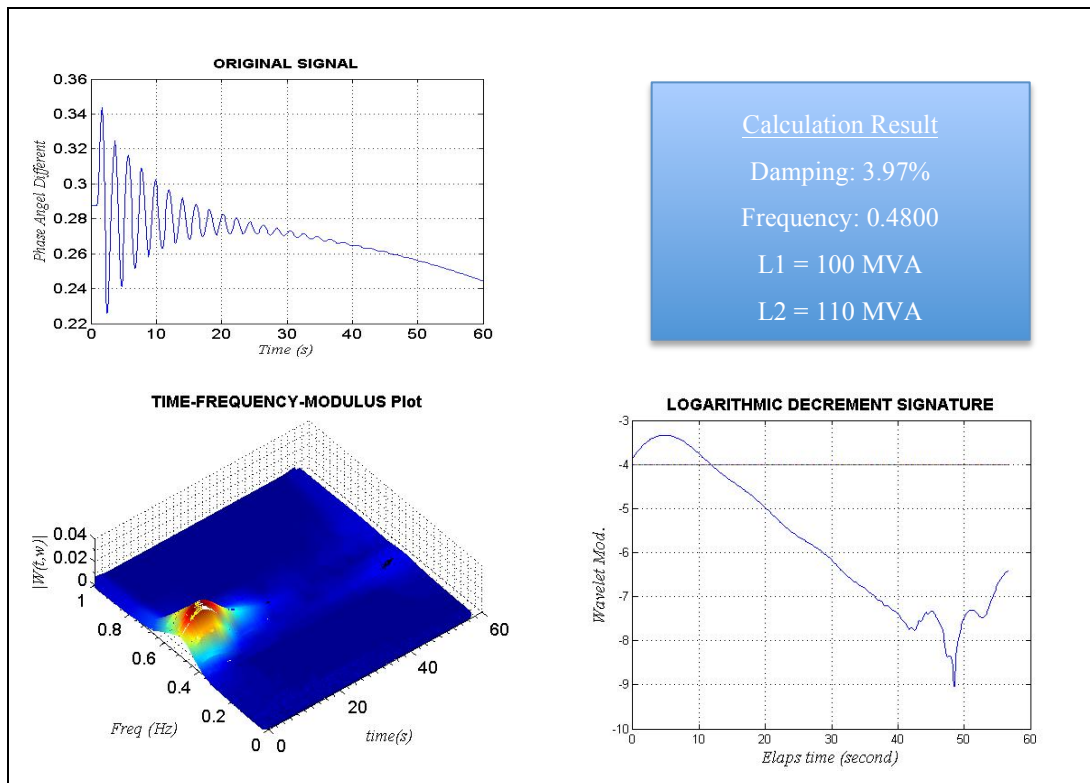
Figure-48. Load in area 1: 100MVA and area 2: 110MVA
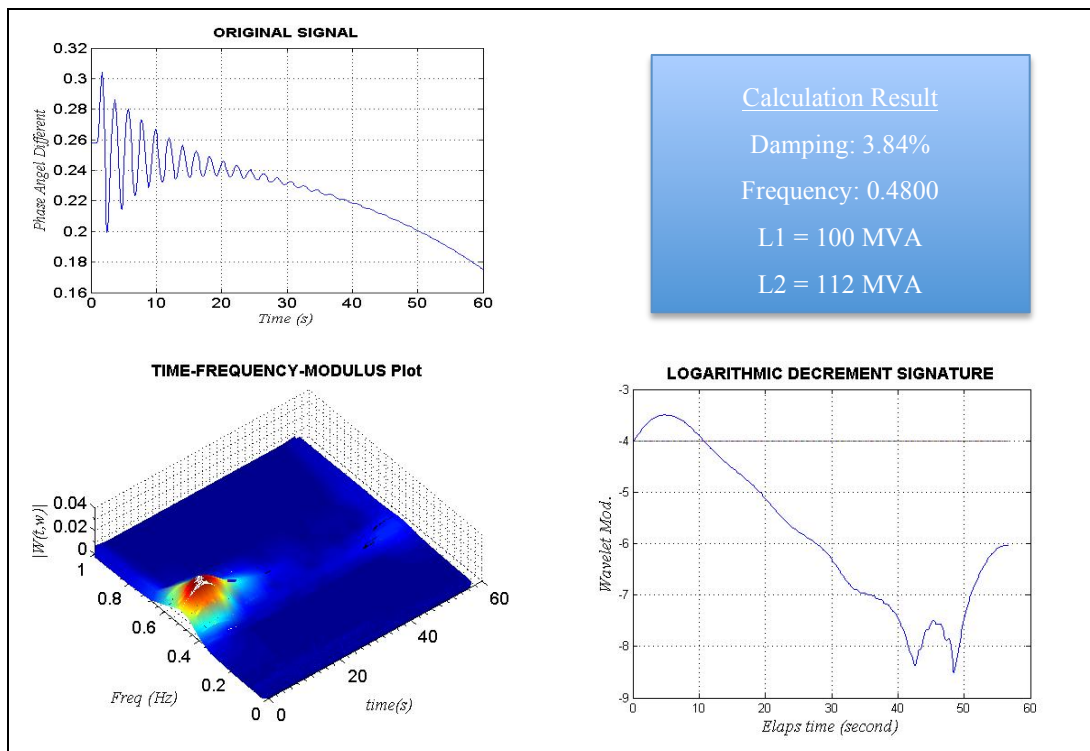


Figure-49. Load in area 1: 100MVA and area 2: 112MVA
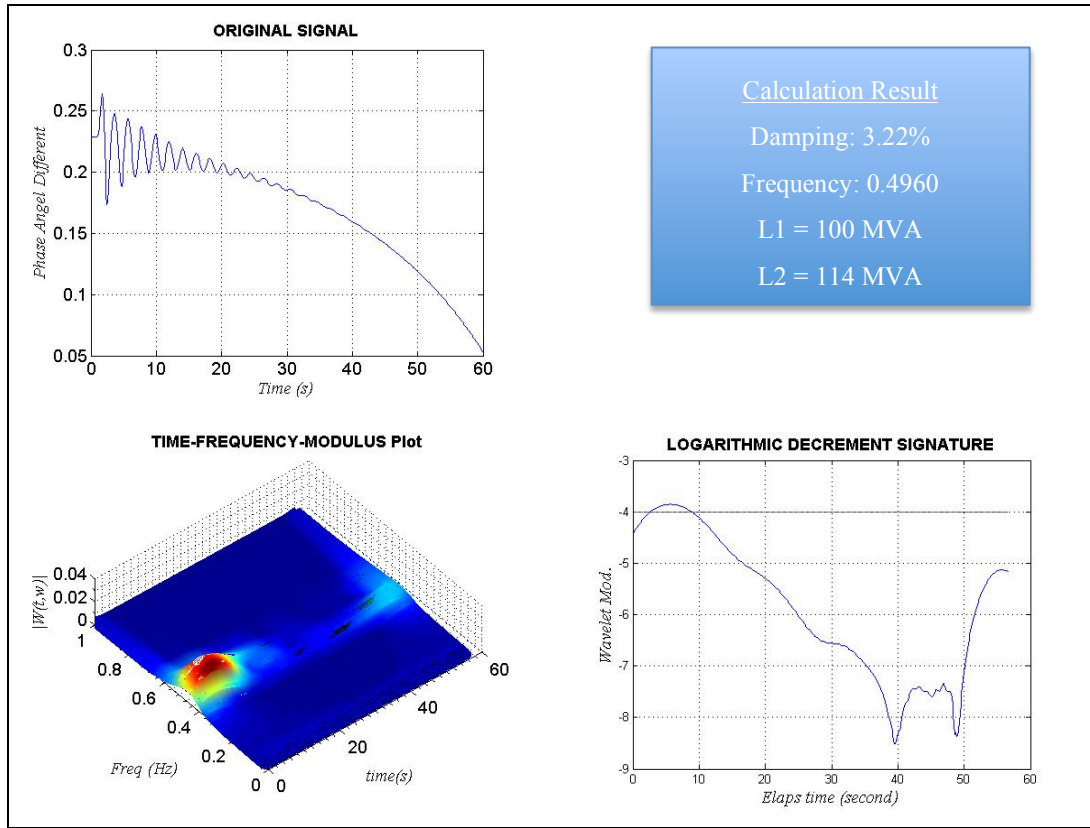
Figure-50. Load in area 1: 100MVA and area 2: 114MVA

### 4.2.3. THE RESULT OF FFT-CWT COMPARED TO EIGENVALUE BASED CALCULATION

Figure-51 and Figure-52 illustrate the accuracy of the proposed method referred to the result of calculation using the PSAT Toolbox. The comparison of the two approaches for every group of simulation also presented in Table-13 and Table-14. It is clearly shown the comparison between the result from the eigenvalue based and the result calculated using the FFT-CWT method. This result confirms that the FFT-CWT method is robust enough to use in small signal stability assessment in a power system.

79

Table-13. Damping by FFT-CWT vs. eigenvalue based, Load simulation in L7

| No. | FFT-CWT (%) | Eigenvalue based (%) |
|-----|-------------|----------------------|
| 1.  | 4.4921      | 4.361                |
| 2.  | 4.0400      | 4.150                |
| 3.  | 3.9055      | 4.270                |
| 4.  | 3.6412      | 3.957                |
| 5.  | 3.5163      | 3.737                |
| 6.  | 3.4193      | 3.570                |
| 7.  | 3.3364      | 3.439                |
| 8.  | 3.2788      | 3.337                |
| 9.  | 3.2770      | 3.280                |
| 10. | 3.1596      | 3.391                |

Table-14. Damping by FFT-CWT vs. eigenvalue based, Load simulation in L9

| No. | FFT-CWT (%) | Eigenvalue based (%) |
|-----|-------------|----------------------|
| 1.  | 4.6039      | 4.438                |
| 2.  | 4.4532      | 4.560                |
| 3.  | 4.4261      | 4.415                |
| 4.  | 4.3481      | 4.282                |
| 5.  | 4.2376      | 4.161                |
| 6.  | 4.1110      | 4.047                |
| 7.  | 3.9722      | 3.937                |
| 8.  | 3.8362      | 3.842                |
| 9.  | 3.2223      | 3.925                |
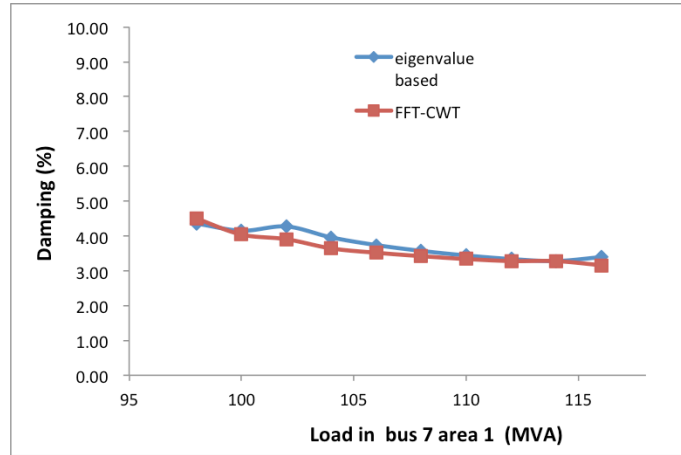
Figure-51. Damping ratio by FFT-CWT vs. eigenvalue based, Load simulation in L7
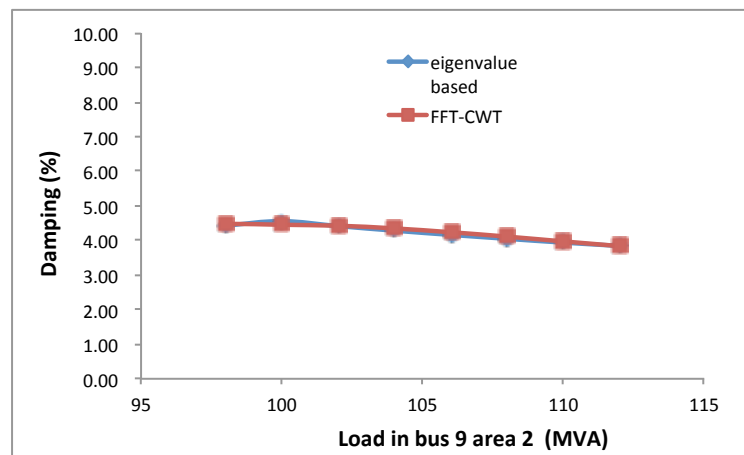


Figure-52. Damping ratio by FFT-CWT vs. eigenvalue based, Load simulation in L9

## 4.3. APPLICATION ON THE REAL PMU DATA ANALYSIS

The difference between simulated data and real data from PMU is that in real data contains some noises and bad form of data such as coinciding data or an impulse peak at the and of signal which can not be analyzed due to no slope to be counted in. the following Figure-53 depicts this situation.
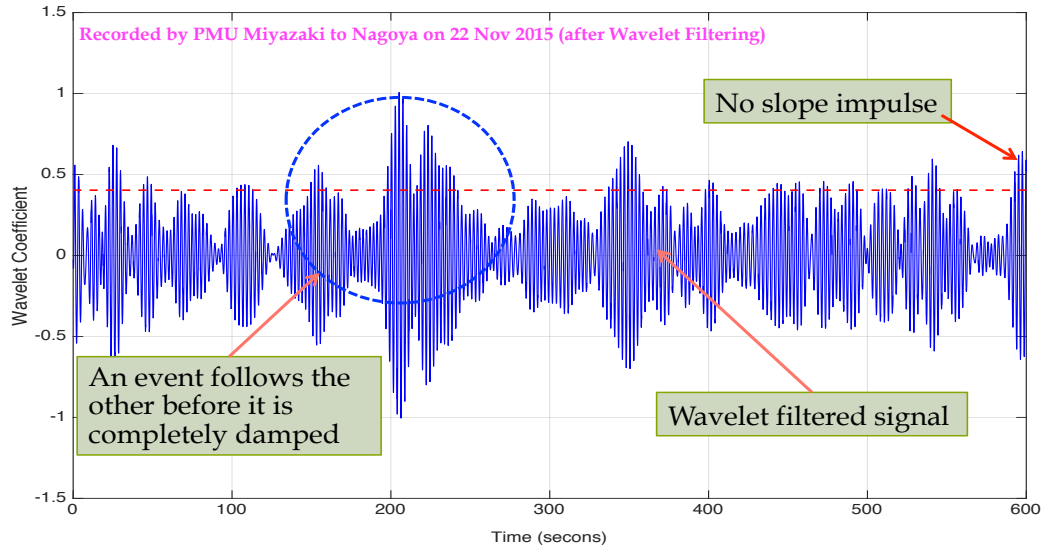
Figure-53. Wavelet filtered signal from PMU data

By introducing a kind of threshold, it can be determined which part of signal can be analyzed. It is noticed that when a higher level of threshold applied, it will collect samples with higher magnitude but less in number. In the other hand, the lower threshold gather more samples but prone to noise interference or coinciding signal.

Assuming the signal behavior is linear and the system is excited by random variations that are Gaussian distributed, the standard threshold is selected as √2.std (Wavelet Coefficient).

Under the assumption that the power system is linier and excited by random variations that are Gaussian distributed, then the average of damping of a set of random decrement defined as:

$$\xi_{av} = \frac{1}{N} \sum_{s=1}^{N} \xi_N(t_s : t_s + \tau)$$

(43)

where $N$ is the number of impulse can be included in the analysis determined from how many impulses touch the threshold level.

Figure-54 presenting the numbers of impulses touched the threshold level.
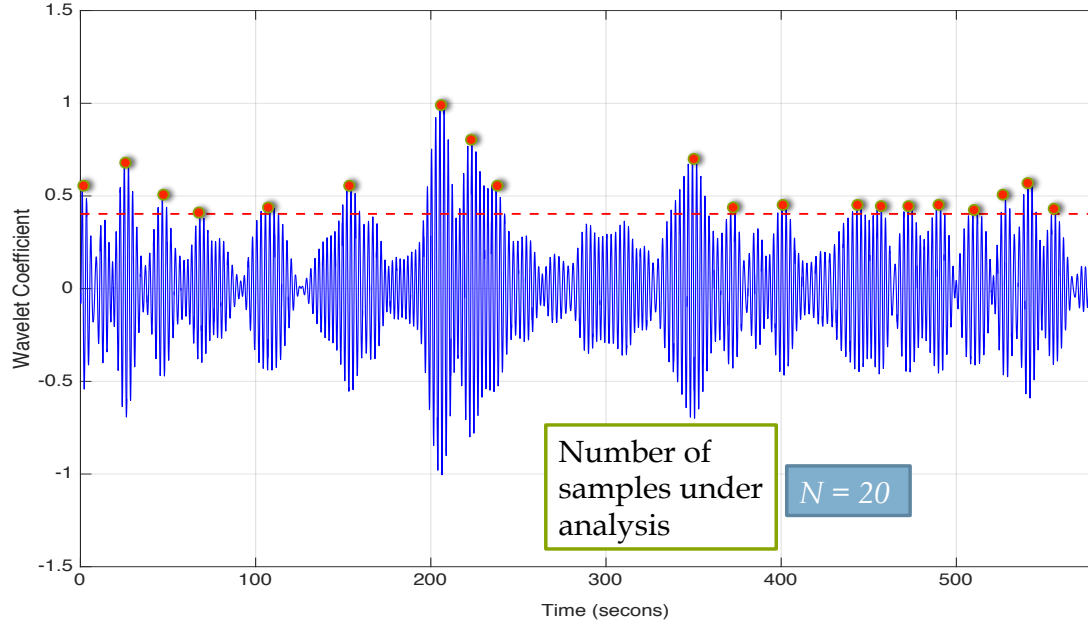


Figure-54. Number of impulses can be counted

Each of wavelet impulse then treated using the equation (38). The interval of analysis time for each segment is around 10 second, which is common happened to inter-area oscillation (P. Kundur, Power system stability and control, p.26) [2]. Figure-55 presents the signal segment lasting from 205th second to 215th second.
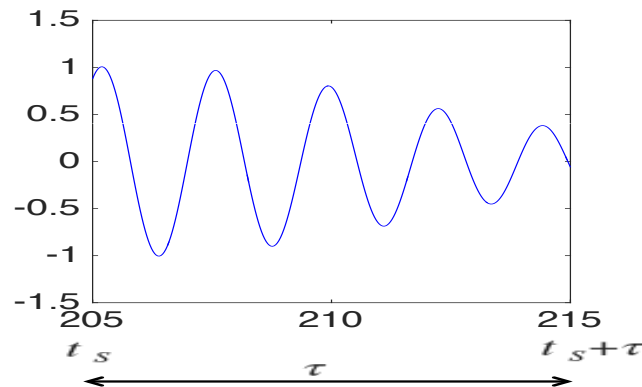


Figure-55. Wavelet coefficient segment of a PMU data

To deal with the real PMU data, some signals from PMU in Japan Campus WAMS are investigated. Figure-56 shows waveforms of phase difference measured between University of Miyazaki and Nagoya Institute of Technology (NIT) from 14:30 to 14:50 in 4th of October 2011. During that time the Genkai nuclear power unit 4 that belongs to Kyushu Electric Power Company stop automatically. The fluctuation pattern of the oscillation is presented in that figure.

Contour plot of the corresponding signal shows the center of oscillation is depicted on Figure-57. It is consistent to the theory that small signal stability appears in the range of 0.4 to 1 Hz [2].
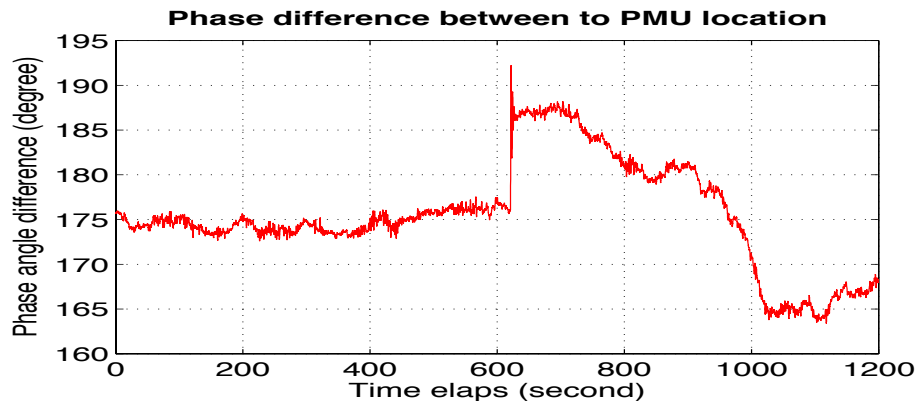


Figure-56. PMU measurement from Miyazaki Univ. to Nagoya Inst. of Technology
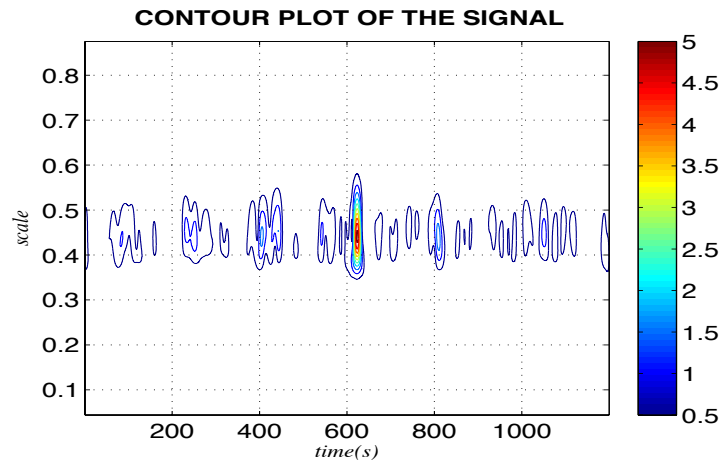


Figure-57. Contour plot of PMU signal on 4th Oct 2011

84
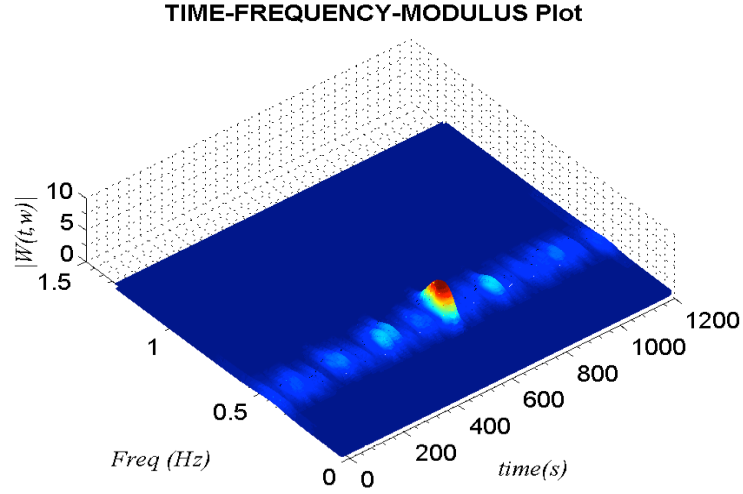
Figure-58. The 3-D plot of Wavelet of PMU signal on 4th Oct. 2011

From Figure-58, it can be clearly seen the ridge of the signal oscillation. The damping ratio can be calculated from demodulating the slice signal at the center of frequency oscillation. Figure-59 and Figure-60 show logarithmic decrement and phase decrement plot of the signal from the ridge of the oscillation until the oscillation disappears at 624 second. Using linear regression analysis the value of $\alpha_d$ and $\omega_d$ can be estimated and based on the equation (38) the damping ratio is determined as 0.045 at damped frequency $f_d = 0.4462$ Hz.
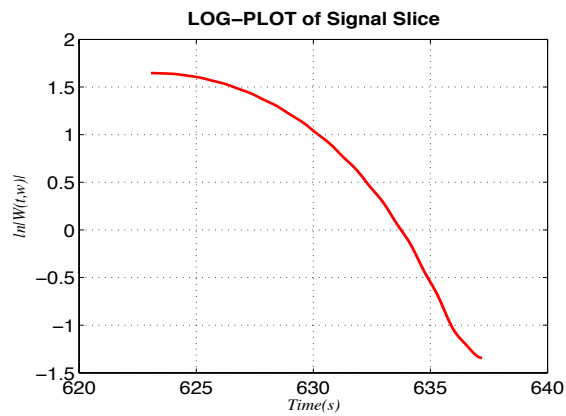


Figure-59. Logarithmic decrement of Wavelet Signal

85
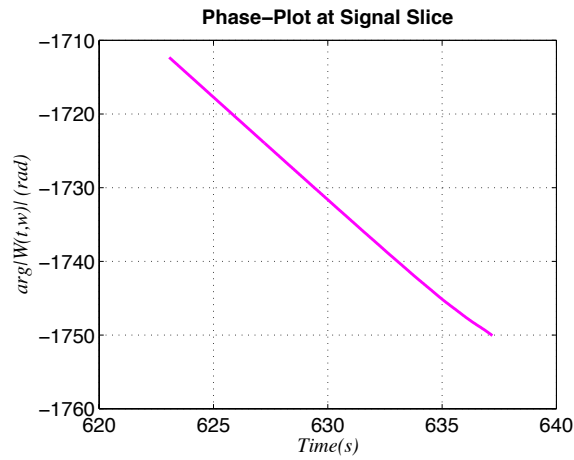
Figure-60. Phase plot of PMU signal

The next evaluation is the event on 24th August 2003, when one unit of power plant in Kanda near Kitakyushu was shut down due to technical problem at around 18:50 to 19.10 time interval of PMU gathering data as shown in Figure-61. From the figure, it can be seen there was a sudden change of patterns in around 700th second to 800th second of data recording.
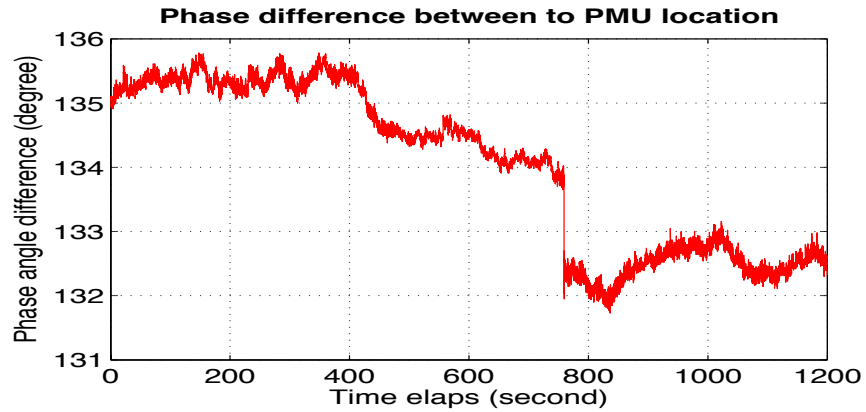


Figure-61. PMU data on 24th August 2003

Using the same procedure from the previous analysis, logarithmic decrement and phase decrement of the signal skeleton are given in Figure-62 and

Figure-63 respectively. The damping ratio for this time event is 0.051 at 0.4143 Hz damped frequency.
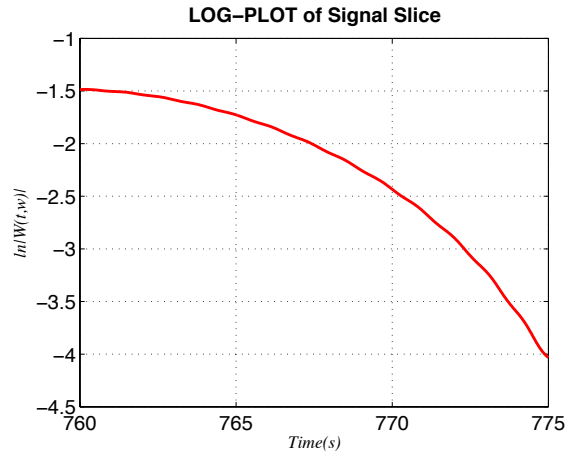


Figure-62. Logarithmic decrement of PMU signal
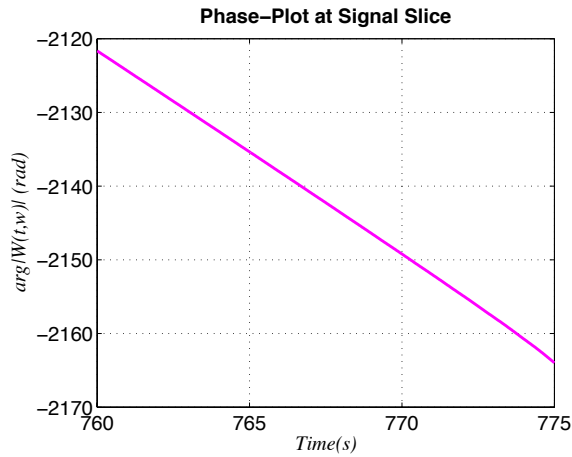


Figure-63. Phase decrement of PMU signal

To monitor the system stability during the day, a PMU signal from Miyazaki to Nagoya at the same day as aforementioned disturbance is evaluated. Damping ratio trend for 24 hours at the day Genkai shutdown on 4th of October 2011 is presented in Figure-64. The fluctuations are in between 2% to 4% that means the system is still remains on stable region.
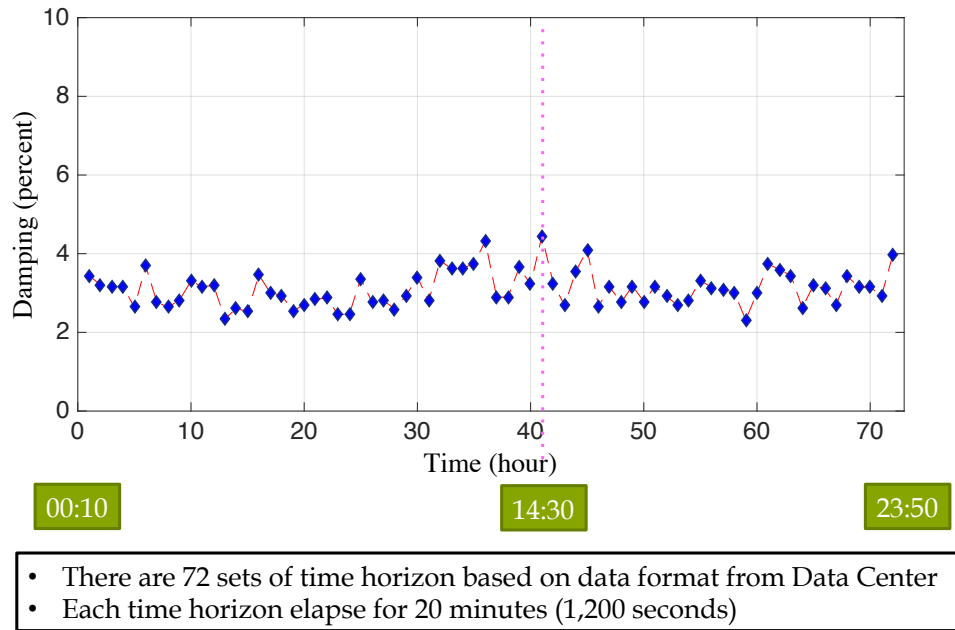
Figure-64. Damping ratio trend for 24 hours monitoring

## 4.4.  SUMMARY

This FFT-CWT approach is robust enough to identify inter area oscillation mode in the system as well as to calculate the damping ratio based on the information extracted from the PMU data without knowing the parameters of the system. The accuracy of this method was verified by comparing to the result of the PSAT toolbox calculation. It was demonstrated that the results of the two approaches confirmed each other, means that this FFT-CWT is reasonable to estimate the damping ratio of a small signal oscillation in a power system. The novelty of this method is that system parameter are not involved in the calculation process such as in the PSAT toolbox.

It also presented the FFT-CWT approach is capable to detect modal frequency oscillation as well as calculating the damping ratio based on the information extracted from the PMU data without associating the parameters to a power system model.

88

# Chapter 5.

# WIDE AREA SIGNAL DAMPING CONTROLLER

## 5.1.  INTRODUCTION

Power System is a complex system consisting of generations, transmissions and loads. Load centers are connected to generator through transmission network. When the growth of demand is not followed by expanding of new power plants and transmission line capacity, it will forced the power systems operator drive the system close to its operation limits.

In some countries, where mostly consist of generations that un-evenly distributed, a large amount of power is transferring through a weak transmission lines between subsystems having surplus of generations to the heavily loaded subsystem. These conditions weakened the power systems and hence becoming more vulnerable to any disturbance. If a disturbance occurs, generators will oscillate each other. Lack of damping torque will lead to an un-damped oscillation, and cause loss of synchronism among generators.

To prevent system from un-damped oscillation witch will cause domino effect to the system and lead to cascading failure to the overall power system, a well design damping controller should be provided. However, to deal with this

issue, some challenge must be addressed. One major challenge in damping control design is the selection of feedback input signals.

The damping itself is defined as the energy dissipation properties of a system. Power oscillation can be damped, when extra energy is injected or consumed to compensate the decelerated or accelerated system. The damping energy must have the correct phase shift relative to the accelerated or decelerated system as incorrect phase angles can even excite the oscillations. Figure-65 shows the different possibilities to damp power system oscillations [67].
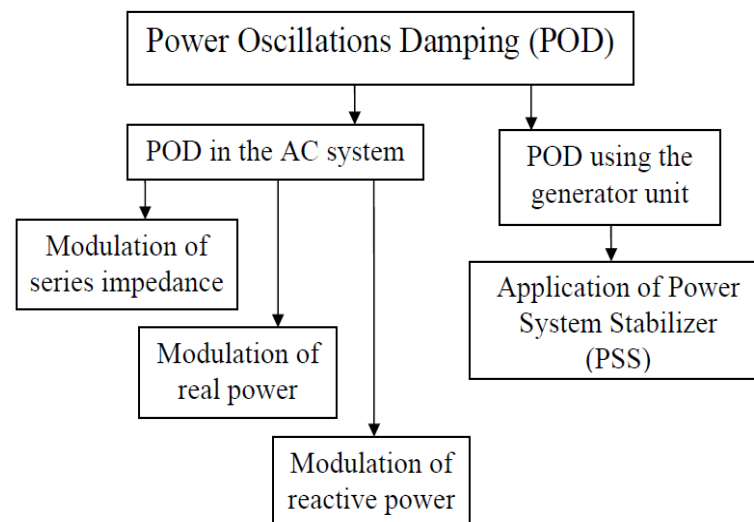


Figure-65. The possibility of damper technique in power system

Conventionally, Power System Stabilizers (PSSs) uses local measurements as the input signals such as active power in the outgoing transmission line, generator speed, and frequency at the terminal bus. With the availability of signals from phasor measurement units (PMUs), choices of inputs are not only limited to those local but now include wide-area signals.

## 5.2. POWER TRANSFER AND SMALL SIGNAL STABILITY

Small-signal stability is one form of the angle stability commonly observed in power systems. It refers to the ability of a power system to withstand small but continuous disturbances in a system. Small-signal stability problems usually appear as poorly damped oscillations in the system, which often cause security violations. They might even lead to system-wide blackouts such as the events discussed in chapter one of this thesis.

To make clear the relationship between power flow and the small signal stability, the observation through a simple Single Machine Infinite Bus (SMIB) system is exercised. Transfer function of SMIB considering the field circuit dynamic and effect of excitation system can be seen as in Figure-66.

Through Automatic Voltage Regulator (AVR), the field flux variations are induced by the field voltage variations as a supplement to the armature reaction. The flux variation is given in (44).
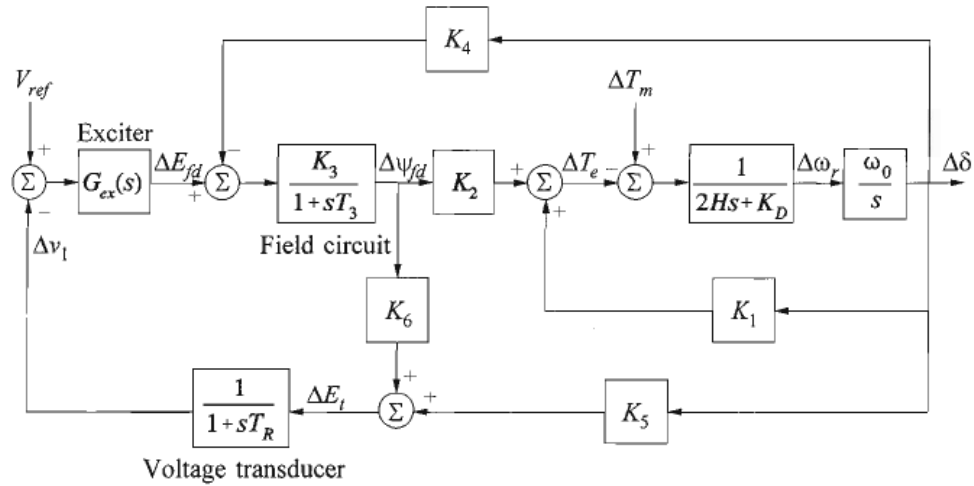


Figure-66. Effect of excitation to the system dynamic

$$\Delta\psi_{fd} = \frac{-K_3(K_4(1 + sT_R) + K_5 G_{ex}(s))}{s^2 T_3 T_R + s(T_3 + T_R) + 1 + K_3 K_6 G_{ex}(s)}\Delta\delta \qquad (44)$$

And the air gap torque due to change in field flux linkage is:

$$\Delta T_e = K_2 \Delta\psi_{fd} \qquad (45)$$

Since the effect of term $K_3\big(K_4(1 + sT_R)\big)$ are relatively small compared to term $K_5 G_{ex}(s)$, damping torque is primary influenced by K5. Torque due to the change of flux linkage is depends on K2, K3, K4, K5 and K6. The constant K2, K3, K4 and K6 usually positive, however K5 can be positive or negative depending on the external network and operating condition (generator output). With K5 positive, the effect of the AVR is to introduce a positive damping torque component. The constant K5 is positive for low value of external system reactance and low generator output. High value of external system reactance and high generator output cause K5 become negative [68].

## 5.3.  DESIGN OF CONTROLLER

The inter-area oscillations often suffer from poor damping since power systems generally operate closely to their maximum transfer capability due to some reason as discussed in section 5.1 in this chapter. In that case, the inter-area oscillations must be effectively damped. Conventionally, they are damped together with the local mode oscillations by tuning power system stabilizers (PSSs) installed on the excitation systems of the synchronous generators or designing decentralized local controllers.

The effectiveness of such controllers to damp inter-area oscillations is limited due to the inter-area signals are not always controllable or observable or both from the local signals [68]. With the development of wide-area measurement system (WAMS) and deployment of synchronized phasor measurement units,

wide-area damping controllers based on PMU signals have been proposed to enhance the damping of the inter-area oscillations [68], [69], [70], [71].

In the practical application, implementation of wide area damping controllers will require a communication channels to transmit the signals. This transmitting signal process will result such a time delays into the control-loop of the controller. It can typically range from tens to several hundred milliseconds, depending upon the type of communication channels, routines of signal transmission, transmission protocols, and communication loads. The time delays would degrade system damping performance or even cause system instability without properly encounter in the system design.

The proposed design of the wide area damping controller is shown in the Figure-67.
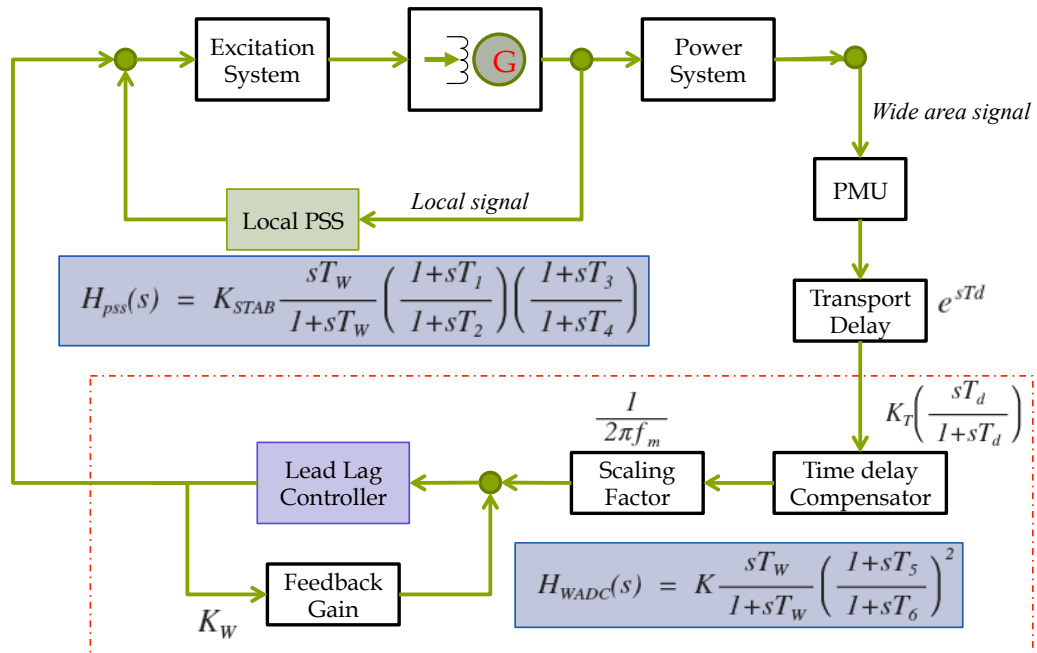


Figure-67. Configuration of wide area damping controller

## 5.4. SIMULATION RESULT

To verify the contribution of the wide area signal input to the inter-area oscillation damping, the Two Area Four Machine model in Figure-68 is used again here. Two PMUs are located in bus 2 and bus 4 correspondingly. Because of bus 2 and bus 3 are identical, including its generator capacity then allocating one PMU in one of them will represent the subsystem in area 1. Bus 2 will represent the area 2 and one PMU is allocated on it.

In a bigger system with multiple PMU, it should be determined the most dominant path that contributes the dominant inter-area oscillation in the system. Since it is more complicated then it will not discussed here. It should be a future work after this thesis.

A three-phase fault in the middle of weak tie line is applied. The Simulink model for this simulation is given in Figure-69 and Figure-70.
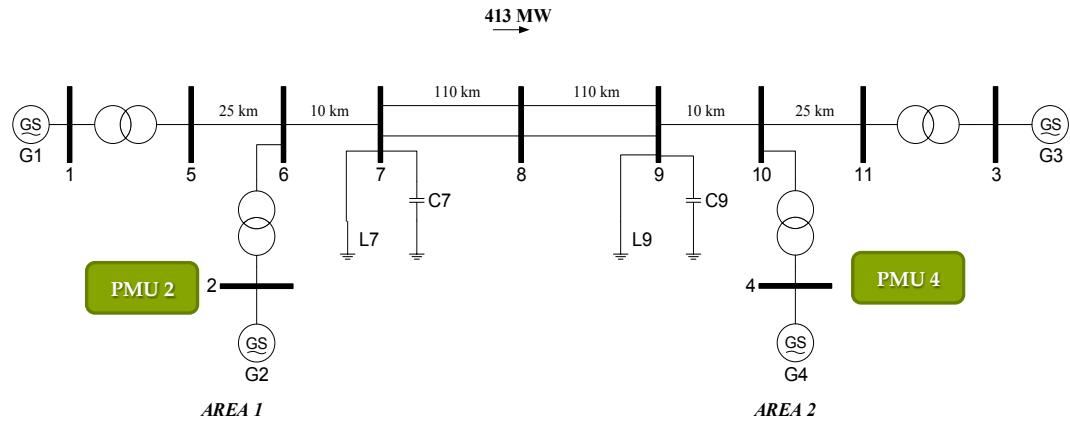


Figure-68. Two Area Four Machine System model with two allocated PMU

The results of simulation, where some loading scenarios are employed and a three-phase fault occurs in the system, are presented in Figure-71, Figure-72 and Figure-73 correspondingly.

From those three figures, it can be confirm that on a situation where the inter-area exist and the local controller failed to maintain the system stability, the

wide area damping controller together with the existing local controller successfully keeping the system stable as shown in Figure-72.
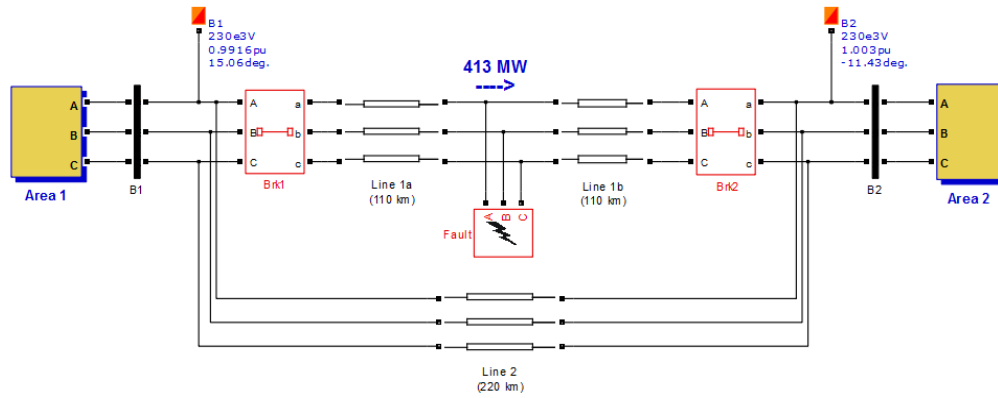


Figure-69. Simulink model of TAFM on 3 phase fault occurring
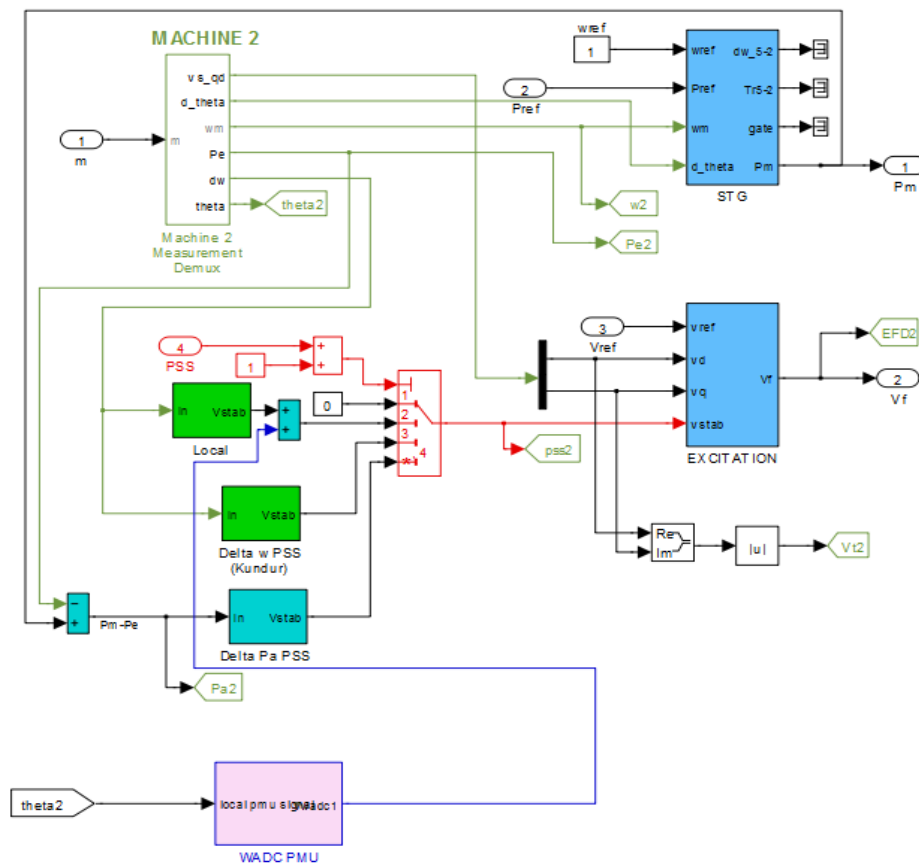


Figure-70. Configuration of Local and wide area controller
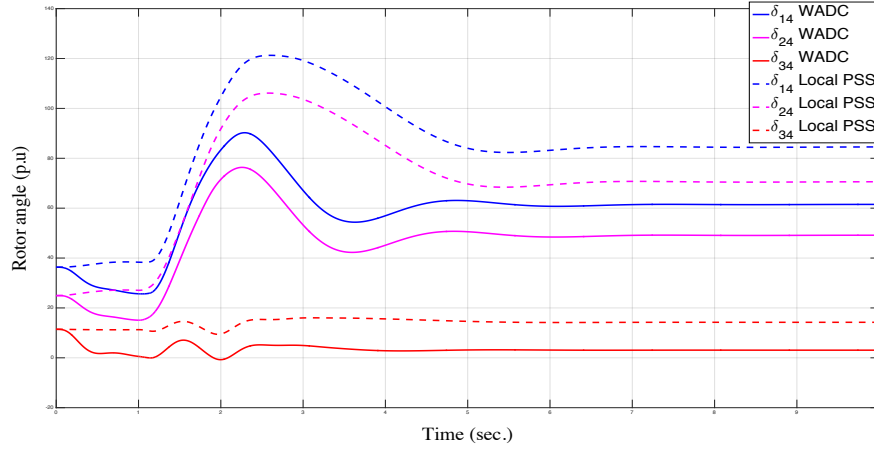
Figure-71. Performance of damping controller on load configuration L7:95% and L9:100%
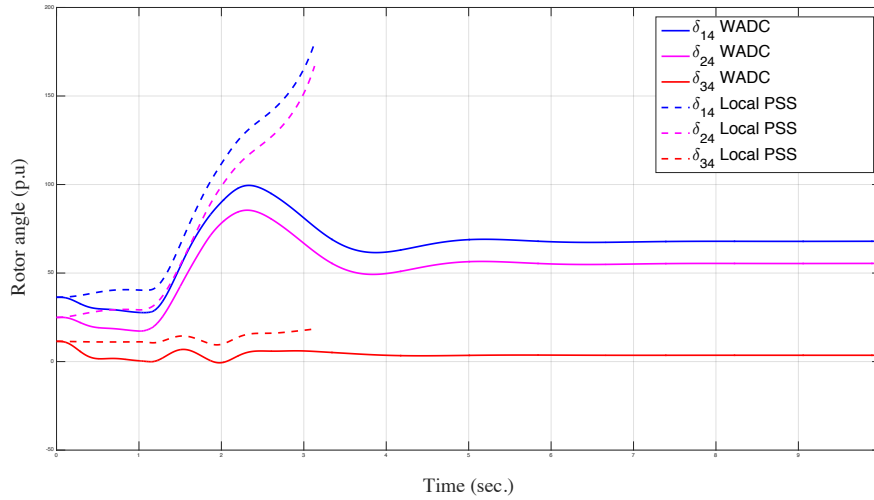


Figure-72. Performance of damping controller on load configuration L7:90% and L9:100%

In this simulation, the control limit of the wide area is kept under 5% and the local controller limit is 10%. In the future work it should be explored the application of such an intelligent system to manage the responds of both wide area and local controller towards any kind of oscillation whether it is local or inter-area oscillation signal.
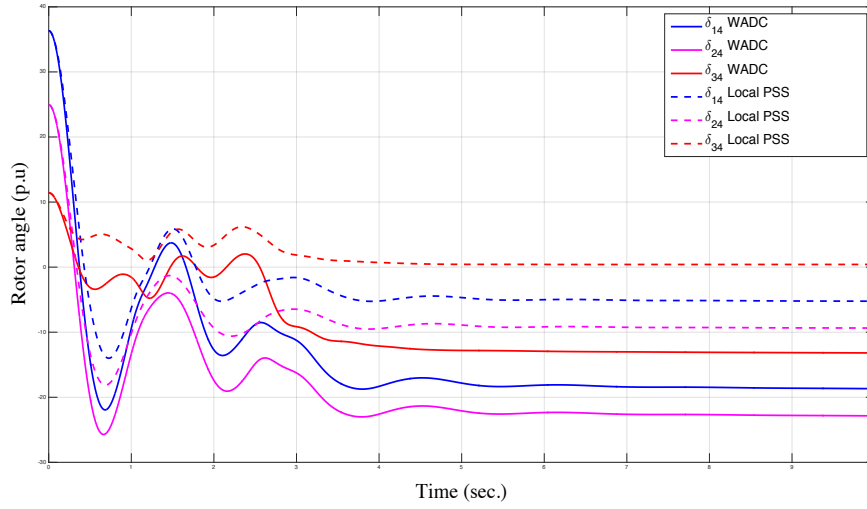
Figure-73. Performance of damping controller on load configuration L7:100% and L9:50%

## 5.5.  SUMMARY

It has been demonstrated the contribution of wide area signal input to the damping controller when an inter-area oscillation exist. In such a case only local oscillation, from the simulation result, local controller showed a better response to the system stability. Therefore in the future work, such an intelligent system to manage the contribution of both local and wide area controller towards the kind of oscillation of the system should be developed. In addition, for a larger system, it should be examined the most dominant path of the inter-area oscillation to provide a better wide area signal input.

# Chapter 6.

# CONCLUSION AND FUTURE WORK

## 6.1. CONCLUSION

This combination of Fast Fourier Transform and Continuous Wavelet Transform approach is capable to identify the center of frequency oscillation as well as calculating the damping ratio based on the information extracted from the PMU data with no information of the parameters of the system required.

The legitimacy of this method is verified by comparing to the result of eigenvalue-based calculation. As it has been demonstrated, the results of the two approaches are about the same that means this FFT-CWT is practicable to estimate the damping ratio of a small signal oscillation in power system.

The outstanding of this method is that information of system parameter are not needed, hence this approach is very applicable to apply in the case of Japan Campus WAMS or in other WAMS project where gathering data from multiple electric companies is not practicable.

From the Simulink based simulation, it shows the prospective of application of PMU signal in power system damping control

## 6.2. FUTURE WORK

In the future work, such an intelligent system to manage the contribution of both local and wide area controller towards the kind of oscillation of the system should be developed.

In addition, for a larger system, it should be examined the most dominant path of the inter-area oscillation to provide a better wide area signal input for the hybrid controller, local - wide area damping controller.

# Appendix A

# Power System Analysis Toolbox

The Power System Analysis Toolbox (PSAT) was developed by Prof. DR. Federico Milano from School of Electrical, Electronic and Communications Engineering, University College Dublin, Irelands. PSAT is a Matlab toolbox for electric power system analysis and simulation. The command line version of PSAT is also GNU Octave compatible. All operations can be assessed by means of graphical user interfaces (GUIs) and a Simulink-based library provides a user-friendly tool for network design.

The main features of PSAT are: Power Flow; Continuation Power Flow; Optimal Power Flow; Small Signal Stability Analysis; Time Domain Simulation; Complete Graphical User Interface; User Defined Models; FACTS Models; Wind Turbine Models; Conversion of Data Files from several Formats; Export results to EPS, plain text, MS Excel and LaTeX files; Interfaces to GAMS and UWPFLOW Programs; Command Line Usage; and GNU Octave Compatibility.

This software is a free license. The toolbox and tutorial can be downloaded from http://faraday1.ucd.ie/psat.html#download.

# Appendix B

# Two Area Four Machine System Data

**400 MW**
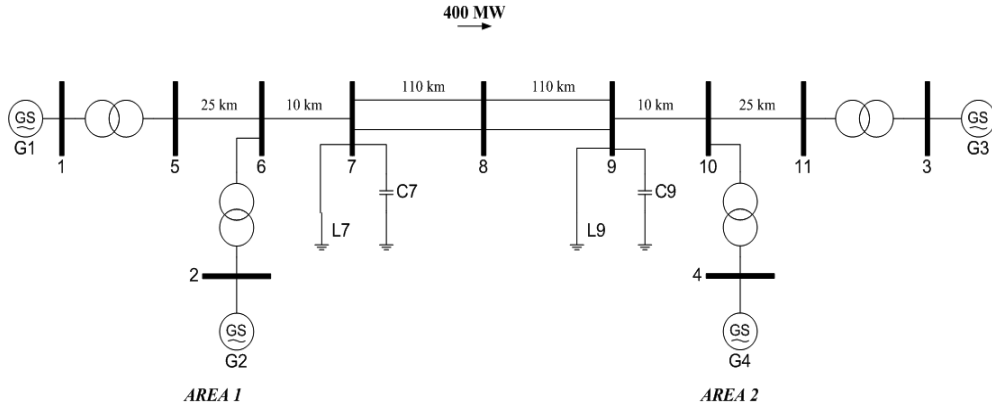


The system consists of two similar areas connected by a weak tie. Each area consists of two coupled units, each having a rating of 900 MVA and 20 kV. The generator parameters in per unit on the rated MVA and kV base are as follows:

$$X_d = 1.8 \qquad X_q = 1.7 \qquad X_l = 0.2 \qquad X_d' = 0.3 \qquad X_q' = 0.55$$
$$X_d'' = 0.25 \qquad X_q'' = 0.25 \qquad R_a = 0.0025 \qquad T_{d0}' = 8.0 \text{ s} \qquad T_{q0}' = 0.4 \text{ s}$$
$$T_{d0}'' = 0.03 \text{ s} \qquad T_{q0}'' = 0.05 \text{ s} \qquad A_{Sat} = 0.015 \qquad B_{Sat} = 9.6 \qquad \psi_{T1} = 0.9$$
$$H = 6.5 \text{ (for G1 and G2)} \qquad H = 6.175 \text{ (for G3 and G4)} \qquad K_D = 0$$

Each step-up transformer has an impedance of $0 + j0.15$ per unit on 900 MVA and 20/230 kV base, and has an off-nominal ratio of 1.0.

The transmission system nominal voltage is 230 kV. The line lengths are identified in Figure E12.8. The parameters of the lines in per unit on 100 MVA, 230 kV base are

$$r = 0.0001 \text{ pu/km} \qquad x_L = 0.001 \text{ pu/km} \qquad b_C = 0.00175 \text{ pu/km}$$

The system is operating with area 1 exporting 400 MW to area 2, and the generating units are loaded as follows:

| | | | |
|---|---|---|---|
| G1: | $P = 700$ MW, | $Q = 185$ MVAr, | $E_t = 1.03\angle 20.2°$ |
| G2: | $P = 700$ MW, | $Q = 235$ MVAr, | $E_t = 1.01\angle 10.5°$ |
| G3: | $P = 719$ MW, | $Q = 176$ MVAr, | $E_t = 1.03\angle -6.8°$ |
| G4: | $P = 700$ MW, | $Q = 202$ MVAr, | $E_t = 1.01\angle -17.0°$ |

# Appendix C

# Example of PSAT Calculation Result

```
EIGENVALUE REPORT

P S A T  2.1.9

Author:  Federico Milano, (c) 2002-2013
e-mail:  federico.milano@ucd.ie
website: faraday1.ucd.ie/psat.html

File:  C:\ResearchProject\FinalProjectforPSAT_CWT_Comparison\d_kundur_Bab5.mdl
Date:  23-Jan-2016 09:59:10


STATE MATRIX EIGENVALUES

Eigevalue       Most Associated States    Real part    Imag. Part   Pseudo-Freq.  Frequency

Eig As # 1      e2q_Syn_2                 -36.4978     0            0             0
Eig As # 2      e2q_Syn_3                 -36.4268     0            0             0
Eig As # 3      e2q_Syn_1                 -34.0439     0            0             0
Eig As # 4      e2q_Syn_4                 -32.7347     0            0             0
Eig As # 5      e2d_Syn_4                 -30.4808     0            0             0
Eig As # 6      e2d_Syn_2                 -30.2548     0            0             0
Eig As # 7      e2d_Syn_3                 -23.3781     0            0             0
Eig As # 8      e2d_Syn_1                 -21.7203     0            0             0
Eig As # 9      omega_Syn_2, delta_Syn_2  -0.57444     6.7862       1.0801        1.0839
Eig As #10      omega_Syn_2, delta_Syn_2  -0.57444     -6.7862      1.0801        1.0839
Eig As #11      delta_Syn_4, omega_Syn_4  -0.5558      6.603        1.0509        1.0546
Eig As #12      delta_Syn_4, omega_Syn_4  -0.5558      -6.603       1.0509        1.0546
Eig As #13      omega_Syn_3, delta_Syn_3  -0.14624     3.3501       0.53318       0.53368
Eig As #14      omega_Syn_3, delta_Syn_3  -0.14624     -3.3501      0.53318       0.53368
Eig As #15      e1d_Syn_2                 -5.7762      0            0             0
Eig As #16      e1d_Syn_4                 -5.8287      0            0             0
Eig As #17      e1d_Syn_3                 -4.3759      0            0             0
Eig As #18      e1d_Syn_1                 -3.482       0            0             0
Eig As #19      e1q_Syn_2                 -0.18076     0            0             0
Eig As #20      e1q_Syn_4                 -0.17336     0            0             0
Eig As #21      omega_Syn_3               -0.07759     0            0             0
Eig As #22      omega_Syn_1               0.02501      0            0             0
Eig As #23      omega_Syn_3               0            0            0             0
Eig As #24      delta_Syn_3               0            0            0             0

PARTICIPATION FACTORS (Euclidean norm)

          delta_Syn_1  omega_Syn_1  e1q_Syn_1  e1d_Syn_1  e2q_Syn_1

Eig As # 1   0.00049      0.00049      0.0023     8e-005     0.25545
Eig As # 2   0.00039      0.00039      0.00187    8e-005     0.2106
Eig As # 3   0.00046      0.00046      0.00081    0.00062    0.34448
Eig As # 4   0.0002       0.0002       0.00035    0.00171    0.16326
Eig As # 5   0.00063      0.00063      1e-005     0.01223    0.00097
```

Simulation 1: L7 98 MVA and L9 100MVA

# Glossary

***Hopf bifurcation***: is a local bifurcation in which a fixed point of a dynamical system loses stability as a pair of complex conjugate eigenvalues of the linearization around the fixed point cross the imaginary axis of the complex plane.

***Threshold level***: a limit used to detect a signal so that every time the signal $y(t)$ crosses the threshold, a sample of the signal of length $\tau$, y(ts : ts+$\tau$), is collected.

***Damping:*** Damping is an influence within or upon an oscillatory system that has the effect of reducing, restricting or preventing its oscillations due to dissipation of the energy stored in the oscillation.

***Signal to noise ratio:*** signal-to-noise ratio, often written S/N or SNR, is a measure of signal strength relative to background noise. The ratio is usually measured in decibels (dB).

# Bibliography

[1] P. Kundur et al., "Definition and Classification of Power System Stability," *IEEE Transaction on Power System; Definitions, IEEE/CIGRE Joint Task Force on Stability Terms and*, July 2003.

[2] Prabha Kundur, Neal J Balu, and Mark G Lauby, *Power system stability and control, EPRI Power System Engineering Series*. New York: McGraw Hill, 1994.

[3] P. Korba, M. Larsson, and C. Rehtanz, "Detection of oscillation in power system using Kalman filtering technique," in *IEEE Conf. in Control Application*, vol. 1, 2003, pp. 183-188.

[4] D.S. Laila, M. Larsson, B.C. Pal, and P. Korba, "Non linier Damping Computation and Envelope Detection using Hilbert Transform and its Application to Power System Wide Area Monitoring," in *IEEE Power & Energy Society General Meeting*, 2009, p. 7.

[5] G. Ledwich, D. Geddey, and P. O'shea, "Phasor Measurement Unit's for System Diagnosis and Local identification in Australia," in *IEEE Power Engineering Society General Meeting*, 2008, p. 6.

[6] G. Ledwich and E. Palmer, "Modal Estimates from Normal Operation of Power System," in *IEEE Power Engineering Society Winter Meeting*, vol. 2, 2000, pp. 1527-1531.

[7] P. Pourbeik and C. Rehtanz, "Wide Area Monitoring and Control for Transmission Capability Enhancement," *CIGRE Special Publications C6.601*, vol. Technical Brochure 330, 2007.

[8] A. Borgetti, C. A. Nucci, M. Paolone, G. Ciappi, and A. Solari, "Synchronized Phasor Monitoring During the Islanding Maneuver of an Active Distribution Network," *IEEE Transcation on Smart Grid*, vol. 2, no. 1, pp. 82-91, March 2011.

[9] J.L. Rueda, C.A. Juarez, and I. Erlich, "Wavelet-based analysis of power system low-frequency electromechanical oscillations," *IEEE Transaction on Power*

*System*, vol. 26, no. 3, p. 17331743, August 2011.

[10] J. Rueda and I. Erlich, "Wavelet-based method for modal identification from power system ringdowns," in *IEEE Power Tech 2011*, Trondheim, 2011, pp. 1-8.

[11] J. Slavič, I. Simonovski, and M. Boltežar, "Damping identification using a continuous wavelet transform: Application to real data," *Journal of Sound and Vibration*, vol. 262, pp. 291-307, April 1997.

[12] W. Staszewski, "Identification of damping in mdof system using time-scale decomposition," *Journal of Sound and Vibration*, vol. 203, no. 2, pp. 283-305, June 1997.

[13] R.E. Wilson and P.S. Sterlina, "Verification of measured transmission system phase angles," *IEEE Transaction on Power Delivery*, vol. 11, no. 4, pp. 1743-1747, October 1996.

[14] Z. Yao, "Fundamental phasor calculation with short delay," *IEEE Transaction on Power Delivery*, vol. 23, no. 3, pp. 1280-1287, July 2008.

[15] Hashiguchi Takuhei et al., "Identification of characterization factor for power system oscillation based on multiple synchronized phasor measurements," *Electrical Engineering in Japan*, vol. 163, no. 3, pp. 10-18, February 2008.

[16] Jegatheeswaran Thambirajah, Nina F. Thornhill, and Bikash C. Pal, "A Multivariate Approach Towards Inter-Area Oscillation Damping Estimation Under Ambient Conditions Via Independent Component Analysis And Random Decrement," *IEEE Transaction in Power System*, vol. 26, no. 1, pp. 315-322, June 2010.

[17] Ashfaque Ahmed Hashmani, *Damping of Electromechanical Oscillations in Power Systems using Wide Area Control*. Germany: DR.=ing Thesis Universität Duisburg-Essen.

[18] Xi-Fan Wang and Yonghua Song, *Modern Power Systems Analysis*. Middlesex, United Kingdom: Springer, 2008.

[19] Nagargoje S. and Diwan Seema P., "A Phasor Estimation of a Sum of Complex Exponentials Using Prony And Matrix Pencil Method with Prefiltering," in *32th IRF International Conference*, Pune, India, 2015, pp. 56-61.

[20] Changsong Lee, "Power System Small-Signal Dynamic Monitoring and Stability Control Based on Wide-area Phasor Measurements ," Kyushu Institute of Technology, Kitakyushu, Thesis 2010.

[21] Khairudin, Y. Qudaih, Y. Mitani, M. Watanabe, and T. Kerdphol, "Wavelet-demodulation-method based out of step detection and damping estimation in Japan campus WAMS," in *Power Systems Computation Conference (PSCC)*, Poland, 2014, pp. 1-7.

[22] Jie Yan, Chen-Ching Liu, and Umesh Vaidya, "PMU-Based Monitoring of Rotor Angle Dynamics," *IEEE Transaction in Power System*, vol. 26, no. 4, pp. 2125-2133, November 2011.

[23] Gibbard M.J., Purbeik P, and Vowies D.J., *Small-Signal Stability, Control and Dynamic Performance of Power System*. Adelaide, Australia: University of Adelaide Press, 2015.

[24] Teeuwsen Simon P., *Oscillatory Stability Assessment of Power System using Computational Intelligence*. Germany: Doctotal Thesis, Universitat Duidburg, Dresden, 2005.

[25] Jukka Turunen et al., "Comparison of Three Electromechanical Oscillation Damping Estimation Methods," *IEEE Transaction in Power System*, vol. 26, no. 4, pp. 2398-2407, November 2011.

[26] B. Chaudhuri and Bikash C. Pal, "Robust damping of multiple swing modes employing global stabilizing signals with a TCSC," *IEEE Transaction on Power System*, vol. 19, no. 1, pp. 499-506, February 2004.

[27] S. Bruno, M. De Benedictis, and M. La Scala, ""Taking the pulse" of Power Systems: Monitoring Oscillations by Wavelet Analysis and Wide Area

Measurement System," in *Power Systems Conference and Exposition, 2006. PSCE '06. 2006 IEEE PES*, Atlanta, GA, 2006, pp. 436 - 443.

[28] Samir Avdakovic and Amir Nuhanovic, "Identifications and Monitoring of Power System Dynamics Based on the PMUs and Wavelet Technique," *International Journal of Electrical, Computer, Energetic, Electronic and Communication Engineering*, vol. 4, no. 3, pp. 597-404, 2010.

[29] Abdon Atangana, *Derivative with a New Parameter: Theory, Methods and Applications*.: Academic Press, 2015.

[30] James W. Cooley, Peter A.W. Lewis, and Peter D. Welch, "Historical notes on the fast Fourier transform," *IEEE Transactions on Audio and Electroacoustics*, vol. 15, no. 2, pp. 76-79, June 1967.

[31] S. Mallat, *A Wavelet tor of signal processing*, 2nd ed. San Diego: Academic Press, 1999.

[32] Y. Chen and Feng M.Q, "A technique to improve the empirical mode decomposition in the Hilbert-Huang transform," *Earthquake Engineering and Engineering Vibration*, vol. 2, no. 1, pp. 75-85, June 2003.

[33] Introduction to GPS. [Online]. http://www.nhdfl.org/library/pdf/Forest%20Protection/Introduction%20to%20Global%20Positioning%20System.pdf

[34] A.G. Phadke and B. Kasztenny, "Synchronized phasor and frequency measurement under transient condition," *IEEE Transaction on Power Delivery*, vol. 24, no. 1, pp. 89-95, January 2009.

[35] Rodrigo J. Albuquerque and V. Leonardo Paucar, "Evaluation of the PMUs Measurement Channels Availability for Observability Analysis," *IEEE Transaction in Power System*, vol. 28, no. 3, pp. 2536-2544, August 2013.

[36] Phadke A.G., "Synchronized phasor measurements-a historical overview," in *Transmission and Distribution Conference and Exhibition 2002: Asia Pacific*.

*IEEE/PES (Volume:1 )*, 2002, pp. 476 - 479.

[37] Saugata S. Biswas, "Synchrophasor Technology – Devices (PMUs) and Applications," The School of Electrical Engineering and Computer Science, Washington State University,.

[38] IEEE standard for synchrophasors for power system, "IEEE Std 1344-1995(R200)," 1995.

[39] Cai J.Y., Zhenyu Huang, J. Hauer, and K. Martin, "Current Status and Experience of WAMS Implementation in North America," in *Transmission and Distribution Conference and Exhibition: Asia and Pacific, 2005 IEEE/PES*, 2005, pp. 1-7.

[40] Yih-Fang Huang, S. Werner, Jing Huang, N. Kashyap, and V Gupta, "State Estimation in Electric Power Grids: Meeting New Challenges Presented by the Requirements of the Future Grid," *Signal Processing Magazine, IEEE*, vol. 29, no. 5, pp. 33-43, September 2012.

[41] A. Mazloomzadeh, O. Mohammed, and S. Zonouz, "TSB: Trusted sensing base for the power grid," in *Smart Grid Communications (SmartGridComm), 2013 IEEE International Conference on* , Vancouver, 2013, pp. 803-808.

[42] Zhenyu Huang et al., "Performance Evaluation of Phasor Measurement Systems," *IEEE Power Engineering Society General Meeting 2008, Pittsburgh, PA*, pp. 1-7.

[43] I. Ngamroo and S. Danupaprita, "PMU Based Monitoring of Inter-Area Oscillation in Thailand Power System via Home Power Outlets," *ECTI Transaction on Electrical Engineering, Electronics and Communication*, vol. 5, no. 2, pp. 199-204, August 2007.

[44] US Department of Energy, "Smart Grid Investment Grant Program Progress Report 2," October 2013.

[45] Tianshu Bi, Hao Liu, Daonong Zhang, and Qixun Yang, "The PMU dynamic performance evaluation and the comparison of PMU standards," in *IEEE Power and Energy Society General Meeting, 2012*, 2012, pp. 1-5.

[46] Changsong Lee, K. Higuma, M. Watanabe, and Y. Mitani, "Monitoring and Estimation of Inter area Power Oscillation Mode Based on Application of Campus WAMS," in *16th PSCC July 2008*, Glasgow, Scotland, 2008, pp. 14-18.

[47] T. Hashiguchi et al., "Identification of Characterization Factor for Power System Oscillation Based on Multiple Synchronized Phasor Measurement," *Electrical Engineering in Japan*, vol. 163, no. 3, pp. 10-18, April 2008.

[48] Ota Y et al., "Monitoring of interconnected power system parameters using PMU based WAMS," in *Power Tech, 2007 IEEE Lausanne*, 2007, pp. 1718– 1722.

[49] Jinfeng Ren and M Kezunovic, "Real-Time Power System Frequency and Phasors Estimation Using Recursive Wavelet Transform," *IEEE Transaction on Power Delivery*, vol. 26, no. 3, pp. 1392 - 1402, July 2011.

[50] Soon-Ryul Nam, Jong-young Park, Sang-Hee Kang, and M Kezunovic, "Phasor Estimation in the Presence of DC Offset and CT Saturation," *IEEE Transaction on Power Delivery*, vol. 24, no. 4, pp. 1842-1849, October 2009.

[51] M. Klein, G.J. Rogers, S. Moorty, and P Kundur, "Analytical investigation of factors influencing power system stabilizers performance," *IEEE Transaction on Energy Conversion*, vol. 7, no. 3, pp. 382-390, September 1992.

[52] I. Ngamroo, "Dynamic Events Analysis of Thailand and Malaysia Power Systems by Discrete wavelet Decomposition and Short term Fourier Transform based on GPS Synchronized Phasor Data," *International Journal of Innovative Computing, Information and Control*, vol. 9, no. 5, pp. 2203-2228, May 2013.

[53] Khairudin, Y. Qudaih, M. Watanabe, and Y. Mitani, "Synchrophasor Measurement Based Damping Estimation and Oscillation Mode Detection using FFT-CWT approach in Japan campus WAMS," *International Journal of Smart Grid and Clean Energy*, vol. 4, no. 2, pp. 93-102, April 2015.

[54] H. Su, Q. Liu, and J. Li, "Boundary Effects Reduction in Wavelet Transform for Time-Frequency Analysis," *WSEAS Transaction on Signal Processing*, vol. 8, no.

4, pp. 169-179, October 2012.

[55] Zhao Xiaofeng, "Improved Genetic Algorithm to Extract the Edge of the Selected Threshold," *International Journal of Multimedia and Ubiquitous Engineering*, vol. 10, no. 1, pp. 277-284, January 2015.

[56] Browne T, Vittal V, Heydt G, and Messina, "A Comparative Assessment of Two Techniques for Modal Identification From Power System Measurements," *IEEE Transaction on Power System*, vol. 23, no. 3, pp. 1408-1415, August 2008.

[57] Liu Qing and Y. Mitani, "Application of HHT for oscillation mode analysis in power system based on PMU," in *2nd International Conference on Electric Power and Energy Conversion Systems (EPECS)*, 2011, pp. 1-7.

[58] Brigham EO, *The Fast Fourier Transform and Its Applications*.: Englewood Cliffs, NJ: Prentice Hall; 1988.

[59] Tomasz Tarasiuk, "Hybrid Wavelet-Fourier Spectrum Analysis," *IEEE Transaction on Power Delivery*, vol. 19, no. 3, pp. 957-963, July 2004.

[60] K Hur and S Santoso, "Estimation of System Damping Parameters Using Analytic Wavelet Transforms," *IEEE Transaction on Power Delivery*, vol. 24, no. 3, pp. 1302 - 1309, July 2009.

[61] Tao Lin and Jr Alexander Domijan, "Recursive Algorithm for Real-Time Measurement of Electrical Variables in Power Systems," *IEEE Transaction on Power Delivery*, vol. 21, no. 1, pp. 15-22, January 2006.

[62] Khairudin and Y. Mitani, "Syncrophasor measurement based small signal stability assesment using FFT-CWT approach in Japan-Campus-WAMS," in *Innovative Smart Grid Technologies Conference Europe (ISGT-Europe)*, Istanbul, 2014, pp. 1-6.

[63] J. T., et al. Bushberg, *The Essential Physics of Medical Imaging*, 2nd ed. Philadelphi: Lippincott Williams & Wilkins, 2006.

[64] Phadke A.G. and Thorp J., "History and Application of PHasor Measurements," in

Power System Conference and Exposition, 2006, pp. 331-335.

[65] Permerlani W, Kasztenny B, and Adamiak M, "Development and implementation of a synchrophasor estimator capable of measurements under dynamic conditions," *IEEE Transaction in Power Delivery*, vol. 23, no. 1, pp. 109-123, January 2008.

[66] Federico Milano, "An Open Source Power System Analysis Toolbox," *IEEE Transaction on Power System*, vol. 20, no. 3, pp. 1199-1206, August 2005.

[67] R. Witzmann, "Damping of Interarea Oscillations in Large Interconnected Power Systems," in *International Conference on Power System Transient*, 2001.

[68] S. E. Stanton and W. P. Dykas, "Analysis of a Local Transient Control Action by Partial Energy Functions," *IEEE Transaction on Power Delivery*, vol. 4, no. 3, pp. 996 - 1002, August 1989.

[69] O. Samuelsson and M Akke, "On-off control of an active load for power system damping-theory and field test," *IEEE Transaction on Power System*, vol. 14, no. 2, pp. 608-613, May 1999.

[70] Satnam Singh, "Application of Prony Analysis to Characterize Pulsed Corona Reactor Measurements," Department of Electrical and Computer Engineering, The University of Wyoming, Wyoming, M.Sc Thesis 2003.

[71] IEEE Power and Energy Society, "C37.118.1-2011 - IEEE Standard for Synchrophasor Measurements for Power Systems," *IEEE Standard Association, 2011*.

# Curriculum Vitae

The author obtained his Bachelor degree form University of Sriwijaya Indonesia in 1995. He acquired his Master of Science degree from the University of Manchester Institute of Science and Technology (UMIST) United Kingdom on 1999. Since 2000 he is working for Lampung University Indonesia at the department of electrical engineering. From September 2012 to March 2016 he got sponsorship from the Directorate General of Higher Education (DGHE) Republic of Indonesia for pursuing education to a Doctoral program in Kyushu Institute of technology Japan. Before working for Lampung University he was an electrical engineer in some companies including an electrical engineering consultant in Bandung Indonesia. He used to work in electrical engineering analysis and design. His research interests are in the area of power system stability, demand forecasting and smart grid. He is member of Institute of Electrical and Electronics Engineer (IEEE) since 1998.

Permanent address: Perum. Pondok Kemala Blok B No.7, Hajimena Lampung Indonesia.
Email: khai_hasan@yahoo.com, khairudin@unila.ac.id, m589505b@mail.kyutech.jp
This thesis was typed by Khairudin.